EFFECTIVE DESIGN OF STIFFENERS

ON INDUSTRIAL DUCTS

EFFECTIVE DESIGN OF STIFFENERS ON INDUSTRIAL DUCTS

By Jeff Udall, B.Sc., B.Eng.

A Thesis

Submitted to the School of Graduate Studies

in Partial Fulfillment of the Requirements

for the Degree

Master of Applied Science

McMaster University

MASTER OF APPLIED SCIENCE (2007) McMaster University

(Civil Engineering) Hamilton, Ontario

TITLE: Effective design of stiffeners on industrial ducts

AUTHOR: Jeff Udall, B.Sc. (University of Western Ontario)

B.Eng. (McMaster University)

SUPERVISORS: Dr. Samir E. Chidiac

Dr. Bassam Halabieh

NUMBER OF PAGES: ix, 143

ABSTRACT

Large ducts are used to carry air and flue gases to and from industrial processes and can be subjected to a variety of loading conditions. To maintain the structural integrity of the ducts, stiffeners are attached to the casing to form a more rigid frame. Stiffeners protect the duct casing by reducing the unsupported span of the plate, hold the original shape of the duct, and are used for overall duct support or restraint.

Current methods used to size stiffeners on industrial ducts are derived from standard equations used for beam design in buildings with some accommodation for the composite section formed by the beam and casing plate. These methods are shown to be significantly conservative with a safety factor in the order of four to five. This large conservatism in the design results in higher capital costs and construction costs.

To determine the actual capacity of a stiffener beam relative to the design limit, an experimental program was developed. A box was fabricated with a removable top plate that incorporated one of two different beam stiffeners. The box was subjected to a vacuum pressure and the response of the beams was monitored until their final collapse.

A finite element model was developed to simulate the experiment. Reasonable agreement between the finite element model and the experimental data was found. Subsequently, a parametric study was conducted using the developed finite element model.

An alternative analytical design method was presented that took into account composite action. This includes the location of the neutral axis, the location of the load along the height of the beam, and the contribution of the web to the support of the outstanding compression flange. Each of these factors provides an increase in bending capacity for the stiffener.

The proposed alternative method continues to provide conservative results relative to the point of failure determined by both the experimental program and the finite element analysis. However, the results are substantially less conservative than what is provided through the current design methods.

ACKNOWLEDGEMENTS

The author would like to express his sincere gratitude to Dr. Samir E. Chidiac and Dr. Bassam Halabieh for their guidance and advice throughout this research project, and their support during the completion of the thesis.

The assistance of Peter Golini, Peter Koudys, David Perrett, Maurice Forget, and Bernard Nieuwenhuis is also greatly appreciated. Their commitment, long hours, experience, and expertise were critical to the completion of the experimental program.

The financial assistance of The Natural Science and Engineering Research Council of Canada, McMaster University's Centre for Effective Design of Structures, and Babcock & Wilcox Canada is deeply appreciated.

Finally, I wish to thank my wife, Tammy, and my children, Zackary and Justine, for their constant understanding and support during the completion of this study.

TABLE OF CONTENTS

LIST OF FIGURES

LIST OF TABLES

CHAPTER 1 INTRODUCTION

1.1 Background

Many industrial processes require a large supply of air for such things as combustion of fuels. The transport of air, which is generally fed in a controlled manner through series of ducts, is controlled by fans that generate the required upstream pressure and air velocity. Downstream of the combustion process, the waste products are removed through flues with the use of downstream fans. Accordingly, the flues and ducts in industrial applications are significantly larger than those used in residential or commercial HVAC applications, and carry air or flue gases at elevated temperatures and pressures. Common sizes of ducts are in the range of 5 m to 15 m in width and height. For some applications, the size of the duct may be even significantly larger. With regard to temperature, a typical duct from a coal fired boiler at a power station carries flue gases in the range of 400°C to 500°C containing corrosive and abrasive products such as sulfur dioxide and ash particulate.

Figure 1, illustrates typical duct layouts for a coal fired boiler as part of a power plant. Effective structural design of these industrial ducts and flues is the focus of this study.

The structure of a duct or flue consists of a casing, reinforcing stiffeners, supports, and mechanical elements such as expansion joints, dampers, flow straighteners, and process instrumentation. The casing plate is designed to resist the operational pressures held within the duct. A rectangular duct with sufficiently thick plate and small size is usually capable of withstanding the pressures without additional reinforcement. However, with larger applications common in industrial processes, additional reinforcement must be added to minimize the plate thickness. This is accomplished by providing external stiffeners that effectively reduce the supported width of the casing plate.

Design considerations for industrial ducts require the engineer to fully understand the process when performing the mechanical and structural design. Applications for the ducts include, for example, movement of combustion air and flue gasses from power boilers, steel making facilities, or large heating and ventilating systems.

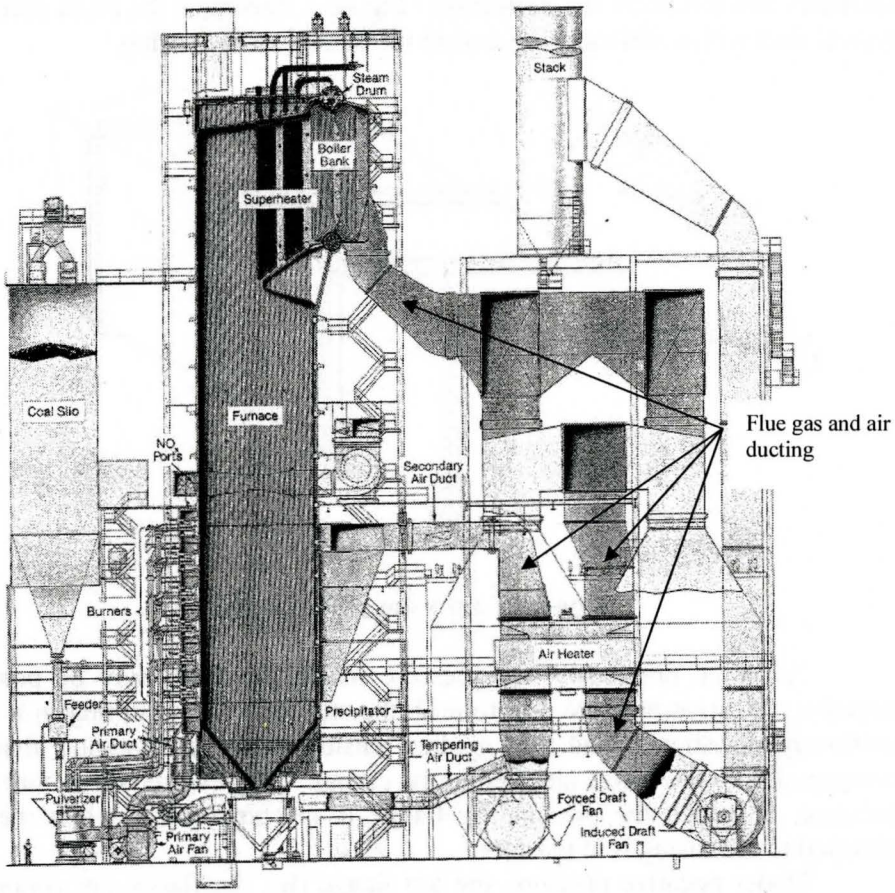

Figure 1: Large coal and oil fired boiler. [17]

Stiffeners are added to maintain the structural rigidity of the duct and are designed to resist operational and external loads, including;

- Internal positive or negative pressure,
- Weight of the casing itself with insulation and lagging,
- Live loads such as wind, snow, seismic, internal ash loads, and
- Other loads such as thermal expansion forces or support loads.

The design of stiffeners is governed by the most critical combination of these loads. Transient internal pressures are often up to ± 8.7 kPa according to the National Fire Protection Association (NFPA) guidelines[16]. Because ducts in industrial applications are quite large, the stiffener spans are similarly long. High loads combined with long spans can result in heavy wide-flanged beam stiffeners. In some cases, internal truss-work is required to limit the size of the reinforcing

stiffeners and minimize the deflection. Figure 2 illustrates the cross section of a typical duct with a stiffener ring around the outside of the casing.

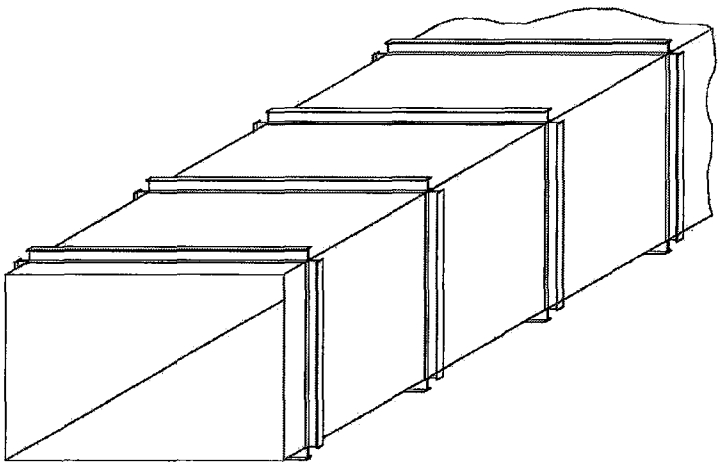

Figure 2: 3m x 4m stiffened duct

As noted previously, the pressure inside the ducts may be positive or negative. Positive pressure acts to push the stiffeners out, resulting in a roughly uniformly distributed load that applies tension to the outstanding flange and compression to the flange attached to the casing. The reverse is true for negative pressure, in which the outstanding flange is in compression while the flange attached to the casing is in tension.

Under negative pressure, the top flange (ie., the flange not connected to the casing) is in compression. Standard practice calls for lateral bracing of the compression flange for long span beams. Since the compression flange in this case is not directly braced, the full span of the beam is taken as unbraced. To reduce the unbraced span, gussets may be added which effectively connect the compression flange to the casing, thereby giving it lateral stability. Figure 3 illustrates the gusset plates as they would typically be installed.

Installation of these gussets reduce the required size of the beam and make a more cost effective design. However, the cost effectiveness comes at the extra expense of adding the gusset plates. Although the cost of the metal itself is relatively inexpensive, the labour and material handling costs can be substantial for very long ducts. This study aims to investigate the effectiveness of the current design method for industrial duct stiffeners as well as the need for adding gusset plates.

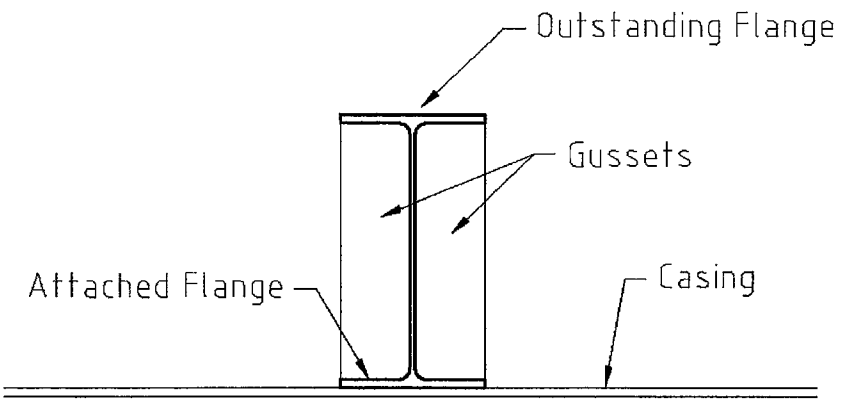

Figure 3: Gusset plates provide stability to top compression flange

1.2 Stiffener Design Method

Design methods commonly used for stiffeners are adapted from structural steel codes and modified to account for the unusual service conditions. A common code used for this purpose is the American Institute of Steel Construction (AISC), Allowable Stress Design Manual[2]. Since many of the larger engineering firms that design industrial ductwork are based in the United States, AISC steel code is generally accepted as the code of choice. This is discussed further in the ASCE Air and Gas Duct Design book[1].

> Traditionally, structural engineers have used the provisions of the American Institute of Steel Construction's (AISC) *Specification for Structural Steel Buildings – Allowable Stress Design and Plastic Design (ASD)* presented in the *AISC Manual of Steel Construction – Allowable Stress Design (AISC-ASD)* when performing the structural design of air and flue-gas ductwork. Since the AISC-ASD Specification is intended to apply to conventional structures at ambient temperatures, the design of structural steel considering the effects of high temperatures has always been left up to the judgment of the responsible structural engineer. This ASCE Special Publication anticipates the traditional use of the AISC-ASD Specification with adjustments and additional considerations for the high metal temperatures. (Sect. 1.2.2, Application of Building Codes and Design Codes)

The AISC design manual also recommends that the design method be based on using allowable stress rather than limit states since the various expected

loads will also come with various temperatures and thus altered material properties. The probability of simultaneous occurrence of the various loads also cannot be determined. This makes a factored design approach difficult and time consuming. As a result, actual loads and allowable stresses are used.

The design process of the duct and stiffeners is briefly summarized as follows;

- The size of the duct is generally defined by the process requirements of the system. The air or flue gas quantities are known according to the process, and the duct size is determined by limiting air or gas velocities through experience and the standards of each design office.
- The critical loading conditions for the duct panels are determined by considering all applicable loads.
- The maximum stiffener spacing on the duct is then determined according to the loading conditions and geometry of the duct. The spacing of the stiffeners is governed by the allowable stress or deflection in the casing plate. If the stiffener spacing is too large, the casing will be overstressed or will deflect excessively and result in permanent deformations or cracking at critical locations. The stiffeners provide reinforcement for the casing and create casing panels that are sufficiently small to withstand the loads applied to them. If the width of the duct is less than the required spacing, then no stiffeners are required. Stress in the plate is determined by using a simple strip beam analogy, or by considering a large deflection analogy to include membrane and bending stresses.
- With the stiffener spacing defined, the loads applied to the stiffener are then defined. A stiffener member is chosen to resist these loads. The stiffeners are generally common steel shapes such as angles, channels, or wide flanges.
- The beam section is chosen by determining the required section modulus of the beam/plate composite section that has a resultant outer fibre stress less than the allowable stress given by the code formulae.
- The maximum deflection of the stiffener is limited by choosing a beam with an appropriate moment of inertia. The casing is often included in the moment of inertia to provide additional stiffness.

The use of the code formulae is modified somewhat by way of the operating conditions of the ducts. Under elevated temperatures, the material properties, namely the yield stress and elastic modulus, are decreased. Since these two material properties are used in the formulae, consideration must be made for their reduction. However, for the purpose of this research, all values are taken at ambient temperature.

Standard design practice assumes the unbraced length of the outer flange to be the full span of the beam when there are no additional attachments or internal trusses. Reducing the unbraced length of the compression flange is

accomplished by adding gusset plates between the flanges of the member. The gussets, shown in Figure 3, provide a load path between the unbraced compression flange and the tension flange that is braced through the attachment to the casing. Very long stiffeners may require the installation of two or more sets of gussets. The gussets do not increase the elastic capacity of the beam, only the buckling capacity. Once the unbraced length is reduced sufficiently, the beam failure is controlled by yielding, rather than buckling, and a smaller size member may be chosen. Reduction of the stiffener size results in substantial cost savings in applications involving large ducts with several tonnes of steel.

1.3 Literature Review

A duct stiffener resisting negative pressure provides unique boundary conditions that have been addressed in varying degrees by other research. This section reviews the literature that determines the capacity of beams with similar boundary conditions.

1.3.1 Bracing of the Tension Flange and Torsional Bracing

Design of beams for use in structural steel is largely based on the unbraced length of the compression flange. The concept of the analysis is that the compression flange generally acts like a column and must be restrained against lateral (out-of-plane) displacement. By keeping the unbraced length of the compression flange below the critical buckling length, the section will fail by yielding rather than by buckling. Bracing is therefore specified at certain intervals along a beam length to maximize the capacity of the beam.

This concept is what is generally considered in the design of duct stiffeners. The flange that is not connected to the casing is in compression when the duct is under negative pressure.

The buckling of a beam involves lateral, out of plane displacement of the compression flange. Equation 1-1 is the standard beam buckling equation[10]. Equation 1-1 is the closed form solution of the differential equation for elastic lateral buckling of a simply support beam under uniform moment; i.e. beam ends may not twist but are free to warp.

$$M_{cr} = \sqrt{\frac{\pi^2 EI_y}{L^2}\left(GJ + \frac{\pi^2 EC_w}{L^2}\right)} \qquad (1\text{-}1)$$

where E is the modulus of elasticity, I_y the moment of inertia about the Y axis, C_w the warping torsional constant, G the shear modulus, J the torsion constant, L the unbraced length, and M_{cr} the critical moment.

A primary consideration in the development of this equation is that the cross section of the beam does not deform. That is, the flanges remain parallel to each other, and the web remains straight and perpendicular to the flanges at all

points along the span. Therefore, for the compression flange to displace laterally in one direction, the tension flange displaces in the opposite direction and the entire cross section twists by an angle, φ (See Fig. 4-a). To the contrary, if the compression flange is braced, the beam will not twist and buckling is prevented. (See Fig. 4-b) Based on this assumption, it can be seen that if only the tension flange is held laterally, the compression flange may still move as the section twists (See Fig. 4-c). Furthermore, it has been shown that providing only lateral restraint on the tension flange has little effect on the buckling capacity[26]. However, if the tension flange is held rotationally about its longitudinal axis, then the compression flange is also held rotationally through the web and twist of the cross section is prevented (See Fig. 4-d). Lateral displacement of the beam without twisting does not constitute buckling since the loading on the beam remains in the strong axis.[26] Thus, torsional restraint of any part of the beam cross section effectively acts as a brace point for the compression flange if the entire cross section, including the web, is able to resist the applied torsional forces. The plate attached to a stiffener may provide some rotational restraint.

Given that a rotational restraint on the tension flange may act as a brace, the question becomes 'is it an effective brace?' For a brace to be effective, it must have suitable strength and stiffness. If either factor is not sufficient, then the buckling mode will not be suppressed.

In 1966, Taylor and Ojalvo[19] addressed torsional restraint as bracing. The authors used partial differential equations for restrained buckling developed by Timoshenko[21]. In their paper, the authors introduced a rotational stiffness coefficient for the restraint that resists lateral-torsional buckling. Accordingly, the critical moment is presented as a function of this coefficient, and the geometry of the beam. The authors examined the cases of continuous restraint and point restraint with equal end moments, centre point load, and uniform load. It is noted that for continuous restraint, the buckling capacity increases unbounded as the torsional rigidity of the brace increases. This is due to the fact that in their model, they assumed no distortion of the cross section as the beam buckles. In the case of a torsional restraint that is not connected directly to the compression flange, the web may bend which distorts the beam cross section making these equations inapplicable.

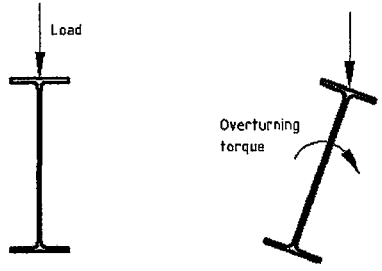

Section is unbraced. At point of buckling, the entire cross section twists, but does not distort

Figure 4-a

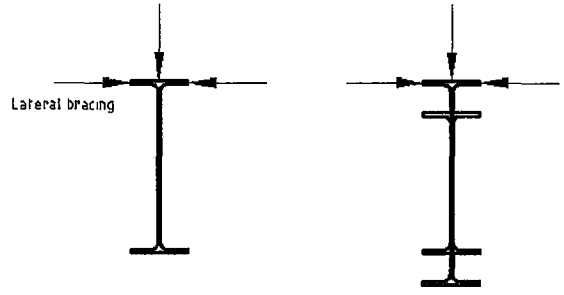

Compression flange is braced and is not capable of buckling laterally. The section fails in yield.

Figure 4-b

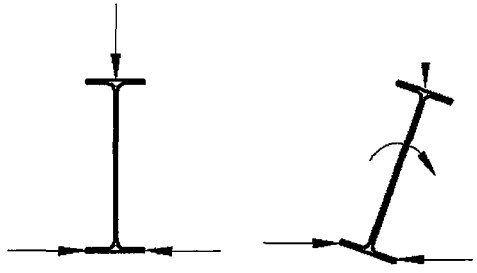

Tension flange is braced laterally. At point of buckling, the compression flange is still capable of lateral displacement, and the cross section will twist with minimal gain in capacity

Figure 4-c

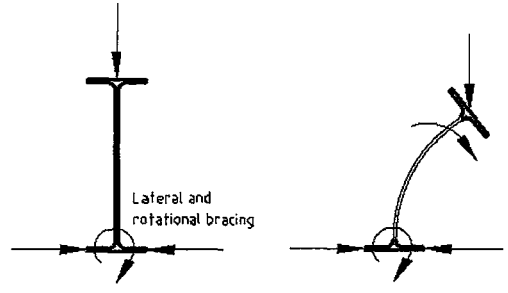

Tension flange is braced both laterally and rotationally. For the compression flange to buckle laterally, the cross section must distort through bending of the web. The compression flange is stabilized if the web is strong enough to prevent the bending, or if gussets are provided.

Figure 4-d

Figure 4: Beam bracing models

In 1975, Milner[14] was the first to address the condition of bracing on the tension flange of a beam that provides infinite positional restraint and finite torsional restraint. The author indicated that there had not been any previous work that considered distortions in the web as buckling occurred. The concept of having the braced and unbraced flanges buckle independently had not been addressed. The model was set up using the principle of virtual work. The author noted that the equations are too difficult to be solved algebraically and resorted to numerical methods. Four buckling modes were established from the characteristic equation and the resulting determinants.

Milner's analysis employed a single variable, K_r, to account for the rotational stiffness of the external brace. He extended this analysis to include the out of plane stiffness of the web in the rotational constant. The stiffness of the web, K_w, was given by

$$K_w = C_1 \frac{Et^3 W}{d} \tag{1-2}$$

where C_1 is a constant, t the thickness of the web, d the height of the web, and W the width of the web beneath the support. Equation 1-2 is derived by assuming that a section of the web acts like a cantilever with length equal to the beam depth and the width equal to the width of the brace attachment. The stiffness is equated to the moment divided by the rotation. By considering only the section of web attached to the brace, the constant C_1 is equal to 1/6. However, the web adjacent to the brace for some undetermined distance provides some contribution to the affect. Therefore, the author suggested that further evaluation of this constant is required.

By combining the rotational stiffness of the external brace and the rotational stiffness of the web, the effective stiffness of the system becomes

$$\frac{1}{K_r} = \frac{1}{K_W} + \frac{1}{K_b} \tag{1-3}$$

where K_r is the rotational stiffness of the entire assembly, and K_b the external brace stiffness

Equation 1-3 presents an upper limit to the effectiveness of an external brace. If the external brace is infinitely stiff, the system stiffness becomes limited by the stiffness of the web. Likewise, if the web is infinitely stiff (or made sufficiently rigid for example by providing web gussets), the system stiffness becomes equal to the stiffness of the attached brace. If both the brace and the web act with finite stiffness, then according to the proposed model of Equation 1-3, the total rotational stiffness is less than the smaller of the two. This concept is illustrated in Figure 5. The consequence of having both the web and external brace acting in series is that if the total stiffness of the combination is not sufficient, then there is no effective brace at this point and the unbraced length of the compression flange cannot be reduced.

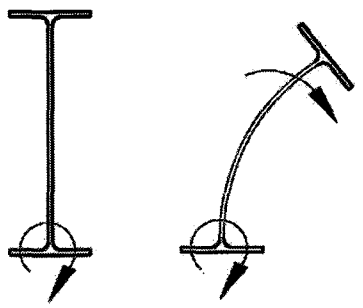

Rotational bracing
and buckling movement
of compression flange

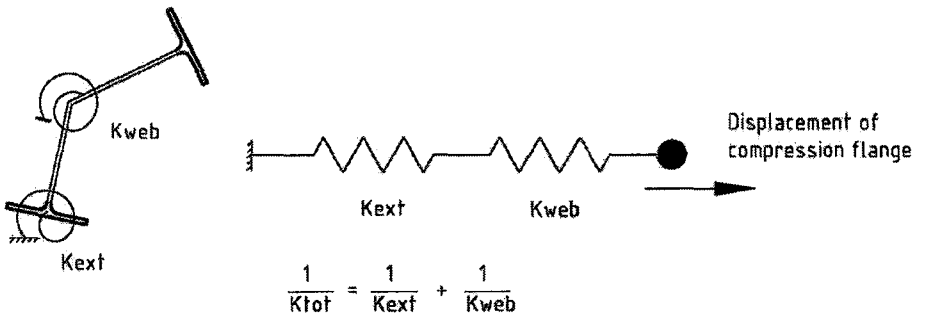

Rotational and linear spring analogy demonstrating effect
of web stiffness on overall bracing stiffness

Figure 5: Spring analogy for web stiffness

With regard to the duct stiffener, the external rotational brace is considered to be the duct casing. However, since the casing is welded to the tension flange, not only does it change the geometry of the beam, but also the section is no longer doubly-symmetric.

In 1977, Milner[15] expanded on his earlier research by deriving a method suitable for engineering design. The proposed method used a series of curves relating the beam properties, span between braces, and the height above the tension flange where the bracing is applied to estimate the rotational stiffness. Accordingly, Equation 1-3 was expanded to include a term for the stiffness of the connection, K_j.

Valentino and Trahair[22] investigated the contribution of torsional restraint on the buckling capacity of a simply supported doubly-symmetric wide flange member. The authors used finite element analysis to generate data required for

developing equations to predict elastic buckling moments. Conditions considered were uniform and non-uniform bending, top, centroid, and bottom flange loading, central (mid-span) torsion restraint, off-center restraint, and continuous restraint. In all cases, the torsion restraint was located at the central height of the web, and web distortion was not considered.

It was noted that the moment capacity of the beam increased without bound as the stiffness of the torsional restraint increased as was found in Milner's earlier work. This is because web distortion was not considered. If the web is not allowed to distort, then no part of the section can twist if the restraint provides infinite torsional stiffness. However, this is not the case in practice. A torsional restraint at only one location of the beam height does not effectively control the twist of the entire section. In the case of the duct stiffener resisting negative pressure, the tension flange is held and the compression flange is free to twist via out of plane bending of the web.

Yura[26] provided a complete presentation on the current state-of-the-art of beam bracing. Much of the information presented in this review is incorporated into the AISC Load and Resistance Factor Design Specification[3] as discussed later.

Yura compared the work of Taylor and Ojalvo[19] with finite element results to discuss the nature of web distortion in the requirements for torsional bracing. He introduced the equation of bracing stiffness used by Milner and further developed the term for web stiffness. The revised term, β_{sec}, included the stiffness of added web stiffener gussets. The addition of gusset plates to the web provides a substantial increase in resistance to distortion. Equation (1-4) shows the revised stiffness term.

$$\beta_{sec} = 3.3\frac{E}{h}\left(\frac{(N+1.5h)^2 t_w^{\,3}}{12} + \frac{t_s b_s^{\,3}}{12}\right) \tag{1-4}$$

where h is the distance between flange centroids, N the length of the attached brace, t_w the web thickness, t_s the thickness of the gusset stiffener, and b_s the full width of both stiffeners on each side of the web.

When the bracing is attached continuously over the length of the beam, an effective unit width replaces the term (N+1.5h). Also, for the case when no stiffener is provided, the terms t_s and b_s become zero and equation (1-4) reduces to

$$\beta_{sec} = 3.3\frac{E}{h}\left(\frac{t_w^{\,3}}{12}\right) \tag{1-5}$$

Equation 1-5 shows similarities to equation (1-2), which is expected since the author had developed the equation based on Milner's work and quantified the constants using the finite element solutions.

Taylor and Ojalvo[19] provided an exact equation for the critical moment of a doubly symmetric beam with continuous torsional bracing,

$$M_{cr} = \sqrt{M_0^2 + \beta_b EI_y} \tag{1-6}$$

where β_b is the brace stiffness, and M_0 is the critical moment of the beam without torsional bracing. The authors indicated that torsional bracing is less sensitive than lateral bracing to conditions such as load height, brace locations, and number of braces. However, it is more sensitive to cross section distortion. They also noted that brace forces can become very large when local flange buckling or web buckling occurs prior to overall lateral instability. After local buckling, the cross section becomes asymmetric and the vertical loads develop very significant out of plane load components.

1.3.2 Load Height

The height of the applied load with respect to the beam centroid is known to affect the capacity of a beam in flexure. The general buckling formulae were developed without considering external torsional forces on the beam. Such forces can be presented by the transverse load if the latter is applied away from the centroid of the section. When the member remains vertical, the load does not apply any torque to the section. As the section begins to twist during the initial stages of buckling, the load no longer acts through the centroid and its distance above the centroid determines the degree of torsion moment that is applied. If the load is applied above the centroid, then the applied torsion acts to increase the torsional forces leading to buckling. When the load is below the centroid, then it acts to resist the buckling torsion forces, essentially providing restorative forces.

The SSRC Guide[10] addresses load height by incorporating it within the moment gradient factor, C_b. The revised factor is given as

$$C_b = AB^{\frac{2y}{h}} \tag{1-8}$$

where A is the moment gradient factor (Table 1), B given by an empirical equation that is a function of W (Table 1), y the distance between the load height and the centroid (positive if below the centroid), and h the depth of the beam. W is calculated according to equation 1-9.

$$W = \frac{\pi}{L}\sqrt{\frac{EC_w}{GJ}} \tag{1-9}$$

Table 1: Load Height Factors

Loading	Maximum Moment	A	B[1]
Central point load, P	$\frac{PL}{4}$	1.35	$1 - 0.180\,W^2 + 0.649\,W$
Uniform Load, w	$\frac{wL^2}{8}$	1.12	$1 - 0.154\,W^2 + 0.535\,W$
Two point loads – equally spaced, L_1 from the ends	PL	$1+\left(\frac{L_1}{2L_1+L_2}\right)^2$	$1-0.465W^2\left(\frac{L_1}{L}\right)+1.636W\left(\frac{L_1}{L}\right)$

Using these factors, and assuming the application of uniformly distributed load, the effect of the load height on the torsional capacity of the stiffener is demonstrated by the following example.
One begins by computing the moment gradient factor for a W12x14 beam that is 4572 mm long, simply supported and subjected to a uniformly distributed load.

1. Torsional properties are taken from reference 9.
   $C_w = 2.164 \times 10^{10}\ mm^6$
   $J = 2.972 \times 10^4\ mm^4$

2. Using Equation 1-9, compute W = 0.945

From Table 1, A = 1.12 and B = 1.36. For the W12x14 beam, h = 303 mm. For top flange loading, y = -h/2 and 2y/h = -1. Negative value implies that the load is above the centroid. Accordingly, $C_b = 1.12 \times 1.36^{-1} = 0.823$. Therefore, the beam capacity is reduced by a factor of 27%. However, if the load is applied at the bottom flange, the value of y changes to +1, and the factor given by Equation 1-8 becomes, $C_b = 1.523$, giving an increase in the capacity of the beam by 36%. The percent difference in the beam capacity from top flange loading to bottom flange loading is then 85%.

It shall be noted that for the case of the duct stiffener resisting negative pressure, the load is applied to the bottom flange. This effect needs to be taken into account in the capacity of the stiffener in resisting transverse loads.

[1] It is noted that the equation for 'B' with two point loads is written incorrectly in the Guide. The L_1/L terms were not included.

1.3.3 Singly-Symmetric Sections

By virtue of being welded to the casing of the duct, the section properties of the stiffener are modified. The neutral axis of the section is lowered due to the added plate on the bottom flange.

The change of section properties is not adequately addressed in the current analytical design methods. Since the stiffener beam is welded to the casing plate, a singly symmetric composite section is created. Under conditions of positive pressure, the casing portion of the composite section is in compression. The width of the casing in compression must be limited to avoid local buckling of the plate. The effective width of the casing in compression is taken as a function of the casing thickness. Various factors are used depending on the source and the design office. The ASCE Air and Gas Duct Design book[1] summarizes a variety of factors that are used.

> The effective width of the plate is determined by the structural engineer and the calculation method may be somewhat arbitrary. There are several rationales that can be used to choose an effective width of duct plate. *Design of Welded Structures*[6], by Blodgett recommends a value of 12 times the plate thickness, t, off to either side of the stiffener edge. The United States Steel Corporation publication *Steel Design Manual* [7], uses $190t/\sqrt{Fy}$ which is 32t for F_y=36.0 ksi; 16t on either side of the stiffener leg. If the limits set for uniformly compressed stiffened elements given in the American Institute of Steel Construction's (AISC) *Specification for Structural Steel Buildings – Allowable Stress Design and Plastic Design (ASD)*[2] are used, the effective width will be $253/\sqrt{Fy}$, which is 42t for F_y=36.0 ksi; 21t on either side of the stiffener leg. Note that even though F_y decreases as the temperature increases, the ambient temperature value of F_y should be used. (Ref. 1, Sect. 8.2.1 Stiffeners – Composite Action)

It should be noted that the suggestion in the previous paragraph to use the ambient value of F_y in the determination of the effective width is not explained, even though doing so would provide a non-conservative design if the intent of the method is followed. Thus, if casing width of '42t' is included in the composite section to derive the overall section properties, the casing should be protected from compressive loads. This then allows the designer to choose an appropriate section with sufficient stiffness to limit the deflection requirements.

This value of effective plate width, as noted above, is relatively arbitrary. It is a value chosen to protect the casing from local buckling near the stiffener. However, it does not accurately reflect the actual contribution of the plate to the composite section. The contribution of plate width can be determined by the longitudinal stresses and how they decrease as one moves away from the stiffener,

which is often referred to as shear lag. At a distance of 21t from the edge of each flange, there may still be substantial longitudinal stress in the plate and should be included in the composite section.

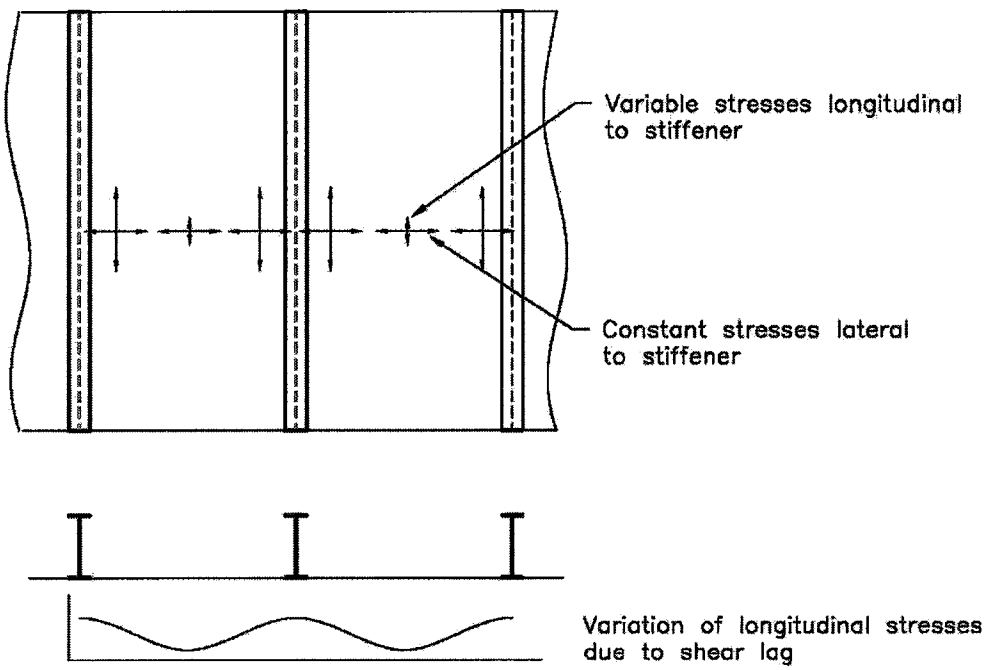

Figure 6: Shear lag and longitudinal stresses in plate

In terms of practical design, the point where the longitudinal stresses are sufficiently small, so that they can be ignored, must be determined. In some cases, the longitudinal stress may not decrease substantially between stiffeners, suggesting that the entire plate width should be included in the analysis. Figure 6 and Figure 7 illustrate the concept of shear lag and its effect on effective plate width.

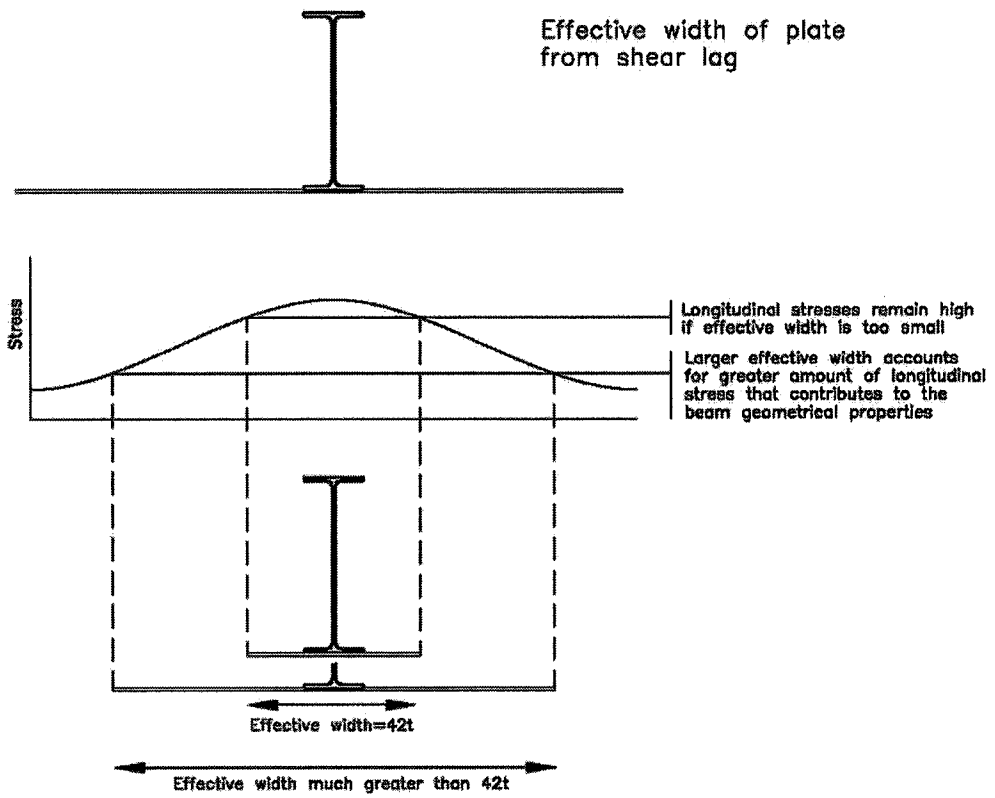

Figure 7: Effective plate width from diminishing longitudinal stresses

By attaching the plate to the beam, the geometry changes from being 'doubly symmetric' (symmetrical about both the Y and X axis) to 'singly symmetric' (symmetric about only the Y axis). Singly symmetric sections have different buckling properties than doubly-symmetric sections.[10]

The SSRC Guide[10] presents the following formula for determining the critical moment for 'monosymmetric beams'

$$M_{cr} = \frac{C_b \pi^2 E I_y \beta_x}{2(K_y L)^2}\left\{1 \pm \sqrt{1 + \frac{4}{\beta_x^{\,2}}\left[\frac{C_w K_y^{\,2}}{I_y K_z^{\,2}} + \frac{GJ(K_y L)^2}{\pi^2 E I_y}\right]}\right\} \qquad (1\text{-}10)$$

in which, the monosymmetry constant, β_x, is given by

$$\beta_x = \frac{1}{I_x}\int_A y(x^2 + y^2)dA - 2y_0 \qquad (1\text{-}11)$$

and K_y and K_z are boundary condition for Y-axis rotation and Z-axis rotation (warping), respectively.

For a wide flange beam, β_x can be approximated according to equation (1-12).

$$\beta_x = \frac{1}{I_x}\left[(h-y)\left[I_{yb} + A_b(h-y)^2\right] - y\left(I_{yf} + A_f y^2\right) + \frac{t_w}{4}\left[\left(h-y-\frac{t_b}{2}\right)^4 - \left(y-\frac{t_f}{2}\right)^4\right]\right] - 2y_0 \qquad (1\text{-}12)$$

The application of these equations to the geometry of the duct stiffener is, however, impractical. The plate that is welded to the beam alters its geometry by lowering its neutral axis, and creates a singly-symmetric section. However, the plate itself cannot be considered as part of the beam when deriving flexural buckling formulae because the plate is completely restrained around its perimeter and is not permitted to deflect in the manner assumed in the derivation of these equations. The plate portion of the composite section does not buckle. Both the lateral displacement and axial rotation are prevented. I_y, which is the weak axis moment of inertia of the entire built up section (plate and beam), essentially becomes very large when considering the length of the plate between stiffeners.

The plate acts to externally restrain the movements of the beam, while also modifying its geometric properties. The geometric properties can be determined by including the plate, but the buckling limit cannot be determined. The buckling limit of a beam or column is primarily a factor of the properties of the compressed side of the member. In the case of the duct stiffener under negative pressure, the casing is in tension. Therefore, a simplification could be achieved by ignoring the tension portion of the assembly and only considering the compressive area. This is the approach taken by AISC ASD steel manual[2] in the equations for allowable bending stress, F_{b1}, F_{b2}, and F_{b3}. The terms in these equations, A_f, r_t etc. only take the compression section of the beam into account.

The depth of the beam in compression is increased with the addition of the casing to the bottom flange. The neutral axis is lowered by a certain amount. Current analysis methods determine the strong axis stiffness of the beam by including the '42t' casing width in the moment of inertia calculation. This is a relatively small section of the plate and its effect on the location of the neutral axis is believed to be minimal.

1.3.4 Warping

In addition to providing lateral and torsional restraint to the beam, and increasing its strength by modifying the geometrical properties, the casing also provides some restraint against warping – also referred to as 'non-uniform torsion'. Warping is the longitudinal displacement of the legs of the member when it undergoes torsion. Since displacement of each leg is different, the cross section of the member does not remain planar. Should this displacement be unrestrained, the torsion is called 'uniform torsion' or 'St. Venant torsion'.

Without restraint, the displacements throughout the length of the member are the same, or uniform. Non-uniform torsion occurs when part of the member is restrained from moving longitudinally. The restraint is generally accomplished by holding the entire cross section of the member in plane at a point along its length. At this point of restraint, additional shearing stresses are present and the torsional stiffness increases. A simply supported beam that experiences lateral torsional buckling will twist about its longitudinal axis. However, since both ends of the beam are held from rotation, the centre of the beam (which is the point of symmetry of the buckled shape) acts as the point of longitudinal restraint. Both ends of the beam try to twist in the same direction resulting in the symmetry point at the centre. This beam will experience both uniform and non-uniform torsion. The classical buckling equation shown in equation (1-1) includes terms for both uniform torsion given by the St. Venant torsional constant 'J', and non-uniform torsion given by the warping constant, 'C_w'.

The method for the derivation of the warping constant C_w is given in Bleich,[5]. The derivation of the overall torsional resistance of a beam is given in several books, including Gaylord et. al.[11]. The derivation of the warping constant is dependant on the location of the shear centre, or centre of twist. For a doubly symmetric wide flange section, the shear centre is coincident with the centroid. Other sections such as channels do not have the shear centre and centroid at coincident points. When a wide flange section undergoes torsional warping, the longitudinal displacement of any point on the cross section is a function of its distance from the shear centre. The four flange tips tend to deflect the most since they are furthest from the shear centre. The direction of warping deflection depends on the relative location of the shear centre, and therefore each flange will deflect in equal and opposite directions.

Warping restraint involves holding all points of one cross section in plane. Studies have been performed to determine the additional capacity given to a beam when warping restraints are installed. The warping restraint in the duct stiffener model does not fit this classical model. In the arrangement of the stiffener welded to the duct casing, the bottom flange is held from longitudinal displacement along its entire length, rather than at one point such as the midspan of the beam. Furthermore, the entire cross section is not held, only the one flange. The web and the top flange are still able to deflect longitudinally. The full area of the cross section of the member does not have the same boundary conditions. Thus, the equations used in the derivation of the warping constants are no longer valid.

1.4 Stiffener Design Guidelines and Code Review

The review presented in the previous section addressed four points that affect the capacity of a beam stiffener from a solid mechanics point of view; namely tension flange bracing, load height, singly symmetric sections, and warping. This section presents a complimentary review of published guidelines and codes for the design of industrial ductwork.

1.4.1 Stiffener Design according to the Air and Gas Duct Structural Design Committee

The Air and Gas Duct Structural Design Committee is part of the Energy Division of the American Society of Civil Engineers.[1] The committee has created a special publication that "has been created by a select committee of structural and mechanical engineers who are extremely experienced in the structural analysis and design of air and flue-gas ductwork for power stations and large industrial boiler applications." The committee represented a working group of 19 individuals in the ductwork industry, including owners, consulting engineers, equipment suppliers and duct suppliers.

This document discusses all aspects of duct design including overall duct layout, material selections, flow distribution devices, insulation and lagging. Section 6.2.1 discusses the design of plate sections of rectangular ducts. The authors suggest that stress analysis of the plate be performed using a strip analogy, where plate "strips" are checked for bending between stiffeners using conventional beam theory. Additional calculations need to be performed in areas close to the stiffener where orthogonal stresses develop.

In Section 6.2.2, the authors note that for typical plate thickness between 5mm and 10mm, the stiffener spacing will usually vary from 0.6m to 1.2m. The spacing may be increased to 1.5m in areas of low stress. Ultimately, stiffener spacing is dependant on loading, material, temperature, method of analysis, and the contribution of stress from the duct global analysis. In addition, the stiffener spacing may be defined by practical panel sizes for the purpose of shipping or construction.

Section 6.2.3 introduces the concept of large deflection theory, where the plate is allowed to develop membrane tension stresses in addition to bending stresses. The authors suggest that an increase in stiffener spacing of up to 20% can be obtained by considering membrane action. This method is commonly used in practice, although some designers may not take large deflection theory into account.

The concept of composite action between the plate and the stiffener is considered in the discussion. The rational behind how much plate contributed to the composite section is noted as "somewhat arbitrary". A variety of different suggestions from various publications are presented, but there is no further

analysis or justification for one method or another. Section 6.3 provides some insight:

> The effective plate width as part of a composite stiffener is specified as a function of plate thickness so that local buckling is limited when the composite area is in compression.[1]

The design of stiffener elements themselves is presented in section 8.2. There are no specific methods or equations mentioned and it is left to the designer to utilize whatever method he/she deems appropriate. The discussion of stiffener sizing is as follows:

> For each loading and direction combination, the structural engineer must calculate the maximum bending stress in the plate and in the stiffener.[1]

Also,

> To design the stiffener correctly, the structural engineer must calculate the stresses at the top of the section and at the bottom, taking into account the axial force and bending moments. Lateral bracing points for the outstanding flange, such as at web/flange stiffener plates or where adjoining stiffener elements frame into the stiffener, must also be considered.[1]

Also,

> The allowable stress for the outstanding flange must be determined taking into account its instability under compression at its design temperature.[1]

To establish the limits of allowable stress, the reader is directed to section 5.2, which recommends the design method of the American Institute of Steel Construction – Allowable Stress Design.[2]

In summary, based on the discussion of stiffener sizing, it is recommended to use a portion of the plate for determining the applied stresses on the beam. The width of plate to be used is arbitrary, and justified only by protecting the plate from local buckling when in compression. The applied stresses are then compared to allowable stresses, which are established by conventional methods that do not take the plate into consideration. The overall design according to the Air and Gas Duct Structural Design Committee is shown by this study to be substantially conservative.

1.4.2 Stiffener Design according to Blodgett

The steel design manual titled "Design of Welded Structures" by Omer Blodgett[6] has been a standard guide for a variety of welded structures for some time. The manual contains a section on panel stiffening. The method suggested by Blodgett is to take a section of the casing panel equal to half the width between the stiffeners, and determine the combined moment of inertia with the added stiffener. Given this moment of inertia, the loading capacity is determined by the standard allowable stress design according to

$$\sigma = \frac{Mc}{I} \tag{1-15}$$

where M is the applied moment depending on the load distribution, c the distance from the composite section neutral axis to the outer fibre of either the panel or the stiffener, and I the moment of inertia of the composite section. If there is a question about the distance between stiffeners being too great, the author refers to an earlier section regarding the compression of plate panels. This section provides formulae similar to the compression of stiffened elements formula in the AISC-ASD[2]. This method does not take into account the limits of lateral torsional buckling. Only the elastic stress is considered.

1.4.3 Code Review

AISC-Allowable Stress Design

The most common structural steel code that is used for the design of stiffener beams is the AISC Manual of Steel Construction, Allowable Stress Design, 9th edition.[2] Due to the large number of power stations and large industrial facilities in the United States, much of the standard design methods have come from American companies. There are no clauses in this code that are applicable directly to the construction of industrial ducting. Therefore, the standard flexural formulas for beam design are used with some of the parameters modified to account for the composite cross section. A design example using this method is presented in Appendix A.

When the duct is subjected to positive pressure, the flange connected to the casing is in compression. A certain width of casing away from the beam flange is therefore also in compression. The AISC-ASD code stipulates limiting width-thickness ratios for compression elements to prevent local buckling. Since the attached casing is considered a thin element in compression, the maximum width of the casing to remain within the allowable limits is determined.

Table B5.1 in the AISC Manual lists a variety of possible geometries for compression elements and provides limits that are a function of the material yield strength. The line in the table commonly used is "All other uniformly compressed stiffened elements, ie., supported along two edges." The limit is given by[2].

$$\frac{b}{t} < \frac{253}{\sqrt{F_y}} \tag{15}$$

where F_y is the material nominal yield strength. Substituting in 36 ksi (the imperial equivalent of 248 MPa, the yield strength for A36, the most common carbon steel plate material used for this application in the U.S.), the limit is b/t < 42.2. This has formed the basis for the standard '42t' used in the design of the stiffener beam and casing composite section. It is noted that for higher yield strength materials, the factor is reduced. However, this reduction is generally not considered despite the stronger materials that are now available.

There are no explicit rules in this code for bracing of either columns or beams, except to note that certain shapes "may require consideration of flexural-torsional and torsional buckling." In section E3, the accepted 'rule of thumb' however is to provide bracing to prevent lateral displacement of the compression flange that will resist 2% of the compressive load in that flange. There is no reference to either displacement or rotational stiffness requirements of the brace. This code also does not address lateral buckling of singly symmetric I-shaped sections or beams with warping restraints.

AISC-LRFD

The American Institute of Steel Construction developed a limit states structural steel code titled Load and Resistance Factor Design[3]. This version of the code provides more explicit rules for bracing. Rather than simply a requirement for the strength of a brace, the stiffness is also required. Both lateral and torsional bracing are addressed. The requirements for the stiffness of a torsional brace were developed from the work of Helwig and Yura and include the formulae presented in section 1.3.1 of this thesis.

Singly symmetric sections are not addressed in the main body of the code. However, Appendix F1 provides an alternative method for singly symmetric sections. The critical moment for buckling is modified to include factors reflecting the geometry of the singly symmetric shape.

CISC – Handbook of Steel Construction

The 8th edition of the Canadian Institute of Steel Construction (CISC) steel handbook[9] incorporates the Canadian Standards Association requirements for structural design[8]. This standard has modified its approach to beam bracing from previous versions by accommodating alternative methods. The first method is identified in clause 9.2.5 Simplified Analysis. In this clause, the brace may be designed to simply have strength of at least 2% of the compressive force in the member. Also, the axial deformation of the brace at this load cannot be greater than the initial deformation of the beam. The second alternative in clause 9.2.6.1 Second Order Method is to perform a second order elastic analysis of the member and its bracing system. A specific method and formulae are not referenced. The commentary provides some explanation of the process but there are no specifics

about the location of the bracing on the beam or torsional resistance. The third alternative in clause 9.2.6.2 Direct Method is a simplified form of the second-order analysis. It states that the brace member must have a factored resistance in the direction of buckling given by

$$P_b = \frac{\beta(\Delta_0 + \Delta_b)C_f}{L} \tag{16}$$

where P_b is the force used to design the bracing system, β a factor depending on the number of equally spaced braces, Δ_0 the initial misalignment, Δ_b the displacement of the bracing system, assumed to be equal to Δ_0 for the initial calculation of P_b, C_f the maximum factored compression in the segments bound by the brace points on either side of the brace point under consideration, and L the length between braces.

Clause 9.2.3 identifies the purpose of bracing and states that the brace system shall provide lateral restraint at the compression flange. There is no reference to torsional bracing or continuous bracing, other than in Clause 9.2.4 that requires twisting be prevented at support locations. These bracing methods are only applicable to building systems, and not for beams with unusual boundary conditions.

1.5 Objective and Scope

Currently there is no governing code for the structural analysis of industrial ducts, particularly for the design of stiffeners[1]. The methods used in the design vary among engineers. Publications have been produced in an attempt to standardize the design, including references 6 and 1.

The current study was undertaken to investigate the adequacy of current stiffener design practices. It is postulated that the current methods do not properly account for three important conditions:

1. Unbraced Length
   The unbraced length of the compression flange is critical to the sizing of the beam. Current design philosophy considers the outstanding compression flange to be braced at the ends (through the connections to the adjacent stiffeners) and at any mid span locations where there are a set of gusset plates. The ability of the web itself to provide lateral bracing is ignored. Gusset plates are substantially more effective than the web at resisting lateral overturning. However, the web does have a significant amount of strength that may be sufficient to brace the flange from lateral motion. For a stiffener resisting negative pressure, the tension flange is held both rotationally and laterally through its rigid attachment to the casing.

2. Composite Section Properties
   The geometrical properties of the stiffener beam change with the addition of the casing welded to the bottom flange. The combined plate-beam section is more stable than a single beam. Current design methods take a certain portion of the plate that is attached to the flange and determine the new properties based on the new section formed by the beam and portion of plate. The amount of plate width generally considered in this composite section is a multiple of the plate thickness and varies between designers. A common value used is '42t', or 42 times the thickness of the plate. The moment of inertia and section modulus are calculated based on this modified section. The beam properties are only briefly accounted for by the consideration of the "42t" effective plate width. However, the buckling formulae used to determine the allowable stress do not consider the modified section.

3. Load Height
   The location of where the load is applied to the beam in terms of the vertical height above or below the beam's neutral axis has a notable affect on the beam's capacity to resist lateral buckling. If the load is applied to the top flange, then as the beam begins to twist in the early stages of buckling, the load acts to provide an added torsion to the beam since it is no longer over the shear center. Likewise, if the load is applied to the bottom flange, it acts to provide a restoring torque that acts against the twisting deformation. This positive or negative torque is not considered in the standard beam flexure formulae. In the geometry of the stiffener and casing, the load is applied to the bottom flange and acts to resist the overturning twist.

These three conditions are investigated and their relative contribution to the capacity of a beam is determined. The working hypothesis is: if the previously mentioned conditions were to be considered, the beam size used for a duct stiffener may be substantially reduced, without the added labour and material costs associated with providing gusset plates.

Engineers that design ducts and stiffeners have noted that the method used is reliable and cite that they are not aware of any failures (aside from catastrophic failures from unforeseeable loads such as explosions etc.) Failures in ducts are usually associated with cracks in the casing at the corners. These cracks are usually the result of acoustic vibration from upstream fans. Reinforcement of the corners or the placement of extra stiffeners reduces the stress in these areas. Stiffener undersize is rarely, if ever, an issue.

Citing a lack of failures to show the reliability of the design method underscores the inherent amount of conservatism. This study will seek to identify the amount of conservatism and offers an effective approach to the design calculations.

1.6 Thesis Outline

This thesis presents the design and results of the experimental program carried out to evaluate the structural behavior of a typical wide flange duct stiffener. The design, construction, and instrumentation of the experimental program are described in Chapter 2. Experimental data are analyzed to determine the elastic response of the box, and to establish the mechanism of failure, namely yielding versus buckling.

Chapter 3 describes a finite element model used to simulate the experimental apparatus. Elastic and buckling results of the model are presented. Comparative analyses between the finite element results and the experimental data are discussed including the location of the neutral axis and the resulting strains on both the top flange and the plate in the vicinity of the beam.

Chapter 4 extends the use of the finite element model by examining the elastic and buckling response of a variety of different beam sections. Several different wide flange sections are analyzed. For each section, two models are considered; the first incorporating the casing plate, whereas the second models the beam without the plate. The capacity of the beams with and without the casing is compared and discussed. Chapter 5 presents the conclusions and recommendations for future research.

CHAPTER 2 EXPERIMENTAL PROGRAM

2.1 Introduction

An experimental program was developed to test the capacity of a stiffener on a duct. Several concepts for the testing apparatus were considered to attempt to simulate the load and boundary conditions of a stiffener beam. The challenge of the design was to be able to generate a controlled negative pressure inside the duct. The concept that was decided upon was a shallow box with a removable top that would hold the stiffener beam that is welded to the plate. The box was to be made reasonably air tight, and a vacuum pressure drawn by way of a vacuum pump. This arrangement simulated a single top section of duct plate with one stiffener. The edges of the box running parallel to the stiffener simulated the next stiffener on either side of the one being tested. The sides of the box at the ends of the beam were the adjacent walls of the duct. Figure 8 illustrates a single section of a duct top plate. The experimental apparatus simulated the stiffener at the center of this section and the plate on either side.

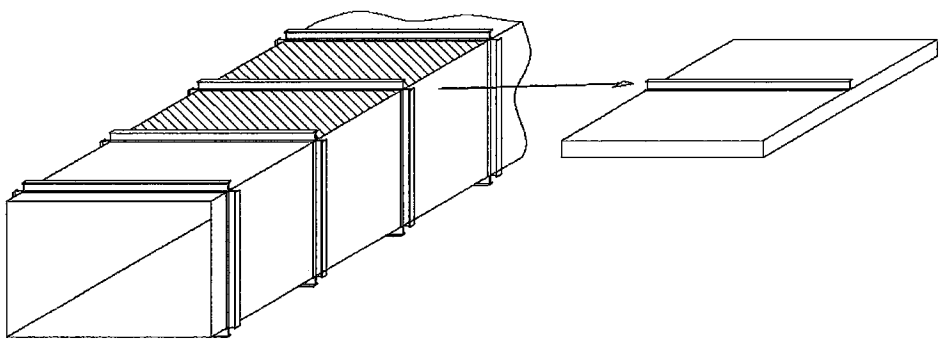

Figure 8: Single section of duct between stiffeners

2.2 Box Geometry and Construction

The box was 4572mm x 2438mm in plan area, and 152mm deep. A 76x76 angle frame around the perimeter of the box acted as a flange for the removable top plate to bolt onto. After each test, the top plate and beam were removed and replaced with a new specimen. ¾" bolts held the plate to the angle frame around the perimeter on 305mm spacing. A rubber gasket and silicone caulking were used to provide the near air tight seal between the top plate and the box. Some leakage occurred during the tests, but the volume capacity of the pump was substantially greater than the leakage at pressures greater than the pressure required to complete the tests.

The removable top plate was a 4.76mm (3/16") thick ASTM 44W steel plate (carbon steel with 300MPa nominal yield strength). The test beams were W310x21 (W12x14) and W200x27 (W8x18)[2] wide flange sections of A992 material (carbon steel with 345MPa nominal yield strength). These sections were chosen based on the required section modulus as calculated in the design example in Appendix A. Both sections have similar section moduli, but different moment's of inertia. As a result, different failure modes for each section were expected. The beams were attached to the plate with 76mm staggered fillet welds on 305mm spacing using E70xxx electrodes on each side of the bottom flange.

The bottom of the box was held stiff using 102x102 angle stiffeners that ran width-wise across the outside of the box. The angles were attached to the box using 76mm fillet welds on a staggered stitch pattern. Due to unbalanced forces, it was found that the box distorted without any significant flexure of the test beam. The beam was stiffer than the box itself, despite the installation of angle stiffeners to the bottom of the box. To restrain the box from distortion, very large wide flange beams were welded to the angle members on the underside of the box. This extra reinforcement ensured that the beam stiffener was the critical element of the test rather than the box to which it was attached.

The size of the beam stiffeners and the size of the box were determined using standard design methods. These calculations are provided in Appendix A.

The negative pressure in the box was drawn using a vacuum pump. The pump was a positive displacement pump capable of reaching near 0 kPa(a). It was attached to the box through standard ABS 1½"[3] pipe and fittings. A ¼ turn manual ball valve placed on the inlet nozzle to the box was used to throttle the air flow out of the box in order to provide controlled rate of pressure drop. A second smaller valve was used adjacent to the control valve to act as an air release point at the end of the test. Figure 9 and Figure 10 illustrate the construction of the box. Figure 11 shows the experimental set up.

The experiment consisted of three tests using a W8x18 beam and three using a W12x14 beam. Not all of the tests used the same strain gauge pattern. Appendix B illustrates the arrangement of gauges for each test.

[2] The imperial designations W12x14 and W8x18 are used throughout this thesis in lieu of the metric equivalents. The beams used in the tests were ordered and supplied according to the imperial size, not the metric size.

[3] 1½" NPS (nominal pipe size)

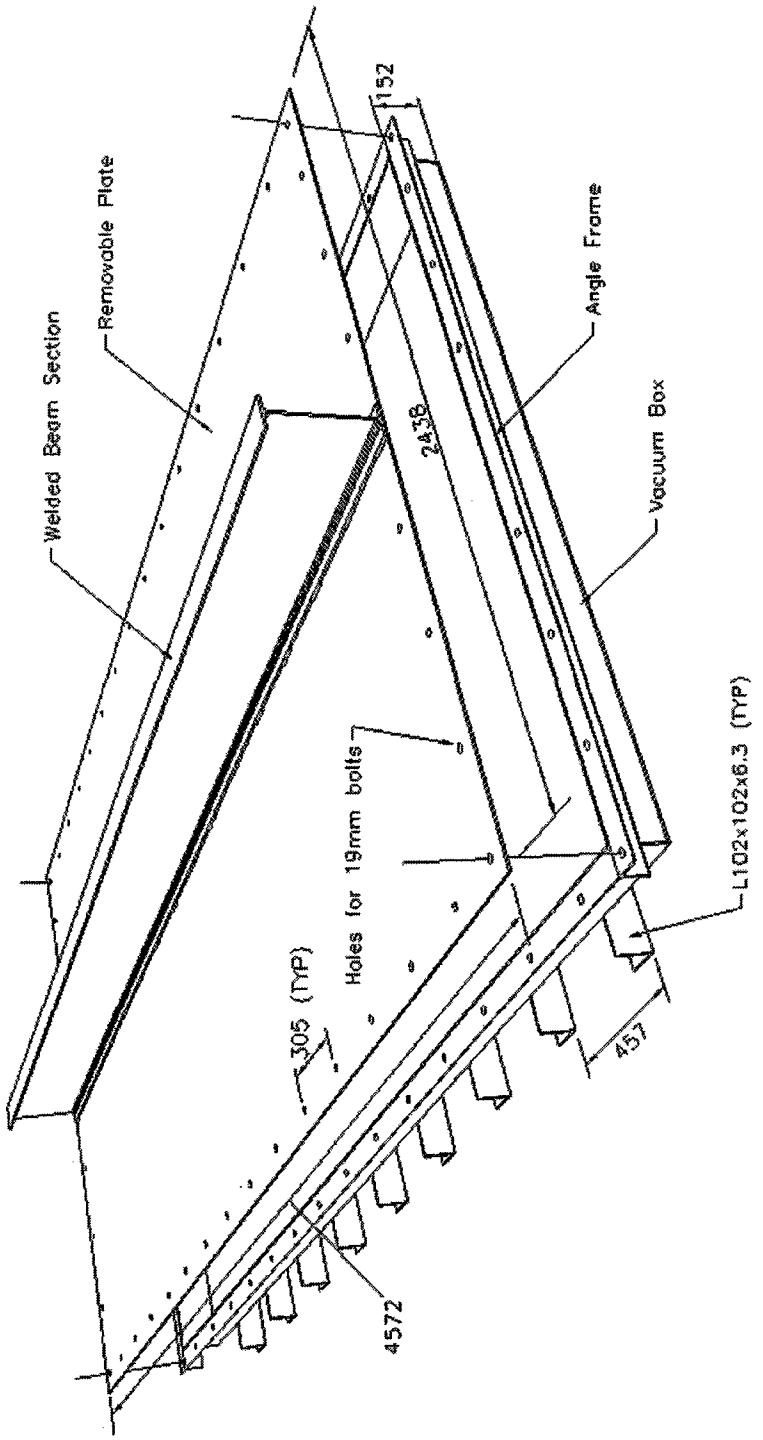

Figure 9: Removable Top Plate Test Specimen

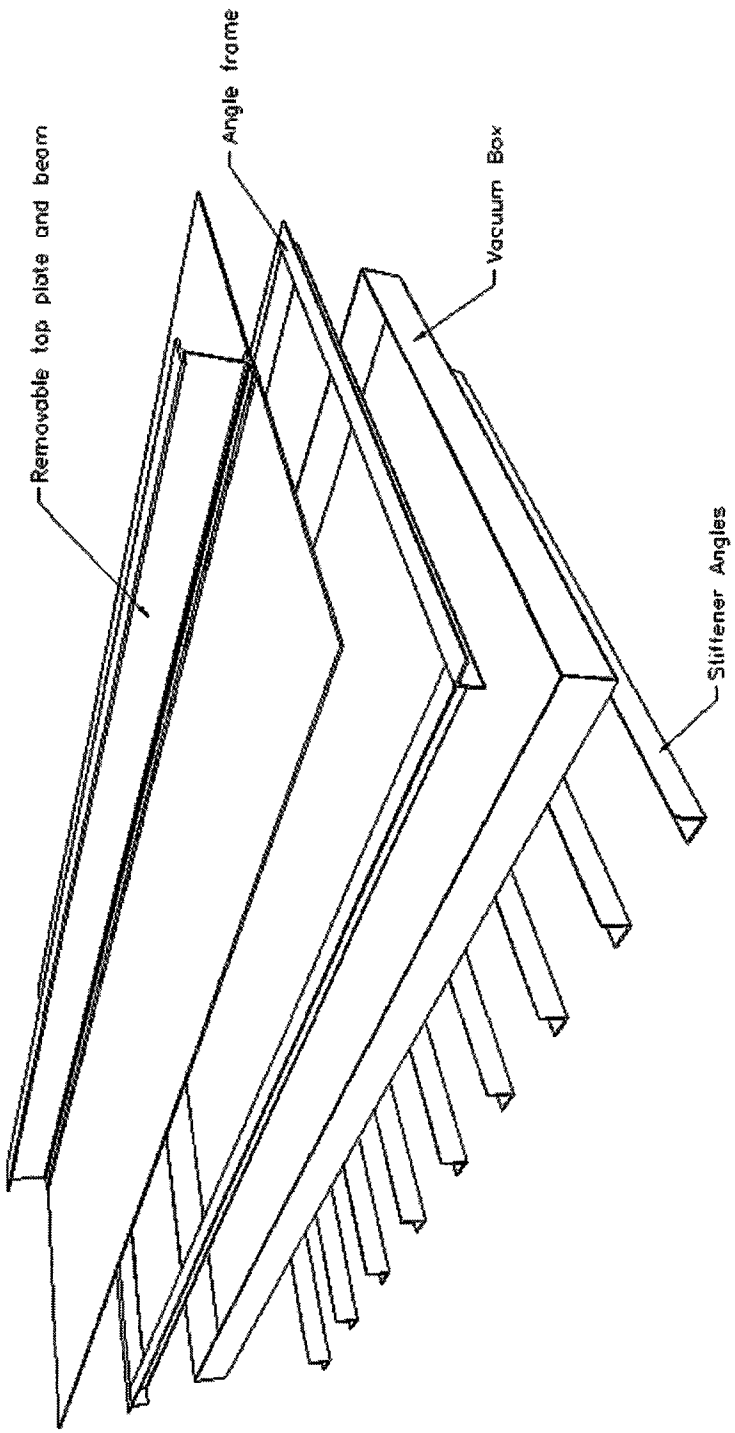

Figure 10: Exploded View of Test Assembly

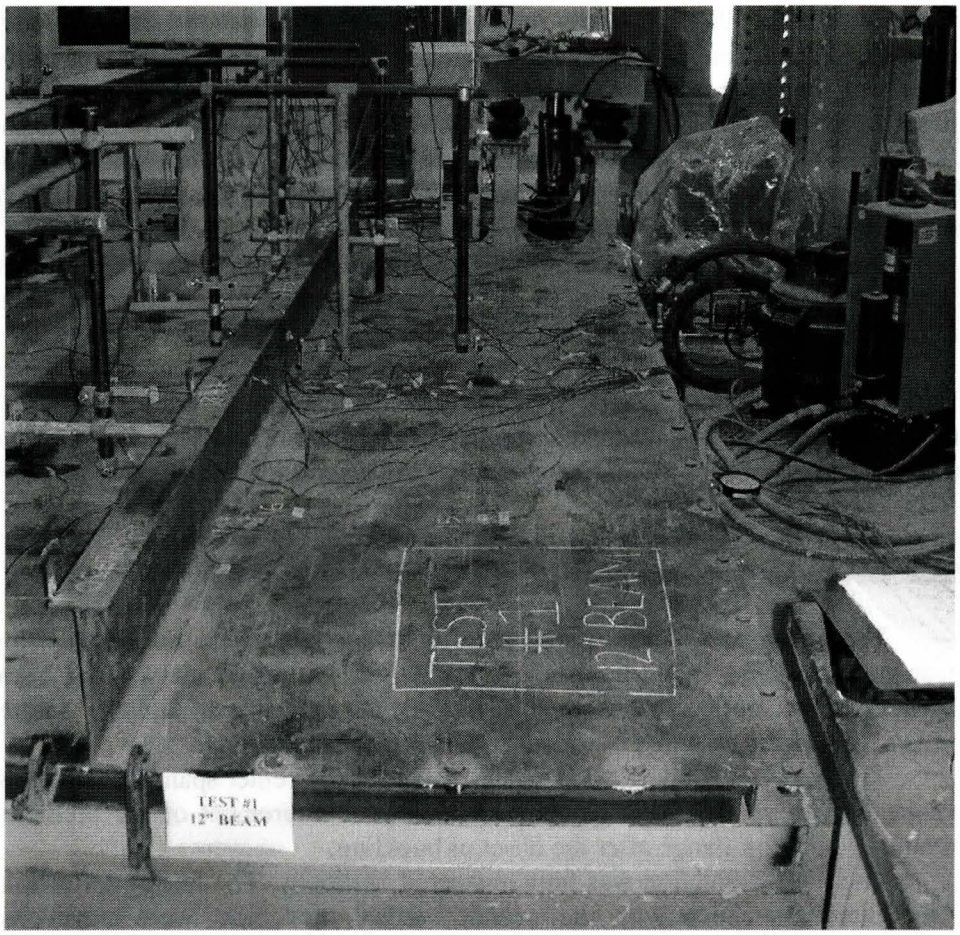

Figure 11: Experimental Apparatus

2.3 Instrumentation

The testing program was designed to determine the capacity of a stiffener on a duct. In order to monitor the response of the apparatus to the applied load, strain gauges and linear voltage displacement transducers (LVDT) were attached to locations that were deemed to be of interest. This section describes the measurement of strain, displacements, and the applied pressure.

2.3.1 Strain Measurement

Strains and deflections of the box and the top beam were monitored during and immediately after the test to track the performance of the apparatus. Strains were measured on the beam and the plate in a variety of locations that were felt to be of interest in this investigation including the midspan area of the beam. Since

this is the point of highest stress in a simply supported bending model, strain gauges were placed on the top flange, the web, the bottom flange in the area of the welds, and the plate both in front of the welds and in between them. Strain gauges were also placed on the top plate in a row close to the bottom flange at the mid-span of the beam. These were used to help determine the contribution of the plate in the composite plate-beam section. The locations of the gauges for each of the six tests are shown in Appendix B.

The plate strains in the lateral (Z) direction were measured at six locations; at the ¼ span, the mid-span, and the ¾ span on both sides of the box. All other strain gauges monitored the strain in the longitudinal (X) direction.

In order to experimentally locate the neutral axis of the composite beam and plate section, strain gauges were placed on the web at various heights as shown in Appendix B. From the strains obtained along the web and the two flanges at the beam centerline, the location of the neutral axis could be reasonably interpolated or extrapolated.

2.3.2 Deflection Measurement

The deflection of the casing plate and the beam were measured using linear voltage displacement transducers (LVDT) at several locations. The beam stiffener vertical deflections were measured at the center span and the quarter points to record the response of the beam under pressure loading.

The beam lateral deflection was measured at the center span, the two ends, and the quarter spans. This pattern enabled the measurement of the predicted curvature of the top flange after the onset of buckling.

The plate deflection was only measured vertically. The lateral deflections of the plate associated with the overall vertical movement were considered negligible.

To support the LVDT's in place over the box, a beam was installed over the box that was supported by two concrete piers. A grid was then constructed using various lengths of pipe and welded to the beam. The LVDT's were attached to the pipe grid and positioned to measure the desired movement. The locations of the vertical and horizontal LVDT's are illustrated in Appendix C.

Figure 12 shows a typical LVDT installation. The photo shows the small plates that were welded to the top flange of the beam at the point of contact with the LVDT. These plates were installed since the actual contact surface of the flange itself was too small, and the LVDT could separate from the flange with the smallest movement. Even with this precaution, many of the LVDTs slipped off of the plate surface after the beam went through large displacements. Figure 12 also shows a short pipe section that was installed beneath the LVDT. This section was used as a bumper to protect the device after the beam moved the full displacement range of the LVDT. Unfortunately, the bumper was often not sufficient to protect the device and several LVDT's were damaged during the final collapse of the beam.

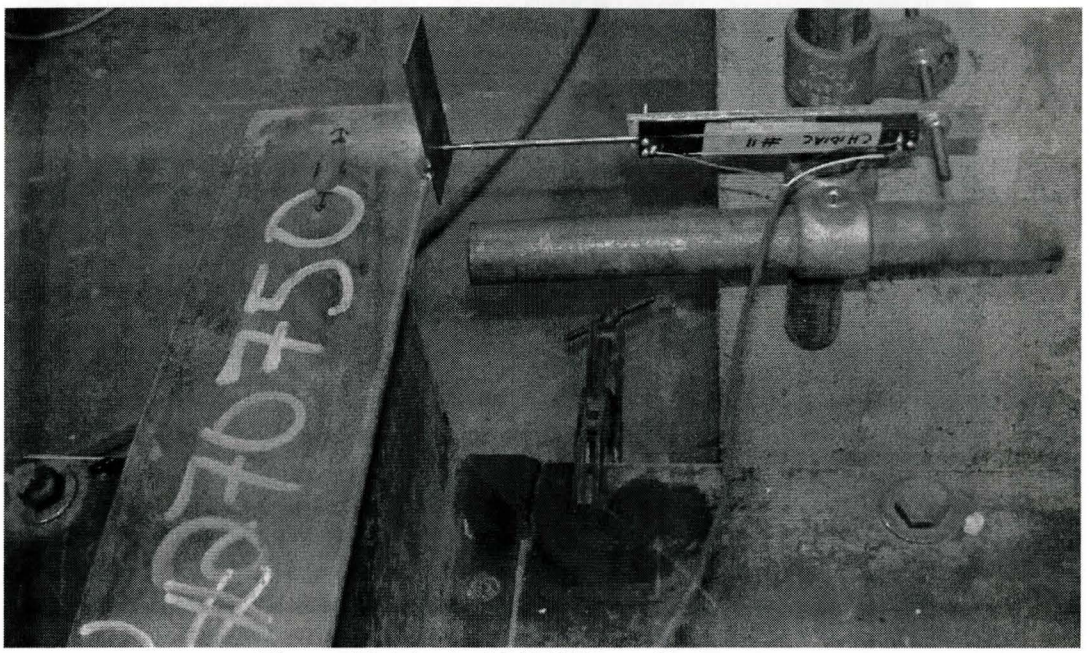

Figure 12: Typical LVDT Installation

2.3.3 Pressure Measurement

Both the deflections and strains of the test box were measured continuously against the vacuum pressure inside the box. Pressure in the box was measured with two gauges; one gauge being an electronic transducer connected to the data acquisition system and the other a standard analog dial gauge used for visual confirmation and continuous visual calibration of the data being retrieved. Calibration data of the pressure transducer is provided in Table 24 of Appendix C.

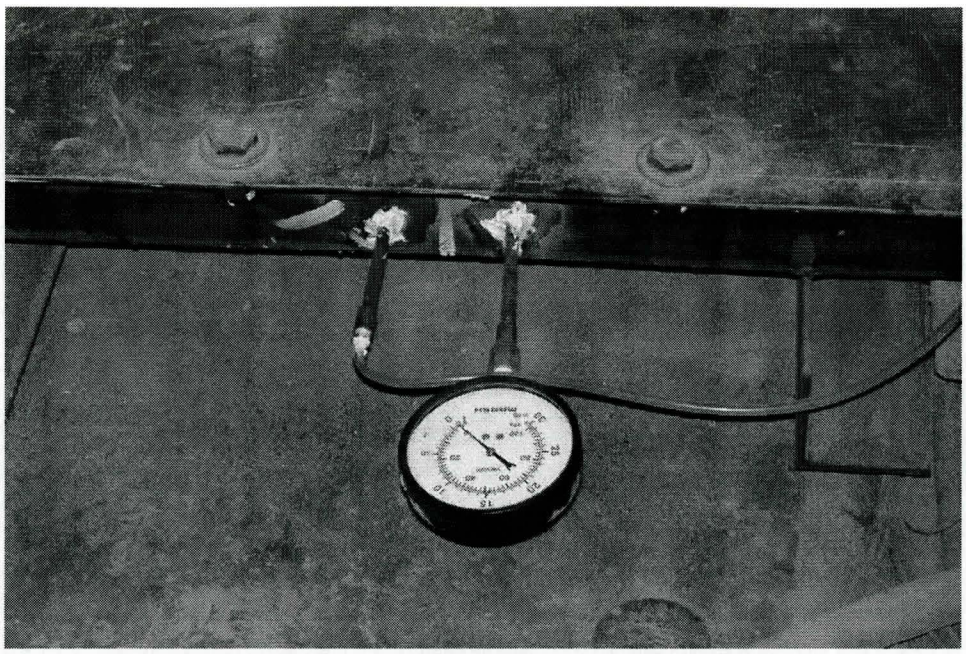

Figure 13: Pressure Transducer and Dial Gauge

2.4 Experimental Results

The discussion in this section focuses on the deflection and strain measurements; in particular the beam's vertical deflection which was measured to compare with finite element predictions, the lateral deflection of the beam measured to determine the elastic response, the onset of buckling and post buckling movement as well as the strain on the top flange measured to determine the onset of yield versus the onset of buckling. Strain measurements on the web were used to determine the location of the neutral axis and subsequent contribution of the plate to the stiffness of the beam. The plate strains were measured in the central area and were used to validate the finite element model, and near the beam flange to further discuss the contribution of the plate to the beam stiffness.

2.4.1 Beam Vertical Deflection

As the vacuum pressure was increased in the box, the stiffener beam began to deflect downwards in response to the downward load. The applied load due to the pressure was approximately uniform across the length of the beam.

Figure 14 shows the vertical deflection of the beam at the midspan against pressure. Table 2 shows the mean, standard deviation, and coefficient of variance corresponding to 20 kPa. This pressure was chosen as the test apparatus is in a state of elastic response and at approximately 50% of the final collapse load.

Comparisons of the measurements to the finite element predictions, presented in the following chapter, correspond to this reference pressure.

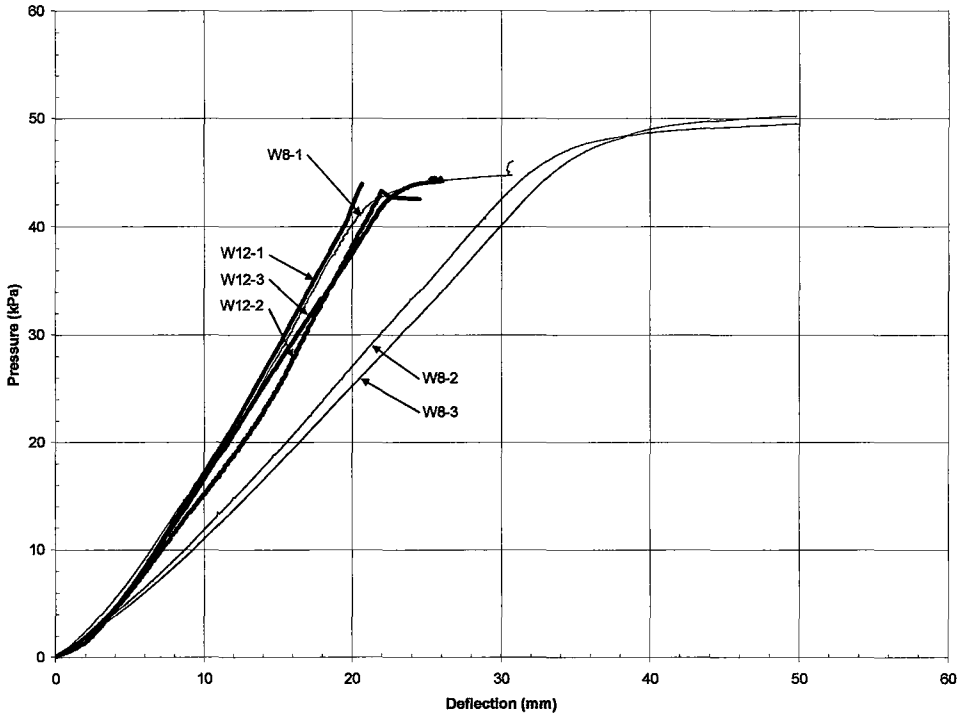

Figure 14: Vertical Deflection at Midspan

Table 2: Vertical deflections at 20 kPa

Test	Deflection (mm)	Test	Deflection (mm)
W12-1	11.3	W8-1	11.41
W12-2	12.61	W8-2	15.53
W12-3	11.59	W8-3	16.38
Mean	11.83		14.44
SD	0.69		2.66
COV	5.8		18.4

Referring to Figure 14, all curves show an adjustment period at the beginning of the test up to approximately 5 to 8 kPa where the deflection is no longer linear with pressure. After the initial adjustment, the relation between pressure and displacement is approximately linear. The response of the two beam sections to pressure show marked differences:

1. The deflection of the W12 beams increased linearly until their final sudden collapse at a mean of 43.59 kPa (σ=0.96 kPa). The curves did not loose their linearity before the beam collapsed.
2. The deflection of the W8 beams also increased approximately linearly through the pressure range of 10 to 45 kPa, but they did not experience the same sudden collapse as the W12's. Instead the failure was of a more ductile nature. The W8 beams began to yield at the top flange with the resistance of the section reaching the plastic limit as reflected by the horizontal slope. At this point, the beam bottomed out in the box and the test was terminated.
3. The W12 sections are stiffer than the W8 sections as they have a higher moment of inertia which is reflected in the slope of the deflection curves. Between 20 kPa and 25 kPa the stiffness of the deflection response of the W12 sections was 2.25 kPa/mm (σ=0.099), and 1.74 kPa/mm (σ=0.383) for the W8 sections.

It should be noted that the curve denoted by 'W8-1' was the first test of the W8 beam size, and as one may observe, its response did not follow the same path as the other two W8 tests. The higher slope indicates a stiffer linear response, and the point of yield appears at a lower pressure (~41 kPa). Each of the W8 tests reached a vertical deflection limit when the top and bottom casing came together inside the box. This discrepancy could not be explained.

2.4.2 Lateral Deflection

Figure 15 summarizes the lateral deflection at the beam midspan of the six test specimens versus pressure. Figure 16 is the same data as Figure 15, but using a different deflection scale to amplify the curvature during the elastic portions of the data. Table 3 lists the deflections of each test at 20 kPa.

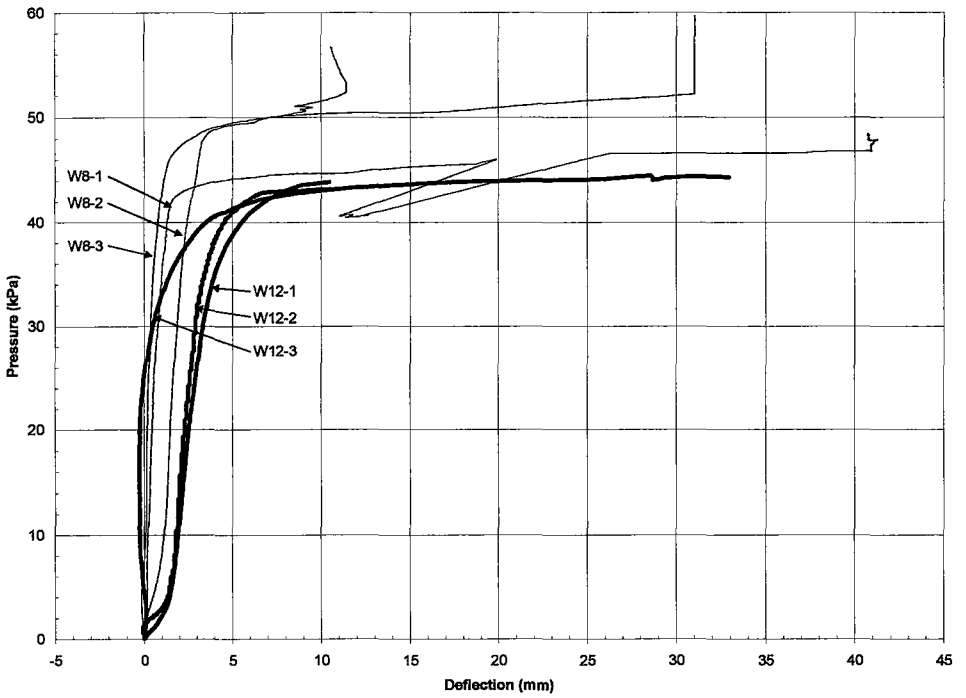

Figure 15: Lateral Deflections at Midspan (1)

Table 3: Lateral deflection at 20 kPa

Test	Deflection (mm)	Test	Deflection (mm)
W12-1	2.52	W8-1	0.444
W12-2	2.3	W8-2	1.468
W12-3	-0.26	W8-3	0.168
Mean	1.52		0.69
SD	1.55		0.685
COV	102		99

The curves denoted by 'W12-1' and 'W12-2' are similar. During an initial adjustment period within the first 3 to 4 kPa, the beam shifted to the side approximately 1.5 mm. The curves then level out to produce a relatively linear response with increasing vacuum pressure. After the pressure reached a level of 30 to 32 kPa, the slope of the lines decreased steadily, eventually becoming nearly horizontal at the final collapse point. Final collapse occurred at about 11 mm of lateral deflection.

Table 3 shows that the spread of the data for the beam tests was quite large, with a coefficient of variance of 102 for the W12 beams and 99 for the W8's. It is noted, however, that with the exception of the third W12 test (W12-3),

which incorporated the midspan gussets, the deflection of the W8x18 beams was consistently less than for the W12x14's. The W12 beams were more susceptible to the lateral overturning moment because of the smaller flange size, relative to that of the W8 beams, which have higher moments of inertia in the beam's weak axis (I_y W8 > I_y W12)

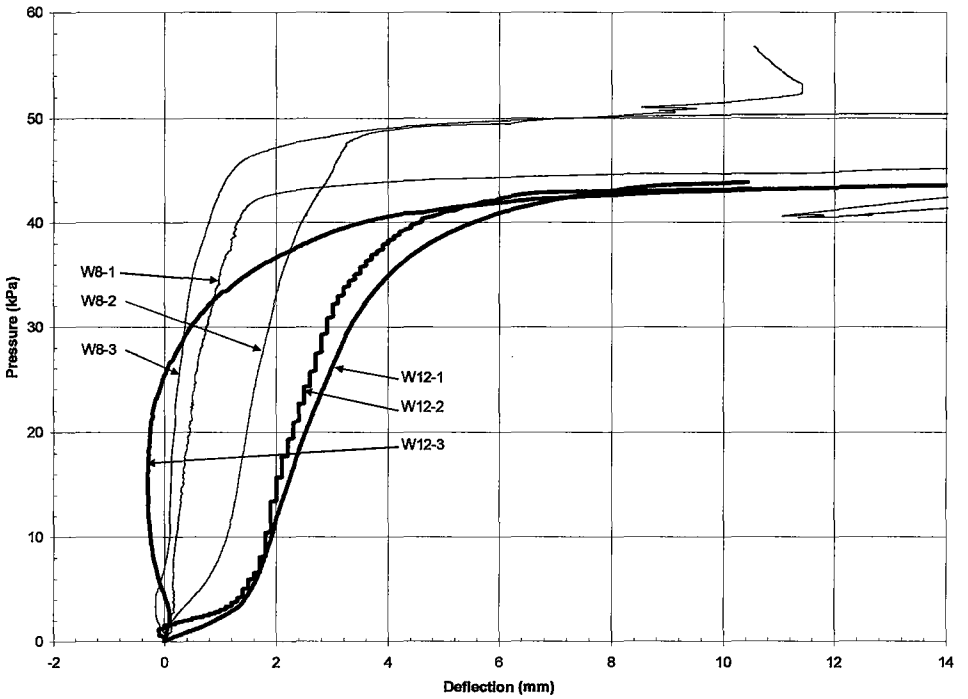

Figure 16: Lateral Deflections at Midspan (2)

The curve denoted by 'W12-3' did not follow the same response as the first two tests, W12-1 and W12-2 due to the gusset plates that were placed at the midspan. The plates were welded to connect the bottom flange to the top flange as would be performed in practice in an attempt to reduce the 'unsupported length' of the beam. The gussets modified the curve during the first 30 kPa of the test, keeping the beam substantially straighter as the pressure increased. However, the weld to the bottom flange was not sufficiently strong and failed during the test as the torsional forces on the beam were ultimately greater than the capacity of the welds. It is noted that this is not a common failure in the field. With the addition of the gussets, this curve did not show the same initial period of settlement. The direction of lateral deflection reversed slightly, in the order of 0.5 mm until 25 kPa. The lateral deflection of the beam was minimal until approximately 30 kPa was reached. The lateral deflection then increased rapidly up to a final collapse point at 32.7 mm and 44.3 kPa vacuum pressure. The final lateral deflection before collapse was greater than the first two tests due to the added lateral strength of the section with the gussets welded to the web. The

failure mode was the same for all three tests. The point of failure of the gusset weld had not been identified during the test.

The W8 test curves were not consistent. Each of the curves showed a period of linearity with the lateral deflection followed by a rapid increase. Furthermore, the pressure at which this increase occurred was different for each test. In the first test 'W8-1', the increase occurred at about 42 kPa. In the second test 'W8-2', the increase occurred at about 48 kPa. In the third test 'W8-3', the increase occurred at about 46 kPa. The maximum deflection measurement of the first test was limited by the LVDT as it reached its full stroke at about 41 mm and 47 kPa. The deflection measurement of the second test was limited by the LVDT as the arm slipped from the small plate attached to the top flange at 31 mm and 52 kPa. The third test reached a maximum deflection of 11 mm at a pressure of 52 kPa before reversing to a reduced deflection point.

The onset of buckling for the W12 beams is identified by noting the departure from the linear response. The curves for W12-1 and W12-2 were the only two which could be used for this determination since the W8 beams did not buckle prior to yielding, and the third W12 test was affected by the gussets. Figure 17 shows these two curves in isolation. A straight line has been superimposed over the curves to illustrate the point of departure from linearity. The W12-1 test departed from a linear response at approximately 30 kPa, with the W12-2 test departing from a linear response at approximately 33 kPa. By definition, these pressures represent the load at the onset of buckling. It should be noted that the beams did not suffer sudden collapse at this point. If the beams were loaded in isolation from the plate, the lateral deflection and torsion would cause the beam to rely increasingly on the weak axis strength to maintain stability. However, the casing provided torsional bracing to the beam and the section maintained substantial post-buckling strength.

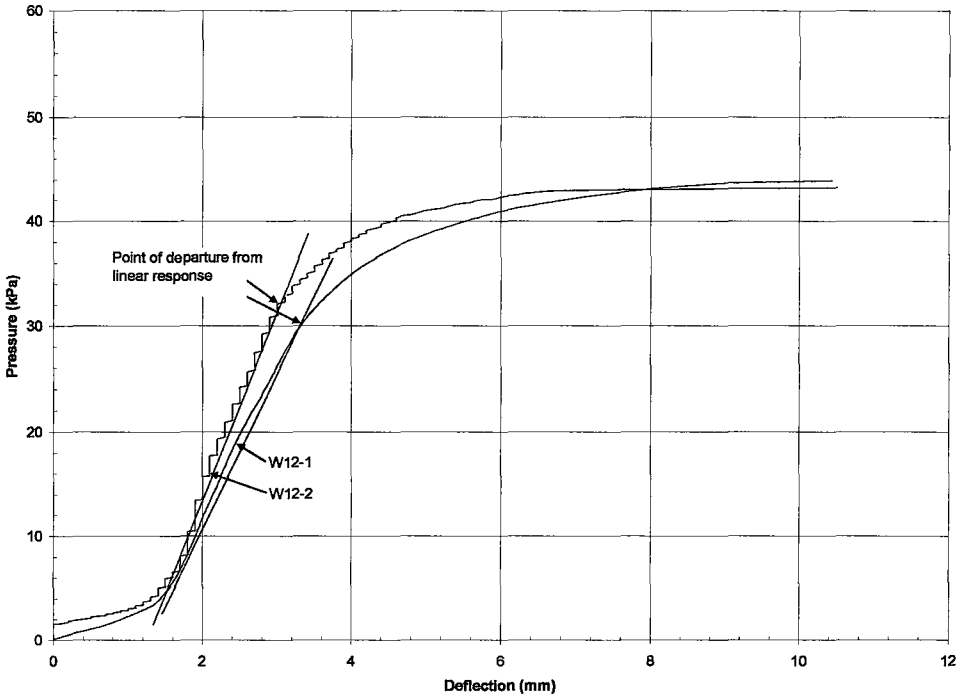

Figure 17: Lateral Deflections at Midspan (3)

2.4.3 Top Flange Strain

The goal of most design practices when sizing a structural member is to ensure that the load or applied stress on the member is less than a given allowable level. In the case of beams, the stress on the outer fibre is generally the limiting factor. In the case of the duct stiffener resisting negative pressure, the beam deflects downwards, or into the duct. As the beam bends in response to the pressure, the top of the beam is under compression and the bottom of the beam is in tension. Due to the unsymmetrical section with the beam attached to the plate, the top flange of the beam will achieve a higher absolute stress than the bottom flange. In this experiment, strain gauges were placed at the centre of the top flange to measure the axial compressive strain of the outer fibre as the beam deflected under pressure. Figure 18 and Figure 19 show the strain versus applied pressure. The two figures show the same series of curves but with a different scale to emphasize the elastic response region.

Under typical duct design rules, the top flange of the beam is designed to reach a stress level of no more than 2/3 of the nominal yield stress of the material. This follows the practice of the AISC ASD structural design code[2]. The curves showing the first two tests for the W12 beams end abruptly at strains of 1684μm/m and 1750μm/m, respectively. This is the point at which the beams

collapsed with local flange buckling. The nominal yield stress of the beams were 345 MPa, which is less than the 400 MPa strength determined by coupon tensile tests, the results of which are provided in Appendix I. This corresponds to a strain of 2000μm/m given a modulus of elasticity of 200 GPa. These beams did not yield prior to final collapse.

The third test with the W12 beam (W12-3), which had been modified to include gussets, had a different result at the point of collapse. Whereas the pressure at failure was similar to the other W12 tests, the strain passed the elastic limit and became plastic. The gusset welds failed during the course of the test, and therefore had no affect on the ultimate capacity of the beam in terms of applied pressure. It did, however, have an effect on the strain levels of the top flange however. This test was not repeated and no conclusions can be drawn from the results.

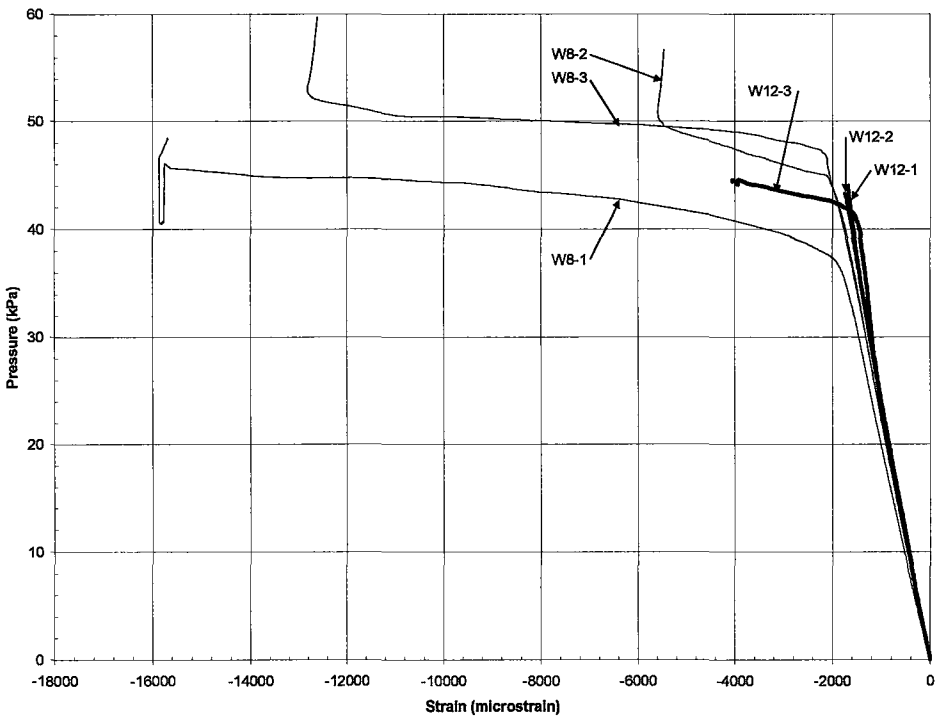

Figure 18: Top Flange Strain at Midspan

Table 4: Top flange strain at 20 kPa

Test	Strain (μm/m)	Test	Strain (μm/m)
W12-1	857.7	W8-1	1009.5
W12-2	860	W8-2	903.9
W12-3	861.5	W8-3	911.3
Mean	859.7		941.6
SD	1.9		58.9
COV	0.2		6.3

As observed in Figure 18, the pressure-strain curves for the three W8 tests were significantly different than the W12 curves, particularly during the final stages. The W12 curves reached the elastic limit but did not become significantly plastic due to the beams buckling prior to reaching this point. The W8 beams however did undergo substantial plastic yielding as pressure increased. There was no sudden failure of these beams by overall section buckling or local flange buckling. The strain on the top flanges increased rapidly after having attained the elastic limit. As with the deflections, the strain curves can be seen to have 'bottomed out' after the apparatus reached its physical limit of deflection. The tests were terminated after an increase in strain was no longer realized with additional pressure.

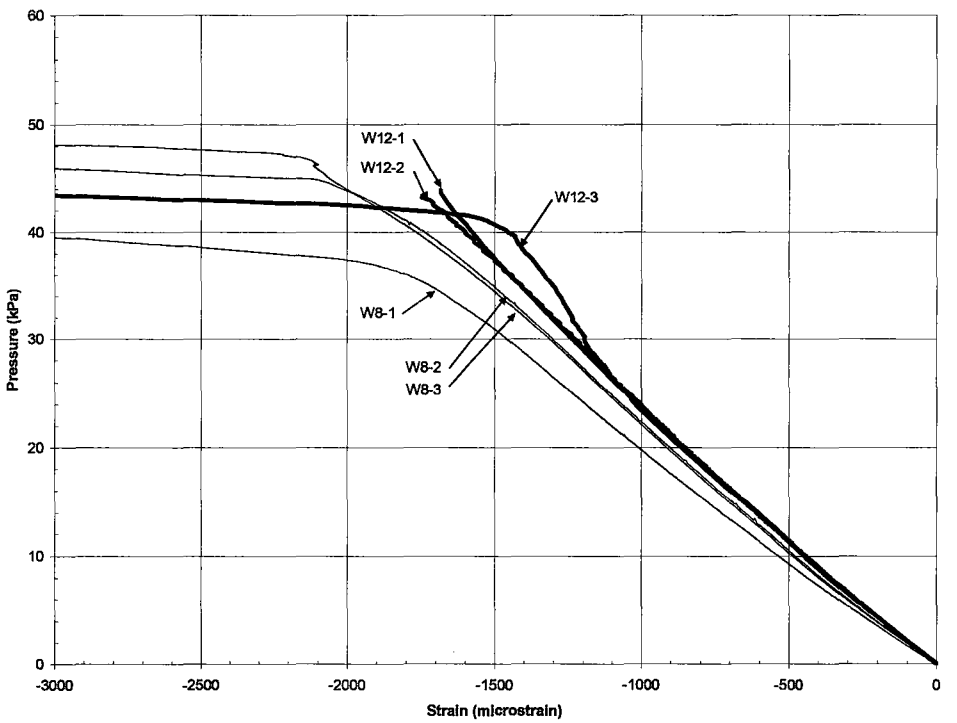

Figure 19: Top Flange Strain at Midspan (2)

Failure of the first W12 beam occurred suddenly. As the pressure was increased, the top flange of the beam developed an approximately sinusoidal curve in the lateral direction. As the middle of the beam deflected in one direction, the ends of the beam deflected in the opposite direction, resulting in a roughly sinusoidal curvature.

With the beam deflecting downwards, the top flange experienced compressive stress as indicated previously. In addition, with lateral deflection superimposed onto the vertical deflection, one side of the top flange experienced a greater compressive stress than the centre line, while the other side of the flange experienced a lesser compressive stress. The combination of stresses on the flange caused one side of the flange to buckle. The sudden loss of strength on one side created a large imbalance in the static forces and the beam collapsed suddenly. Figure 20 shows the beam and box assembly after the failure. The photo shows a sudden change in the lateral curvature at the midspan where the flange failed, creating a plastic hinge in the top flange. Figure 21 is a closer view of the buckled flange. Figure 22 shows the lateral deflection on the post-buckled W12x14 beam.

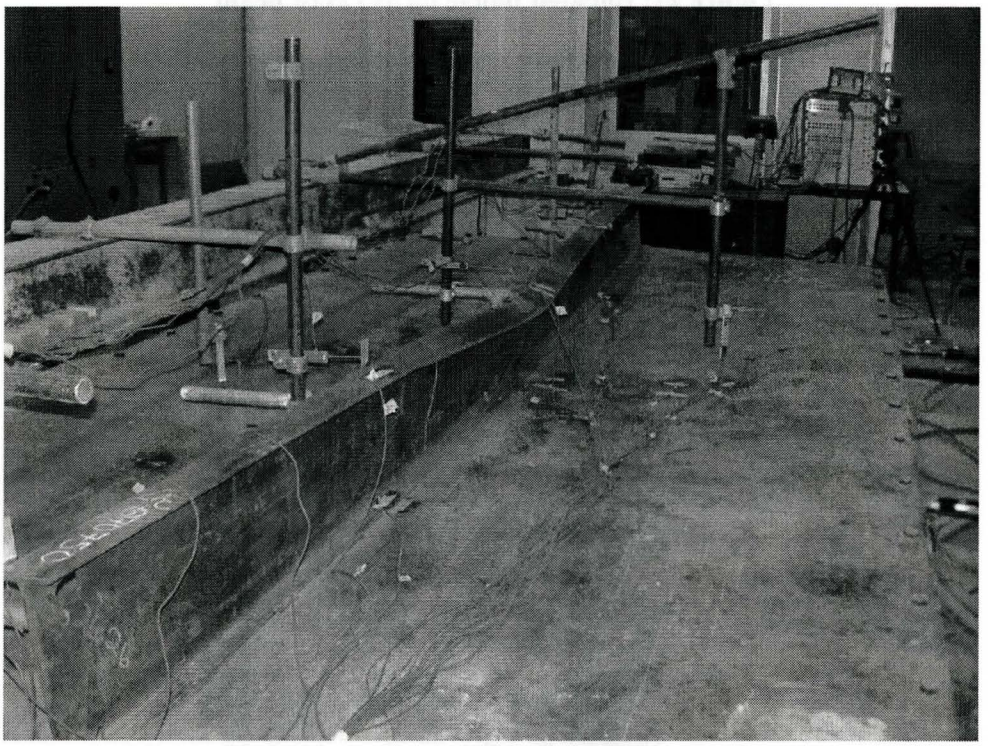

Figure 20: W12x14 beam failing by local flange buckling

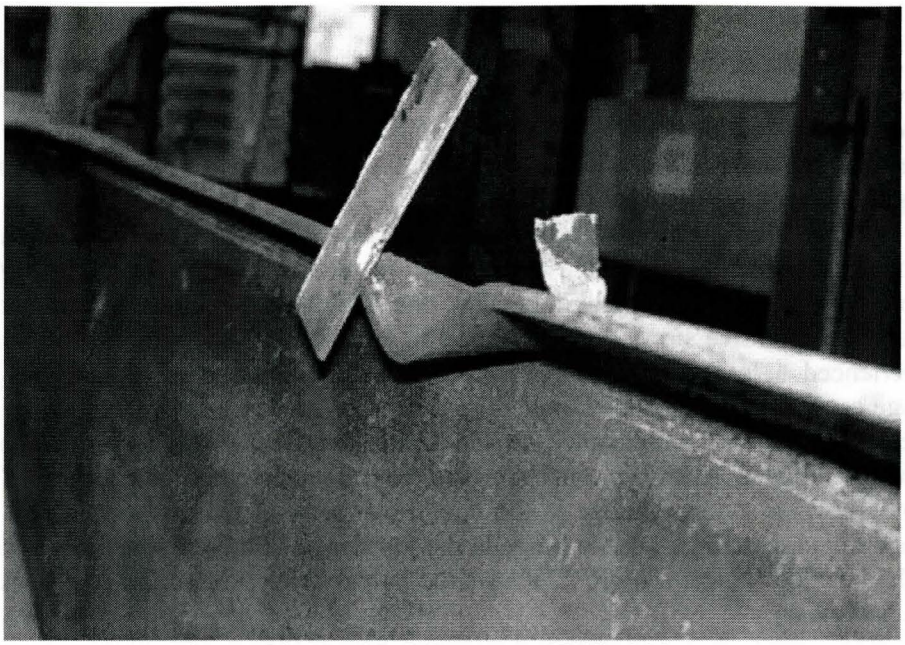

Figure 21: Buckled flange on W12x14 beam

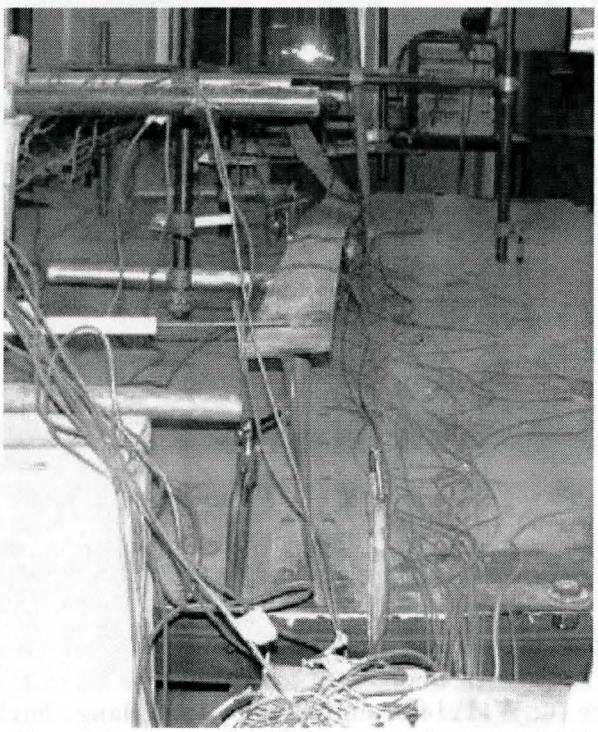

Figure 22: Large lateral deflection on post buckled W12x14 beam

The failed W8x18 beam is shown in Figure 23 and Figure 24.

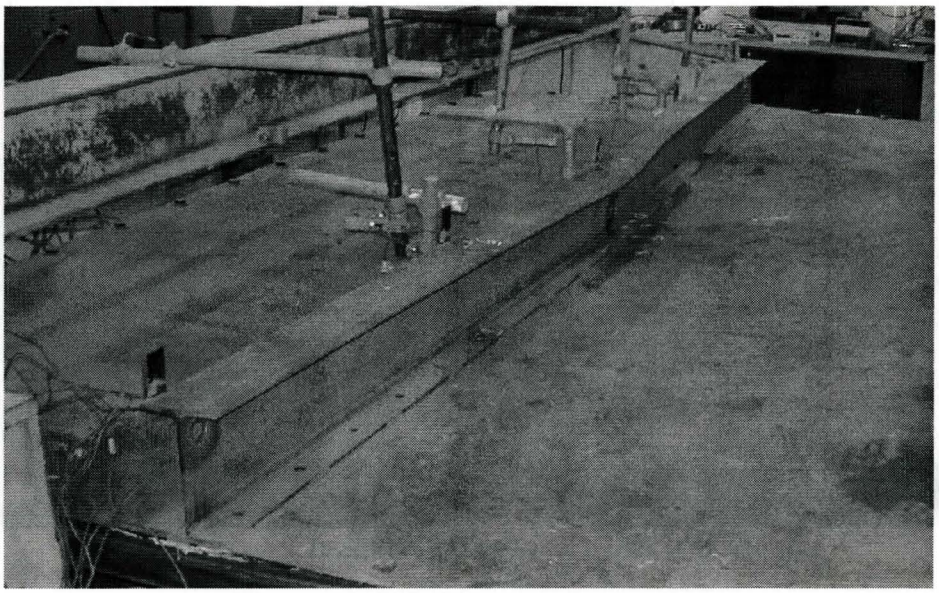

Figure 23: W8x18 beam after testing

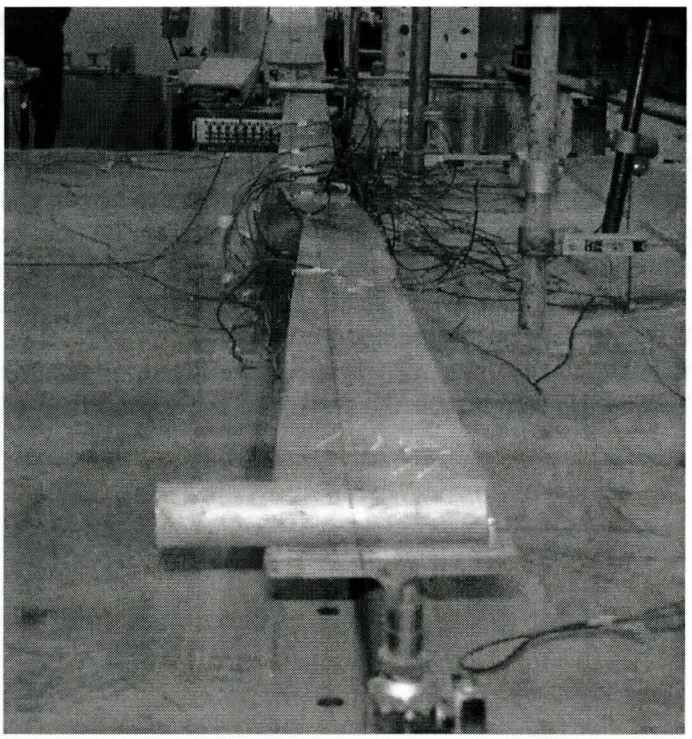

Figure 24: Lateral deflection of post-yield W8x18 beam

An examination of Figure 25 shows the Leuder lines that were apparent at the end of the test. The presence of these lines is indicative of localized yielding.

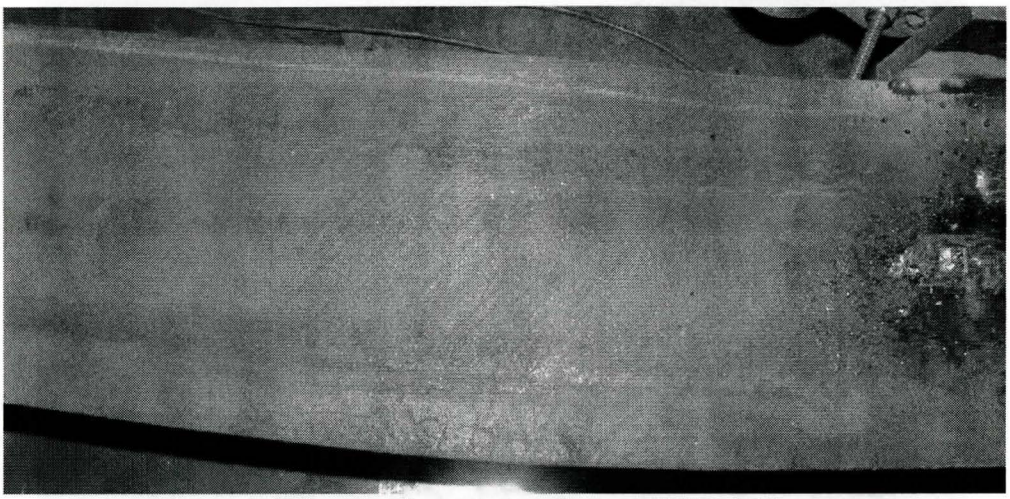

Figure 25: Leuder lines on top flange of W8x18 beam

2.4.4 Neutral Axis Location

To investigate the actual location of the neutral axis of the beam/casing cross section, the data from the strain recorded on the top flange was compared to the strain on the bottom flange. By drawing a linear relation between the top and bottom flange strain, the point of zero strain could be determined which is assumed to coincide with the geometrical neutral axis. From this, the amount of plate that actually contributes to the beam cross section can be calculated.

In the W8 tests, additional gauges were placed on the beam web at midspan. Gauges were placed at the 1/3 and 2/3 height of the web, or alternatively at the '1/3T' and '2/3T' positions. For various reasons, strain gauge measurements on the W12 beams are not presented.

Figure 26 shows the three W8 test curves for the strain recorded on the top flange, the 2/3 and 1/3 heights on the web, and the top surface of the bottom flange.

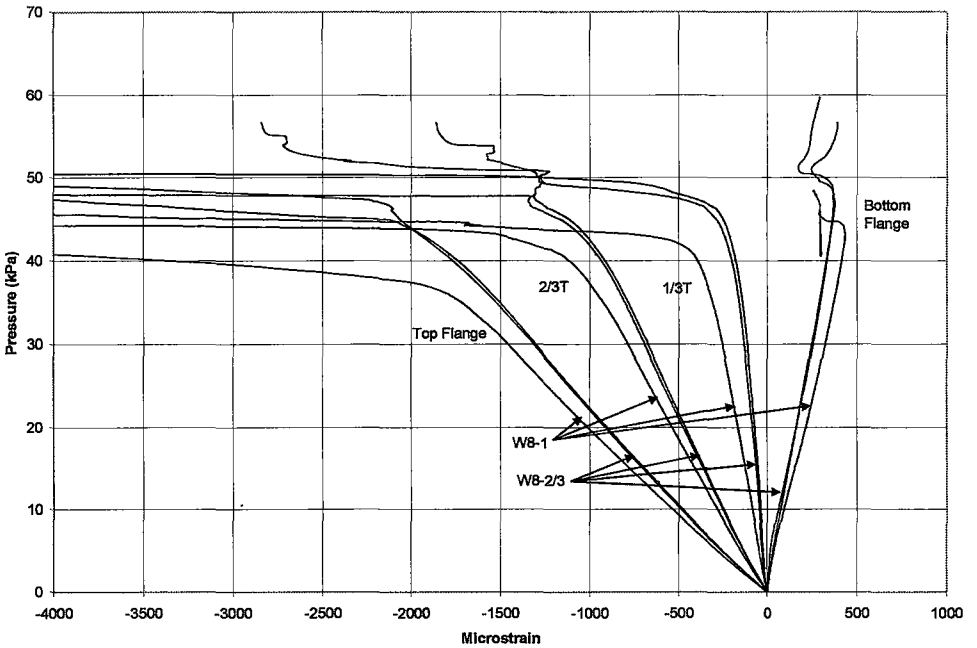

Figure 26: Neutral Axis – Web and Flange Strains – W8x18 Tests

Table 5: Neutral Axis Web Strain (μm/m) at 20 kPa

	Top	2/3	1/3	Bottom
W8-1	-1009.52	-538.375	-166.826	217.369
W8-2	-903.951	-475.969	-84.672	163.619
W8-3	-911.298	-463.438	-72.4407	163.001
Mean	-941.59	-492.59	-107.98	181.33
SD	58.943	40.139	51.328	31.212
COV	6.3	8.1	47.5	17.2

Table 5 shows the strain values at 20 kPa. The coefficient of variance for the top flange strain is very small, indicating the data is consistent between tests. However, the first W8 test gave values that were higher than the other two tests. This is also the case for the 1/3 height, the 2/3 height, and the bottom flange data.

Figure 27 shows the three W12 test curves for the strain recorded on the top flange and the top surface of the bottom flange. The data recorded at 20 kPa is summarized in Table 6. The coefficient of variance for the top flange strain is vary small indicating the data is consistent between tests. The coefficient of variance for the bottom flange, however, is larger. The influence of the welds and drilled holes is reflected in this large variance.

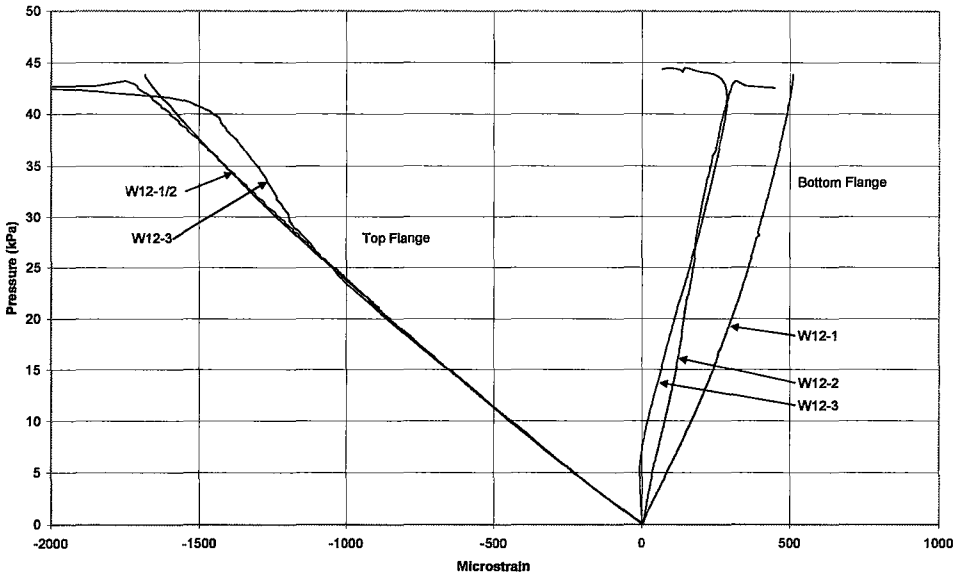

Figure 27: Neutral Axis – Top and Bottom Flange Strains – W12x14 Tests

Table 6: Top and Bottom Flange Strain at 20 kPa for Neutral Axis Calculations

	Top Flange Strain (μm/m)	Bottom Flange Strain (μm/m)
W12-1	-857.7	303.3
W12-2	-850	141
W12-3	-861.4	116.6
Mean	-856.4	187.0
SD	5.8	82.9
COV	0.7	44

Figure 28 illustrates the strain values for each of the three W8 tests and the three W12 tests corresponding to 20 kPa. 20 kPa was chosen as both beams appeared to be responding in a linear elastic manner at this pressure. From Table 9, the predicted location of the neutral axis for the W8 tests using a width of casing equal to '21t' on each side of the flange toe is 68.2mm above the bottom face of the bottom flange. The actual location varied between 44.9mm and 60.1mm, giving a mean of 54.2mm. This corresponds to a contribution of the plate equal to '128t', more than double the standard design value. The linear relationship can be seen between the top flange strain and the web strain for all three W8 tests. The strain on the bottom flange, however, is not consistent with this linear trend, which is attributed to the nature of the bottom flange and the positioning of the strain gauges. The gauges were not located on the centre line of

the beam as they were on the top flange; rather they were on one side of the flange. In addition, the bottom flange contained drilled holes and stitch welds that affected the local strain values.

In light of the inconsistent bottom flange strain values for the W8 tests, the determination of the neutral axis in the W12 tests may not be reliable.

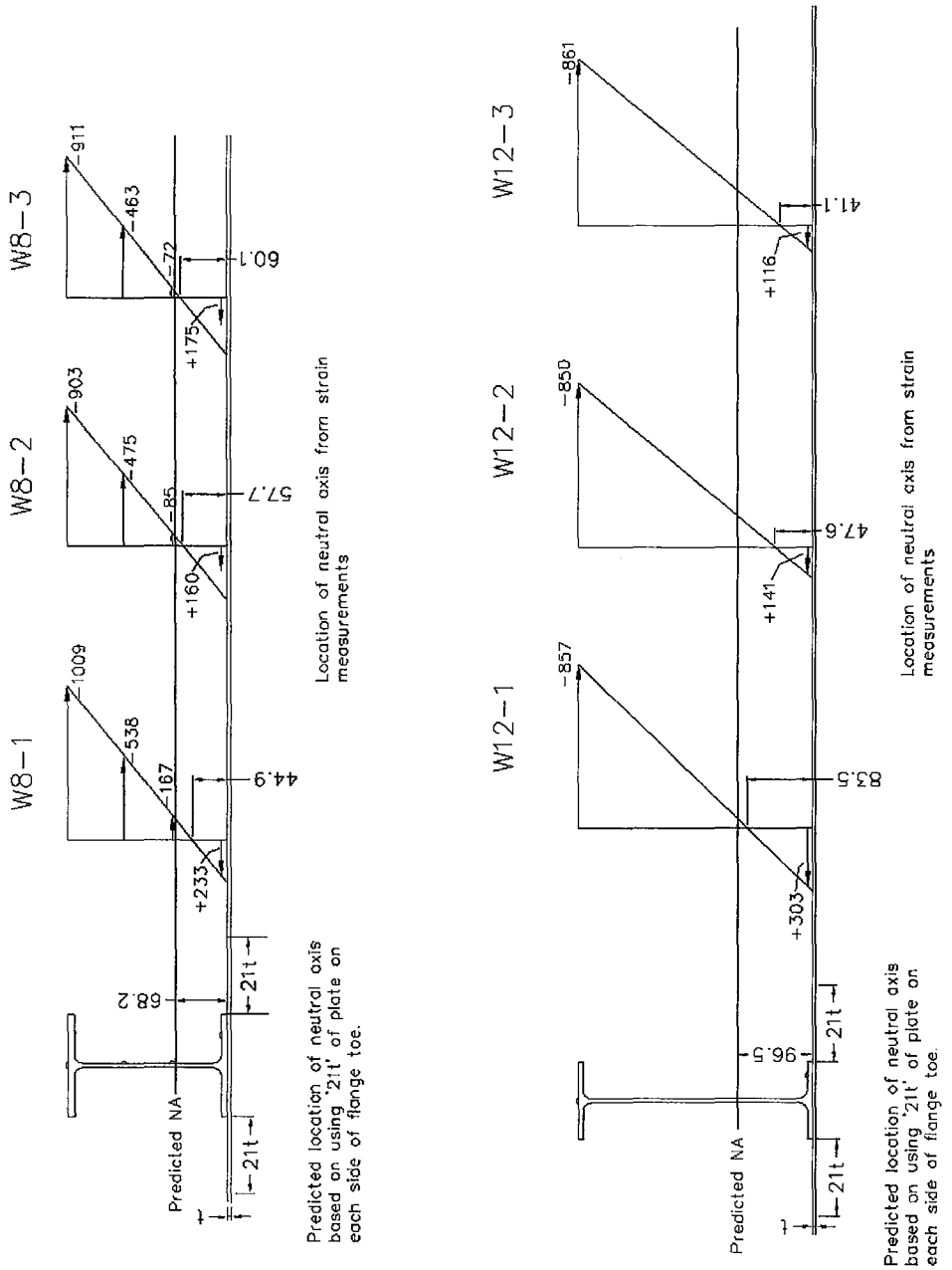

Figure 28: Location of Neutral Axis from Strain Gauge Data

2.4.5 Plate Strain and Deflection

The plate strain perpendicular to the stiffener was recorded at the midspan, the ¼ span, and the ¾ span in the central area of the plate between the beam and the edge of the box. This area represents the casing plate mid-way between stiffeners along a duct.

Figure 29 shows the plate strain for the three W12 tests. The slope of the curves is shallower at the beginning of the tests and increases gradually as the pressure increases. The change in slope of the curves is due to the increasing affect of tensile membrane forces. As the box initially deflects down under negative pressure, the plate will act as a simple beam. The top surface of the plate will be in compression while the bottom surface is in tension. However, as the deflection increases, the edge of the box begins to restrain the downward deflection by resisting lateral movement. This applies tensile membrane forces into the casing which will combine additively with the compressive bending forces.

The edge of the box, which was neither a rigid nor a free restraint provided an elastic type restraint to the lateral movement of the plate. In the configuration of a standard duct with multiple stiffeners along its length, this lateral deflection would not occur. The restraint on the plate in such a case would be rigid, and greater tensile membrane stresses would be expected as a result.

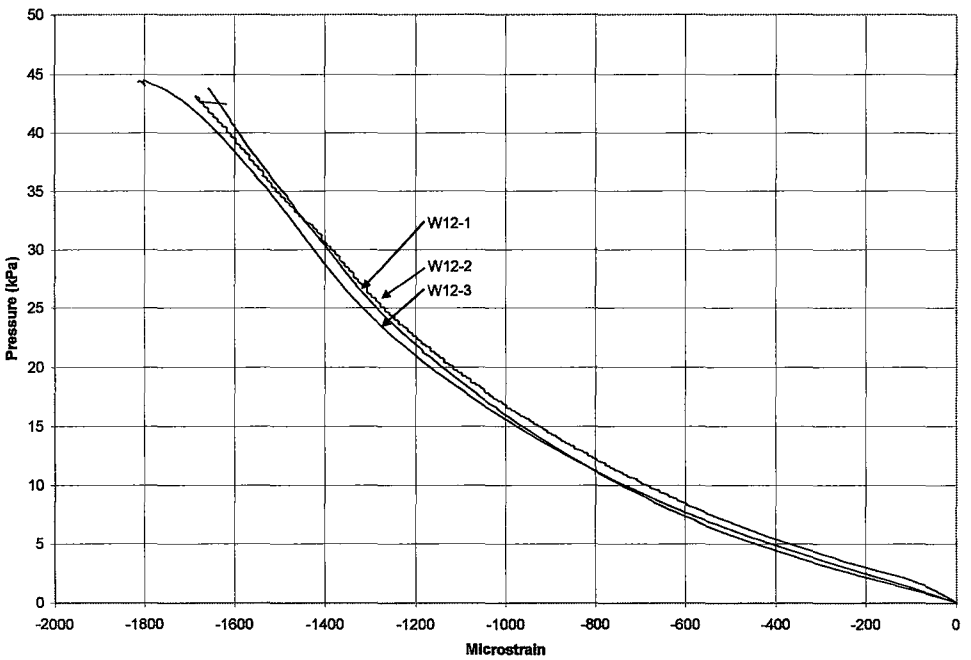

Figure 29: Lateral Plate Strain in Central Area Between Stiffeners

Table 7: Lateral Plate Strain Between Stiffeners

Test	Strain (μm/m)
W12-1	-1143
W12-2	-1118
W12-3	-1167
Mean	-1143
SD	25
COV	2.1

Figure 30 shows the vertical deflection of the plate in the central area at the midspan of the box. The deflection response is similar to the strain response shown in Figure 29. The slope of the curves increases with increasing pressure.

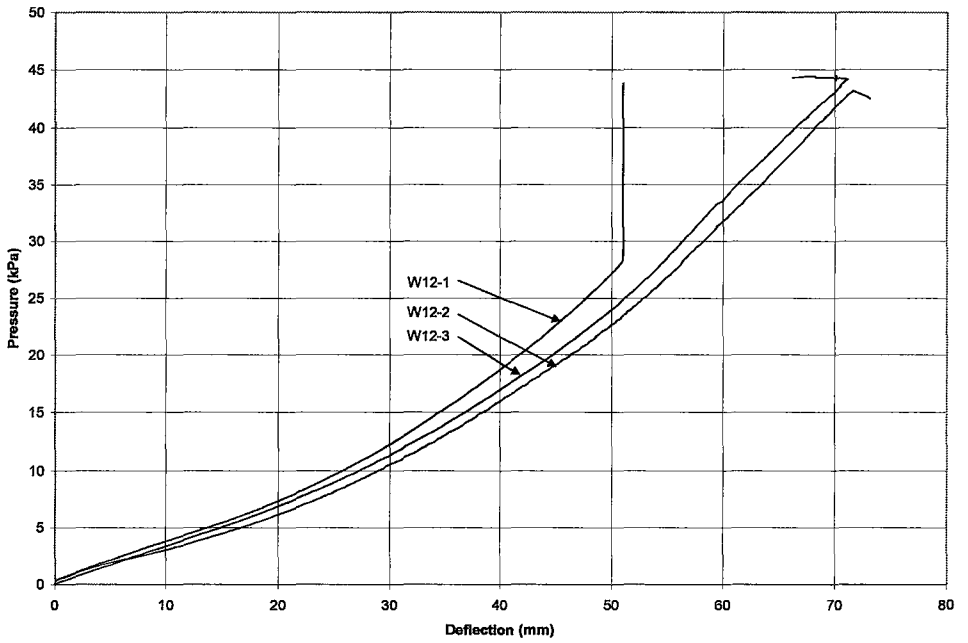

Figure 30: Plate Deflection at Midspan in Areas Between Stiffeners

Table 8: Vertical Plate Deflections (mm) Between Stiffeners at 20 kPa

Test	Deflection (mm)
W12-1	41.8
W12-2	46.3
W12-3	44.6
Mean	44.2
SD	2.3
COV	5.2

2.5 Analytical Analysis

The data from the tests can be used to calculate the location of the neutral axis, the moment of inertia of the composite plate/beam section, and the maximum compressive bending stress on the beam's top flange. Table 9 lists the data that is presented in Figure 28 and section 2.4.4. The table identifies the location of the neutral axis and shows the equivalent plate contribution.

Table 9: Neutral Axis Analysis (at 20 kPa)

	W12x14	W8x18
Neutral Axis Height with respect to bottom flange (mm)	1 - 83.5 2 - 47.6 3 - 41.1 Mean = 57.4 SD = 18.6 COV = 32	1 - 44.9 2 - 57.7 3 - 60.1 Mean = 54.2 SD = 6.7 COV = 12
Equivalent plate contribution	'192 t'	'128 t'
Predicted NA with '42t'	96.5 (31.9% of beam height)	68.2 (33.0% of beam height)

From Table 9 above, the W12x14 neutral axis was 57.4 mm above the bottom surface of the beam and 54.2 mm for the W8x18. The moments of inertia for these beams become:

W12x14 $I_x = 74.1\times10^6$ mm^4 (increased from 38.2×10^6 mm^4)
W8x18 $I_x = 45.7\times10^6$ mm^4 (increased from 26.2×10^6 mm^4)

Using these moments of inertia, the deflection of a simply supported beam under a uniformly distributed transverse load can be predicted by

$$\Delta_{max} = \frac{5\omega l^4}{384EI} \qquad (2\text{-}1)$$

where ω is equal to pressure times stiffener spacing.

Using P = 20 kPa, stiffener spacing = 1219mm, E = 200 GPa, and the corresponding composite moment of inertia from above, the deflection is given in Table 10:

Table 10: Prediction of deflection using moment of inertia

Section	Δ_{max} (eqn 2-1)	Δ_{max} (Measured from Table 2)	% difference (1- Δ_{pred}/ Δ_{act})
W12x14	9.36 mm	11.8 mm	20.7%
W8x18	15.18 mm	14.4 mm	5.4%

Likewise, the moment of inertia can be used to calculate the stress on the top flange if the applied moment is known. Using Equations 2-2 and 2-3, the top flange elastic stress is given by the values in Table 11.

$$M = \frac{\omega l^2}{8} \tag{2-2}$$

$$\sigma_b = \frac{M(c + d_{NA})}{I} \tag{2-3}$$

The actual stress on the top flange as recorded by the strain gauges is also given in Table 11, where σ=E×ε, and E=200 GPa.

Table 11: Actual vs. Calculated top flange stress from moment of inertia

Section	σ_b (eqn 2-3)	σ_b (Table 4)	% difference (1- σ_{pred}/ σ_{act})
W12x14	210.7 MPa	172 MPa	22.5%
W8x18	212.6 MPa	188 MPa	13.1%

One observes from Table 10 and Table 11 that this method of calculating the actual stress and actual deflection is more accurate for the W8x18 section than for the W12x14 section. Referring back to Figure 28, the neutral axis for the W8x18 sections were determined using the strain recordings from strain gauges on the web, rather than by the strain gauges on the bottom flange. The strain recordings from the bottom flange were ignored for this as the reading was influenced by the presence of the stitch welds and the drilled holes. Likewise, the W12x14 strain values on the bottom flange would have been somewhat affected by the welds and drilled holes. However, there were no web strain gauges for these tests. If the strain values on the bottom flange are too low (as is the case with the W8x18 tests), the neutral axis is actually higher than what is shown, and the resulting moment of inertia would be calculated as too high. Subsequently, the deflection and stress are under predicted. Further comparison of the experimental data to the finite element results are presented in section 3.5.

CHAPTER 3 FINITE ELEMENT MODELING

3.1 Introduction

The finite element (FE) model of the stiffened duct is presented in this chapter, which is calibrated and validated using the data from the experimental program. This model is then used to predict the response of other beam sections that may be used in the application of industrial duct stiffening. To simulate the specimens of the experimental program, two FE models were created; one for the W8 beam and the other for the W12 beam. This chapter describes the numerical models, the elastic results, as well as the buckling results.

3.2 Elements and Geometry

The top plate of the tested duct, whose dimensions is 4572mm x 2438mm (180" x 96"), with a centre stiffener, was analyzed using the finite element (FE) program, ANSYS.[4] The FE model was constructed using 8-node shell elements for the plate as well as the stiffener. Three thicknesses were specified in the model corresponding to the casing plate, the stiffener flange, and the stiffener web. The FE model input is included in Appendix D. Figure 31 and Figure 32 show the finite element model for the W12×14 beam and W8×18 beam, respectively.

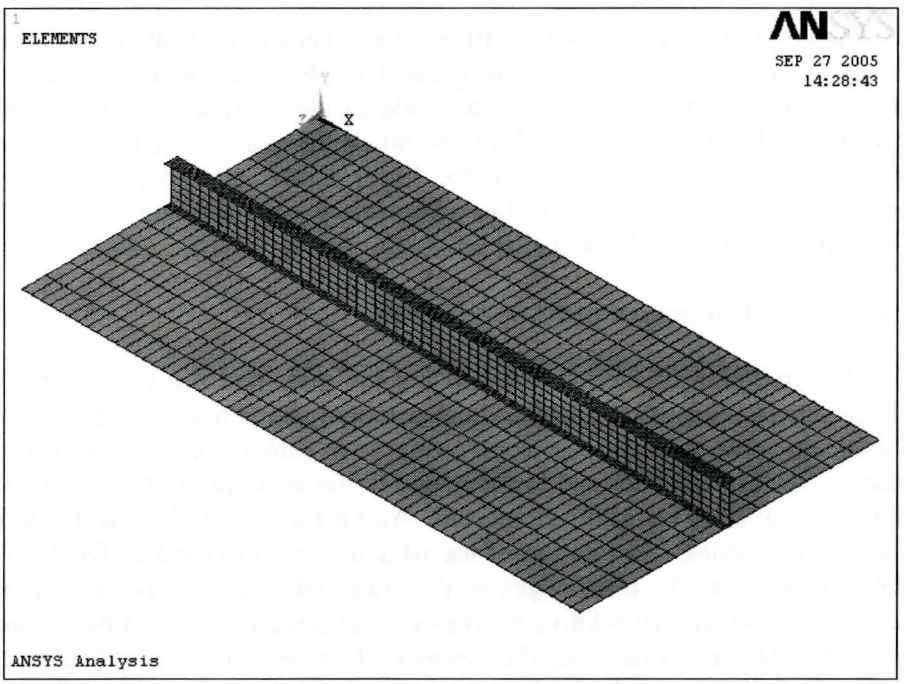

Figure 31: Ansys model for duct and single W12x14 stiffener

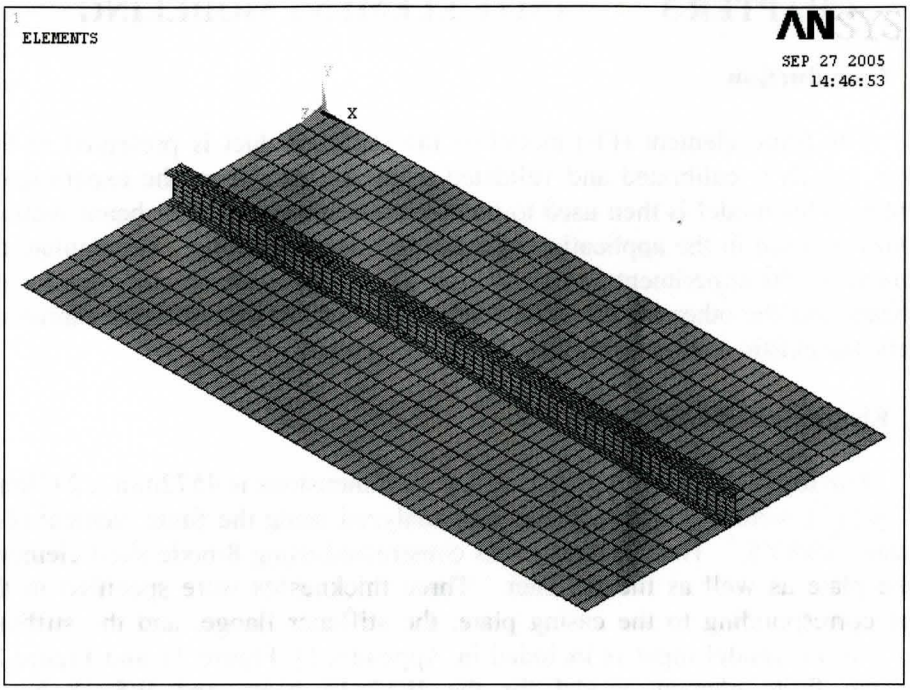

Figure 32: Ansys model for duct and single W8x18 stiffener

The input of the model was configured in a parametric fashion that would enable quick substitution of the beam geometry. For each beam section, the flanges were 6 elements wide (3 on each side of the web) and the web was 6 elements high. The plate was modeled to be 60 elements long, and 6 elements on each side of the beam flange. For the linear elastic analysis, the material properties assigned were the modulus of elasticity with a value of 200 GPa (29.5×10^6 psi) and Poisson's ratio of 0.3.

3.3 Boundary Conditions and Applied Load

The structural interaction between the top plate and the vacuum box is non-linear due to the contact boundary and potential slip between the two edges. This difficulty was resolved by considering two extreme conditions for the boundary reflecting an upper and lower bound to the solution. For the first case, the plate is assumed to be rigidly connected. Accordingly, both the translation in-the-plane of the casing and rotation of the edge axis are modeled as fixed. The vertical translation of the plate edges is also modeled as fixed. For the second scenario, it is assumed that relative movement between the plate and the vacuum box is permitted. For this case, the degrees of freedom corresponding to the translation in the plane of the casing are released. The rotation about the edge axis and vertical translation for the plate edge conditions are modeled as fixed.

The magnitude of the load applied was 6.9 kPa (1 psi). The pressure was applied normal to the bottom surface of the plate in the downward direction.

3.4 Stability Analysis

3.4.1 Elastic Buckling of Casing and W12x14 Stiffener

The finite element model was used to simulate the linear elastic behaviour of the plate. The eigenvalue analysis was also carried out using the two noted boundary conditions.

For Case 1, the first buckling eigenvalue of the model was 4.55. This corresponds to an applied pressure of 31.37 kPa. The corresponding mode shape is shown in Figure 33.

For Case 2, the buckling eigenvalue of the model was 4.07. The corresponding pressure at the point of buckling is 28.05 kPa. The mode shape, which is similar to Case 1, is shown in Figure 34. By fixing the in-plane movement of the plate has yielded an additional 12% increase in capacity. The additional capacity of the buckling can be attributed to the torsional stiffness of the plate. As discussed in section 1.3.1, and Appendix J, and illustrated in the design example of Appendix H, the bracing of the member against lateral buckling is achieved through the torsional stiffness of both the casing and the web of the beam. According to the concept of springs in series between the casing and the web, the stiffness of the least stiff component dominates the overall stiffness of the torsional bracing. The contribution of the casing stiffness is from the out-of-plane flexibility as the top compression flange tries to deflect sideways, creating a moment on the bottom of the beam and attached casing. The casing on one side of the bottom flange will be forced in an upwards vertical displacement, while the other side is forced down. The flexibility of the plate to allow this out-of-plane deflection determines the rotational stiffness of the plate.

By comparing the two finite element results, one observes that restricting the in-plane movement at the plate edge has led to a 12% increase in buckling capacity, and has also provided a reduced flexibility for out-of-plane displacement adjacent to the bottom flange. A review of the results from the experimental program (see Figure 17) shows that the buckling onset occurred in the range of 30 to 33 kPa. The onset of buckling is presented by the increase in rate of lateral deflection. For pressures up to 30 kPa, the lateral deflection of the top flange appeared roughly linear with increased pressure. After this pressure, the lateral deflection increased at a non-linear rate in post-buckling movement. From this comparison, it can be deduced that the fixed edge boundary condition is more representative of the actual restraint of the experimental box than the free one.

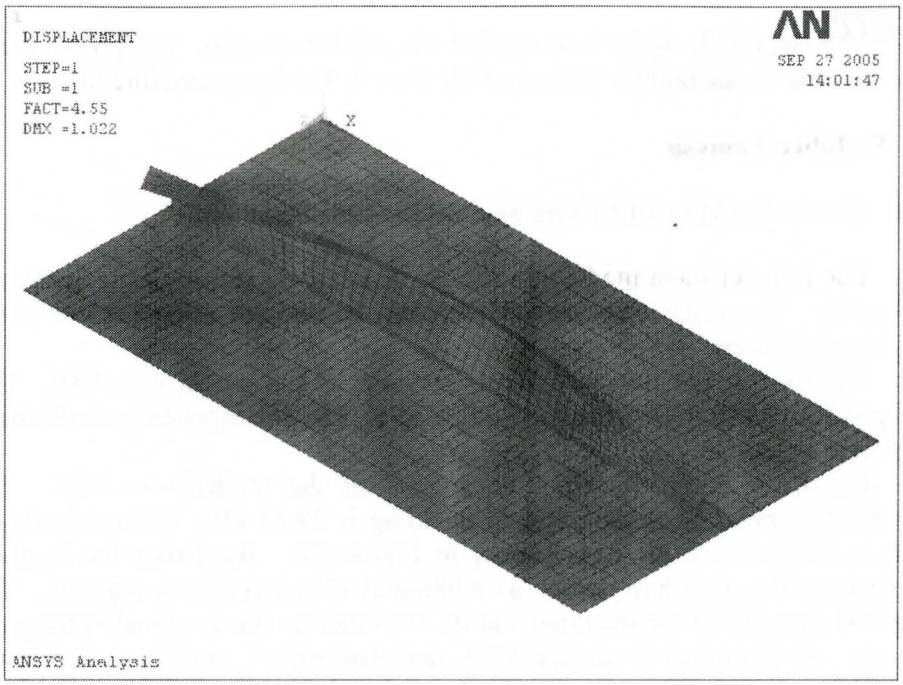

Figure 33: W12x14 buckled shape - long edges held laterally

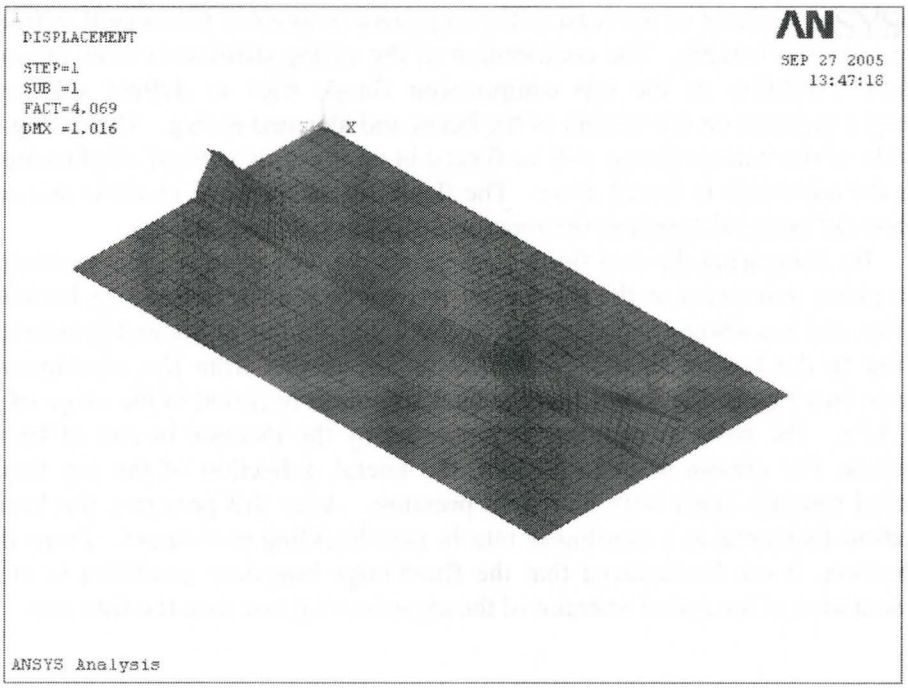

Figure 34: W12x14 buckled shape - long edges laterally free

3.4.2 Elastic Buckling of Casing and W8x18 Stiffener

The finite element analysis was repeated with different parameters representing the W8x18 beam. As before, the analysis was carried out twice to include the different boundary conditions associated with a free in-plane motion and a fixed in-plane motion. Unlike the results for the W12x14 beam, the resulting pressure at the point of buckling for the W8x18 beam was substantially different for the two cases. For Case 1, the applied pressure at buckling is 78.2 kPa (11.34 psi) and for Case 2 the pressure is 43.91 kPa (6.37 psi). This represents a difference of 78%. Both of these pressures are sufficiently high to ensure that highly stressed regions of the beam become plastic, and therefore elastic buckling is not possible. Therefore, determining the buckling load for this beam is not necessary as it is not the critical one. Nonetheless, the result highlights the impact of casing flexibility due to boundary conditions on buckling loads.

For the models corresponding to the W12x14 beam, the difference in buckling load was attributed to the extra flexibility of the casing to resist the overturning moment of the beam. For the models with the W8x18 beam, the casing geometry and boundary conditions were similar to the previous series of simulations, but the difference in buckling capacity between them has increased from 12% to 78%. The large difference in buckling capacity with the W8x18 beam is therefore attributed to the extra torsional stiffness provided by the shorter and thicker beam web. By increasing the stiffness of the web, small changes in casing stiffness can have a greater influence on the overall torsional stiffness of the assembly. The W12x14 web was taller and thinner, and therefore less stiff when resisting overturning moments. With the web and casing closer together in stiffness, small changes in the stiffness of one do not greatly change the overall stiffness. Increasing the stiffness of the web allows small changes in the casing to have a greater influence on the overall stiffness, and thus buckling capacity of the beam overall.

The mode shapes for Case 1 and Case 2 are shown in Figure 35 and Figure 36, respectively. One clearly observes that the two buckling modes are not similar.

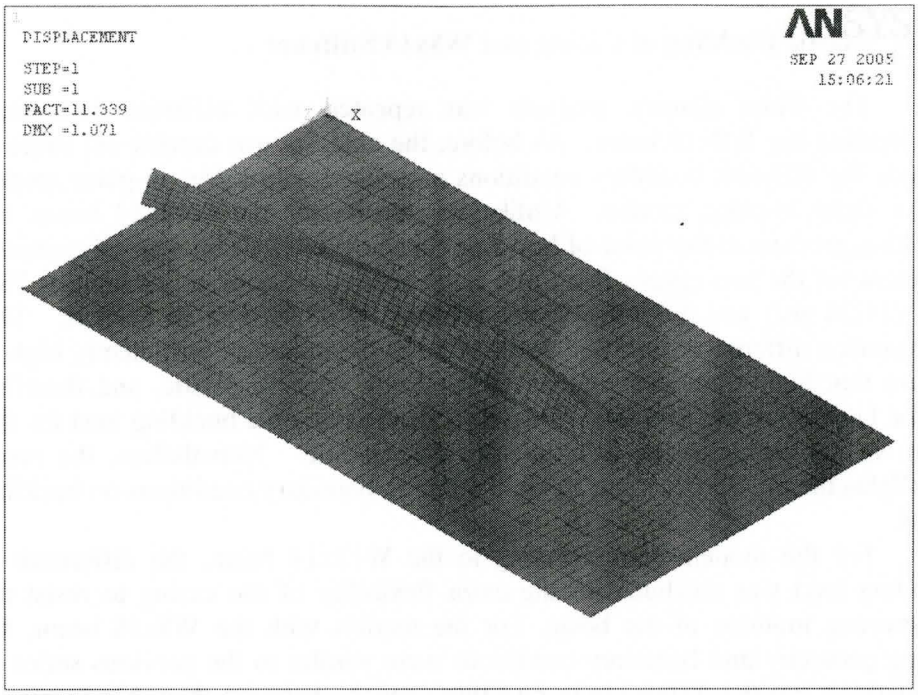

Figure 35: W8x18 buckled shape - long edges held

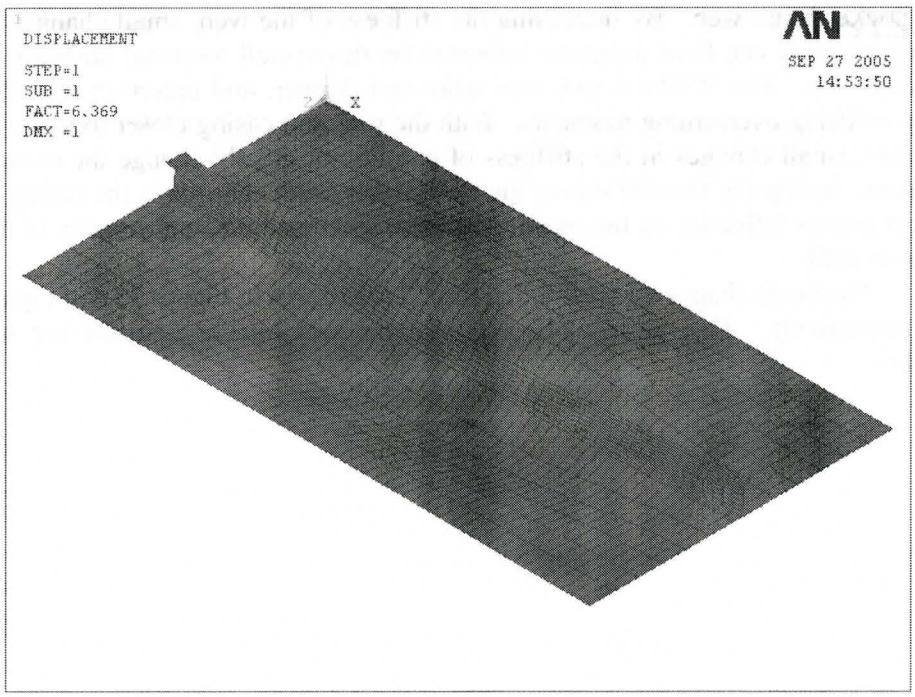

Figure 36: W8x18 buckled shape - long edges free

3.5 Linear Elastic Results

This section presents the finite element results of the stiffened casing plate. Comparisons are made between the finite element results and those measured experimentally to determine the appropriateness of the FE model.

3.5.1 Linear Elastic Analysis of Casing and W12x14 Stiffener

Figure 37 and Figure 38 show the FE results of the vertical deflection contours and profile of the casing and stiffener assembly with a negative pressure applied to the underside of the assembly. The largest deflection is seen in the central area of the plate between the stiffener and restrained plate edge as one might expect. The deflections at key points in the finite element model corresponding to a pressure of 20 kPa are reproduced in Table 12 along with the experimental data. These correspond to the vertical deflection of the beam top flange and the central area of the plate between the edge and the stiffener beam. One can observe that the computed deflection of the beam is smaller than the measured one by 39%, whereas the computed vertical deflection of the central area of the plate is 16% larger than those measured experimentally. This implies that the in-plane stiffness of the plate represented by the FE model is slightly less than the one depicted in the experimental program.

Table 12: Vertical deflections from FE analysis vs. experimental results – W12x14 stiffener

Location	Deflection from FE at 20 kPa (mm)	Deflection from tests at 20 kPa ($\mu \pm \sigma$)	% Difference
Beam – Top flange center	8.5	11.83 ± 0.69 (COV=5.8)	39%
Plate – Central area between stiffeners	51.48	44.24 ± 2.28 (COV=5.1)	16%

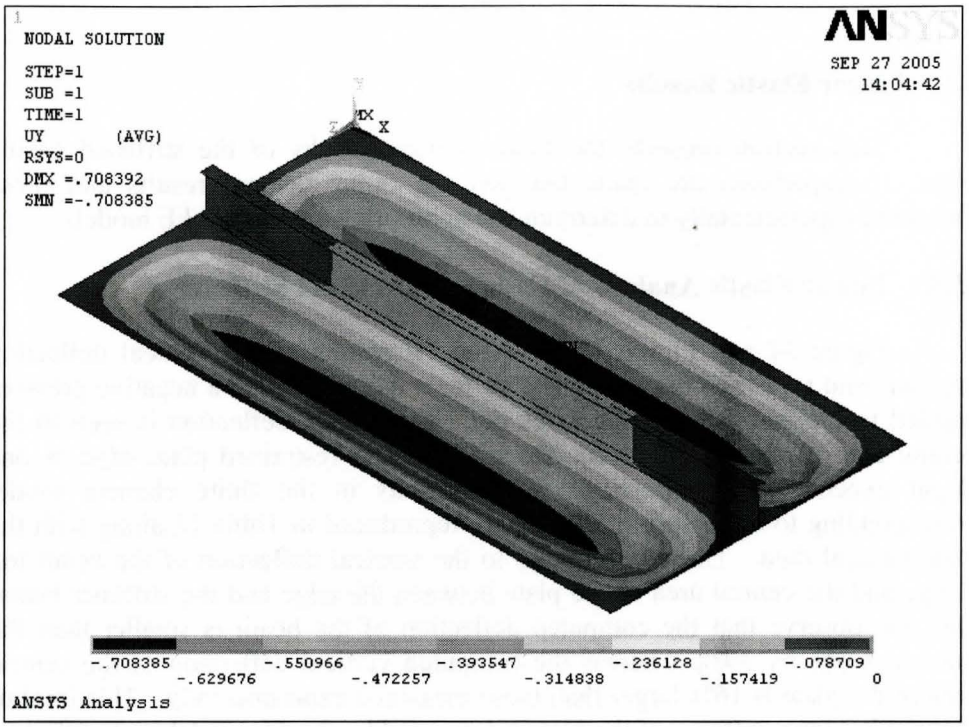

Figure 37: Vertical deflection of W12x14 section, long edges held laterally

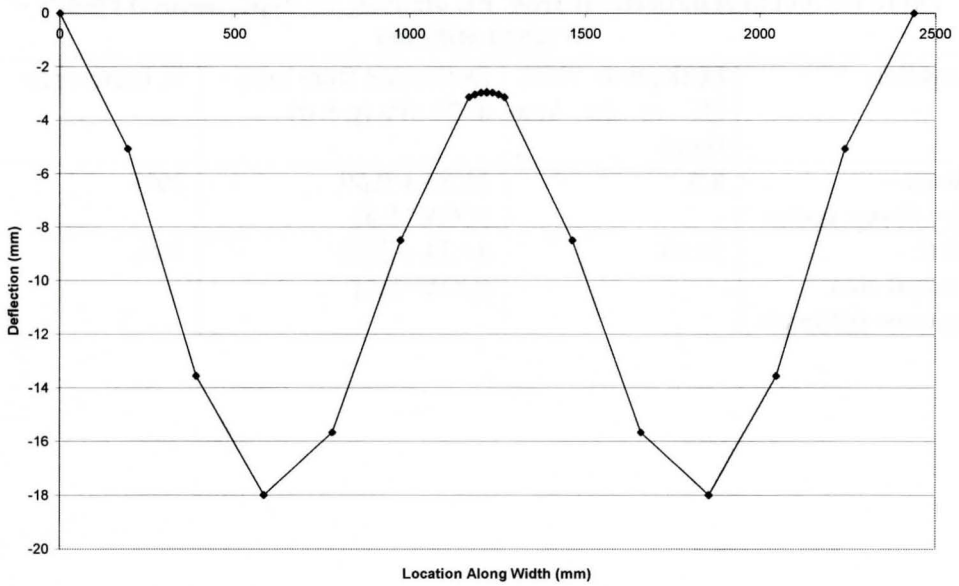

Figure 38: Vertical Deflection at Midspan

Figure 39 is a contour plot of the longitudinal strain. The minimum strain can be seen on the top flange, which represents the largest compressive strain. The strain value from the finite element model is listed in Table 13 along with the experimental result from section 2.4.3. The percent difference in strain between the finite element model and the experimental results is 12%

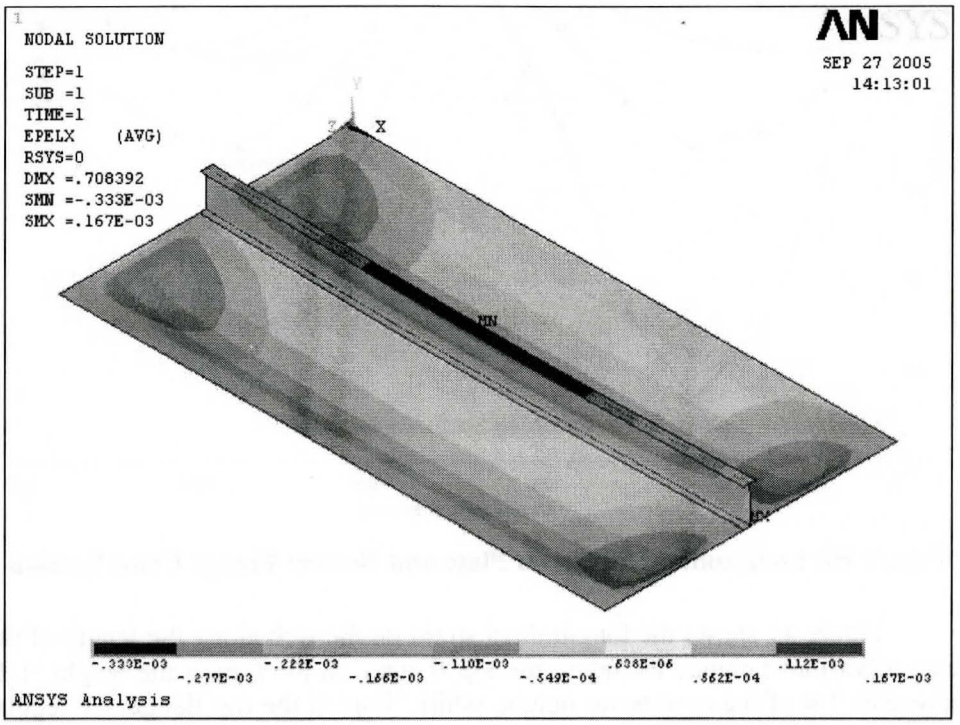

Figure 39: Longitudinal Strain, W12x14 section

Table 13: Strain on top flange at midspan – W12x14

	Finite Element strain at 20 kPa (μm/m)	Experimental strain at 20 kPa (μm/m)	% Difference
Strain (μ)	-966	-860 ±2 (COV=0.2)	12%

Figure 40 shows the longitudinal strain through the cross section of the FE model at various locations along the length of the plate. The top curve (X=2286 mm) represents the axial strain at the centre of the physical model. The bottom curve (X=610 mm) shows a larger axial strain towards the sides of the plate. Figure 39 also illustrates this effect. This increased strain towards the edges of the plate is the result of the larger bending stresses due to the change in slope of the deflection.

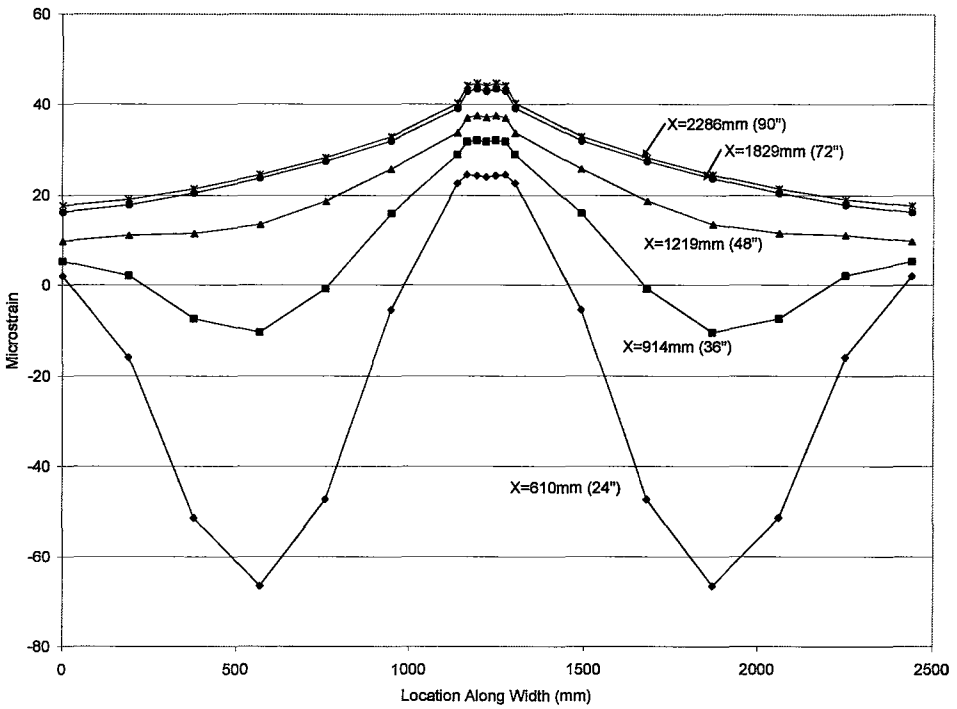

Figure 40: Longitudinal Strain on Plate and Bottom Flange Cross Section

Figure 41 shows the longitudinal strain on the web along the length of the beam at various heights, including the top flange. In the figure, the height '1/6' represents 1/6 of the total beam height, while 'Top' is the top flange. A regular pattern is generally seen with tensile strain on the bottom flange and compressive strain on the top flange as would be expected of a beam with downward loads applied. The ends of the beam show relatively complicated stress patterns that can also be seen in Figure 39. This stress pattern is the result of the unusual support and boundary conditions imposed on the beam. The nature of the pattern and its effect on the beam's capacity was not studied.

Figure 42 illustrates the strain at the midspan of the beam only. The strain on the web and flanges appears to be reasonably linear. The neutral axis of the beam is located where the strain changes from compressive to tensile and has a 'zero' value. From this figure, the neutral axis of the beam with the plate is seen to be at 20% of the beam height. For a beam height of 302mm, this is 60.5mm above the bottom flange. As noted in section 2.5, determination of the neutral axis on the W12 tests from the strain gauge data was influenced by the discontinuities of the bottom flange. However, the result was 57.4 mm above the bottom flange and remains consistent with the finite element data.

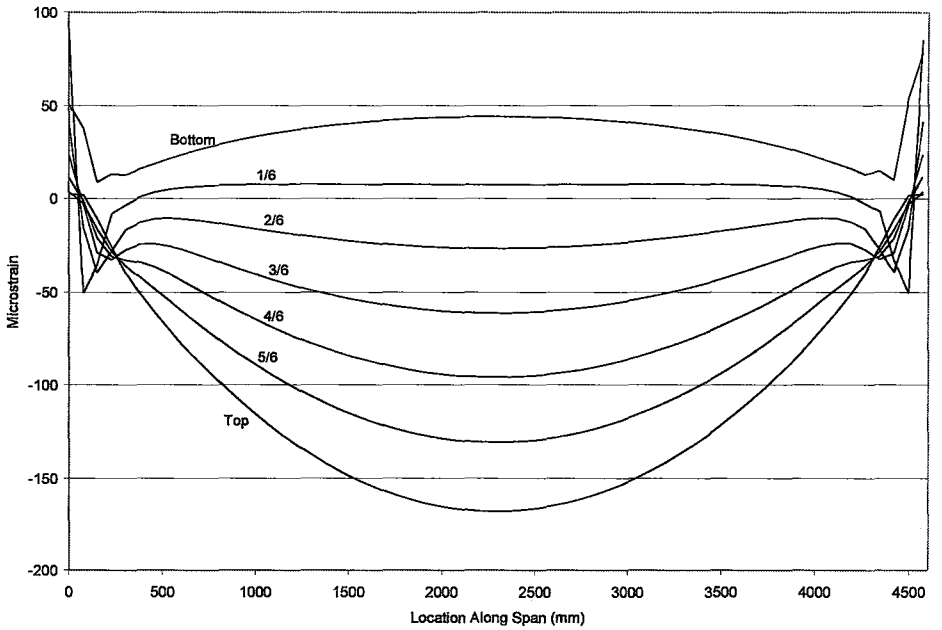

Figure 41: Longitudinal Strain Along Web at Various Heights – W12x14

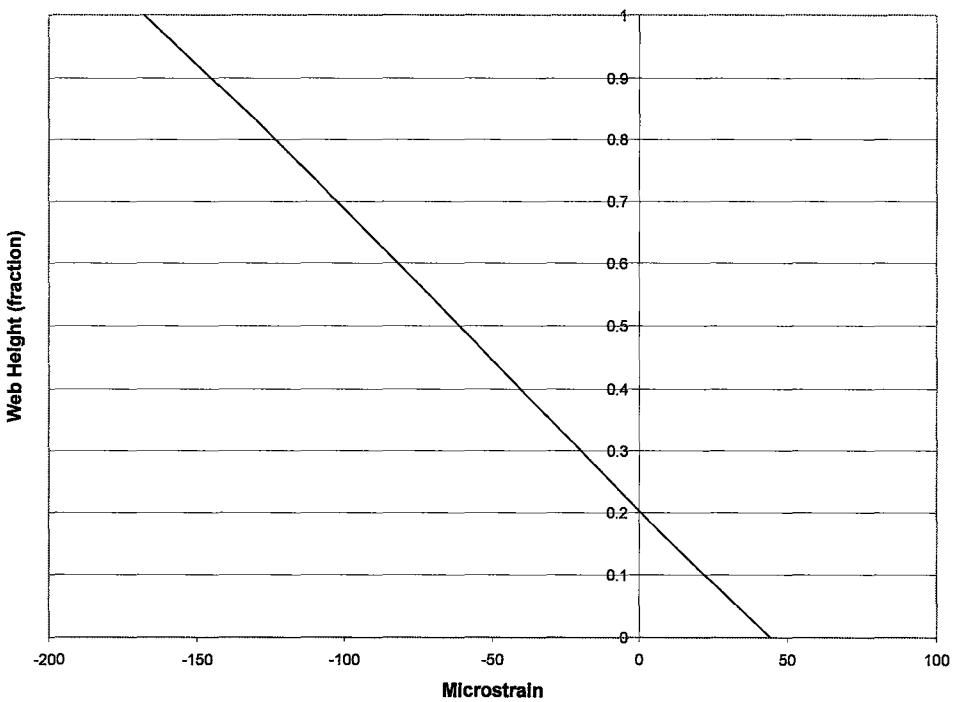

Figure 42: Longitudinal Strain – Location of Neutral Axis – W12x14

Figure 43 and Figure 44 show the lateral strain distribution on the plate ('Z' axis - perpendicular to the beam). The areas around the edge of the plate and beside the beam flange are in tension, while the central area is in compression. The lateral strain in the central area of the plate was recorded as -1143μm/m, which compares with the predicted value of -1267μm/m at 20 kPa. This corresponds to 11% difference.

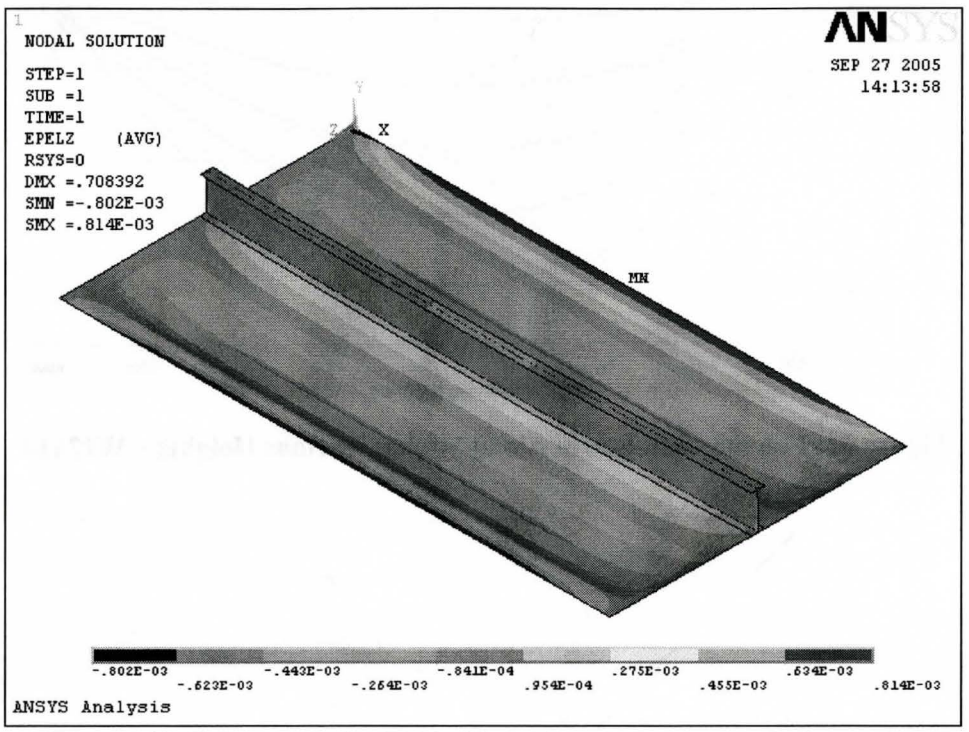

Figure 43: Lateral strain, W12x14 section, long edges held laterally

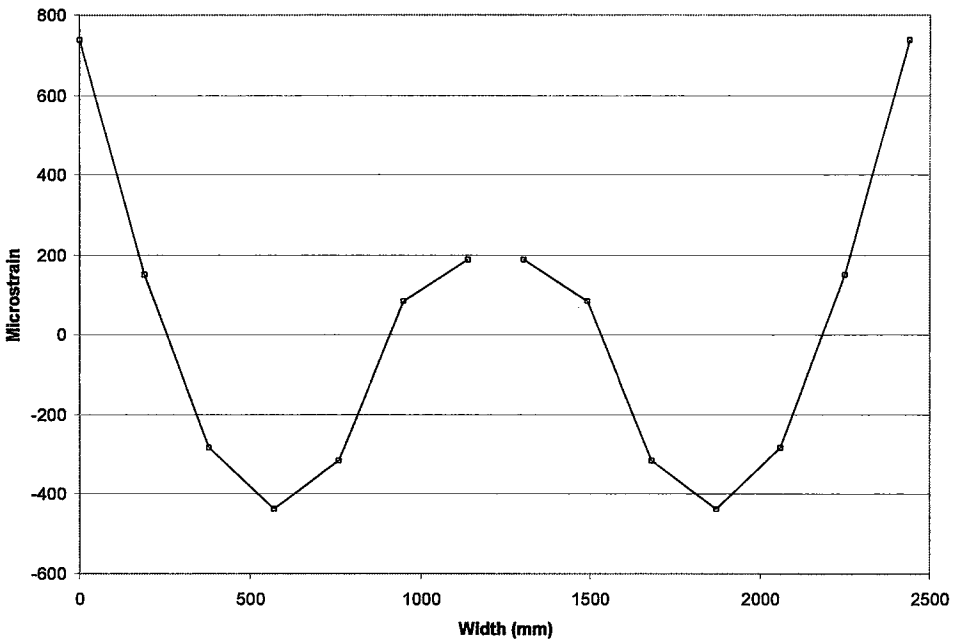

Figure 44: Lateral Strain Across Plate Width

The measured vertical deflection of the test beam was within 39% of the FE predictions. It should be noted that although the percentage difference is fairly large, the absolute difference is only 3.3mm. Due to the size and construction of the box and its elaborate support structure, the two values can be considered reasonably close.

Other measured values differed from the finite element results by approximately 15% or less. These results indicate that the finite element model of the plate with a W12x14 stiffener reasonably captures the experimental data.

3.5.2 Linear Elastic Analysis of Casing and W8x18 Stiffener

Figure 45 and Figure 46 show the vertical deflection of the plate and W8x18 beam under the applied pressure load. Figure 47 shows a contour plot of the beam and plate longitudinal strain. Comparing this plot to Figure 39, which shows the longitudinal strain for the W12 section, suggests that the shear lag on the plate is more evident in the W8 model. The W8 beam is more flexible than the W12, and so the plate must resist higher load resulting in higher deflection and strains local to the beam.

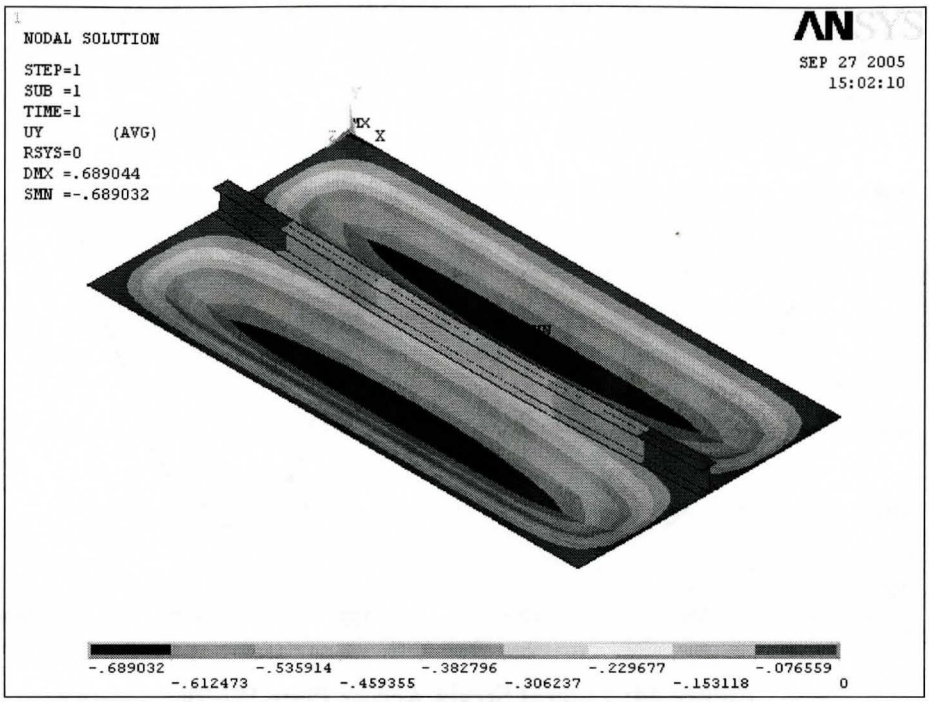

Figure 45: Vertical deflection of W8x18 section

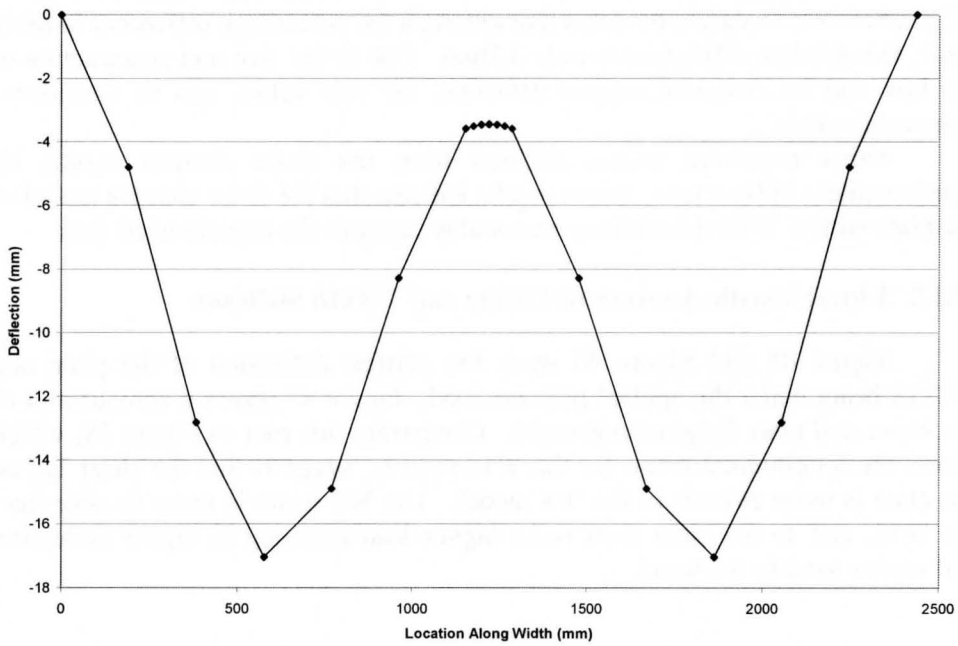

Figure 46: Vertical Deflection of Plate at Midspan

Table 14: Vertical deflections from FE analysis vs. experimental results – W8x18 stiffener

Location	Deflection from FE at 20 kPa (mm)	Deflection from tests at 20 kPa ($\mu \pm \sigma$)	% Difference
Beam – Top flange center	13.2	14.44 ± 2.66 (COV=18.4)	9%
Plate – Central area between stiffeners	50.7	44.2 ± 2.3 (COV=5.2)	15%

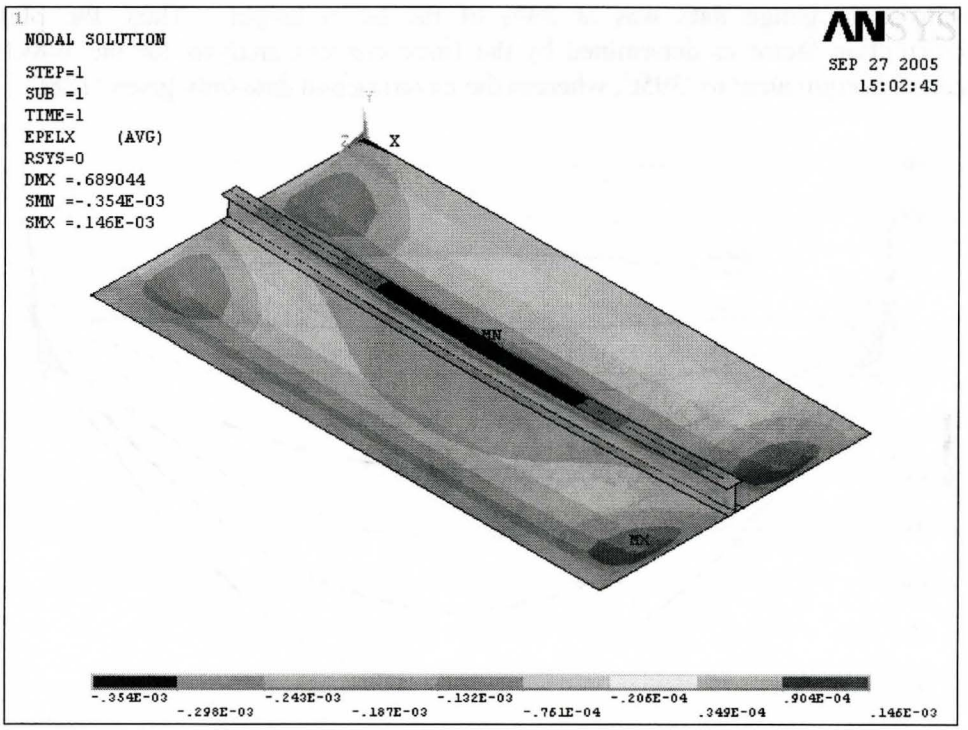

Figure 47: Longitudinal Strain, W8x18 section

Table 15: Strain on top flange at midspan – W8x18

	Finite Element strain at 20 kPa	Experimental strain at 20 kPa	% Difference
Strain (μ)	-1017	-942 ±59 (COV=6.3)	8.0%

Figure 48 shows the finite element results for the axial strain along the web of the W8x18 beam. The line of zero strain is the position of the neutral axis and can be seen to generally follow the curve representing 1/6 of the beam height. A cross section of the strain at the midspan is shown in Figure 49. The strain is nearly linear throughout the beam height, and crosses the zero line at 15% of the beam height. Results of Table 9 revealed that the beam neutral axis determined from strain gauge data was at 33% of the beam height. Thus, the plate contribution factor as determined by the finite element analysis for the W8x18 section is equivalent to '395t', whereas the experimental data only gives '128t'.

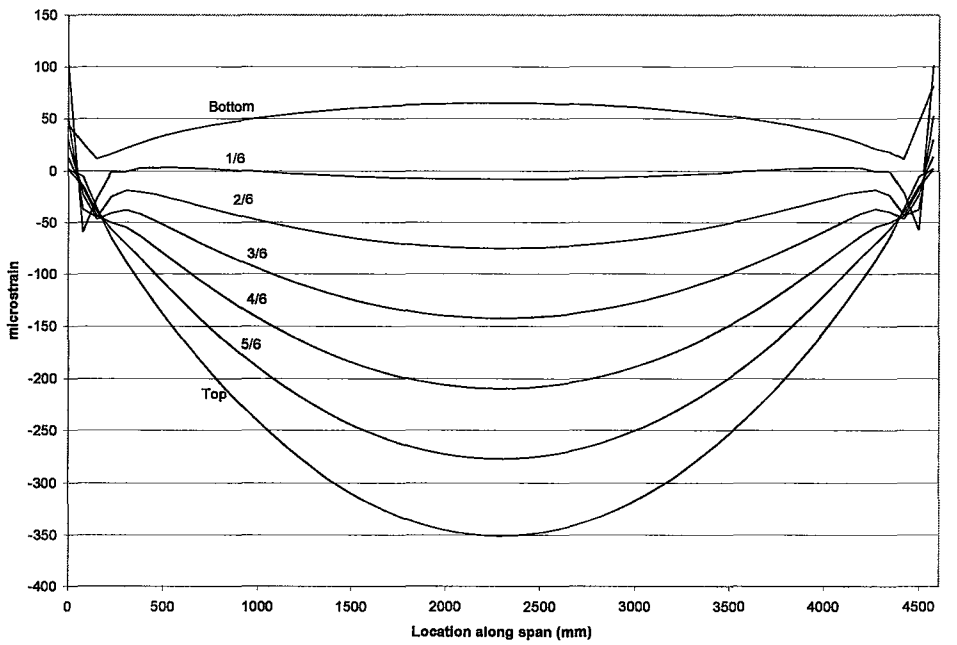

Figure 48: Longitudinal Strain Along Web at Various Heights – W8x18

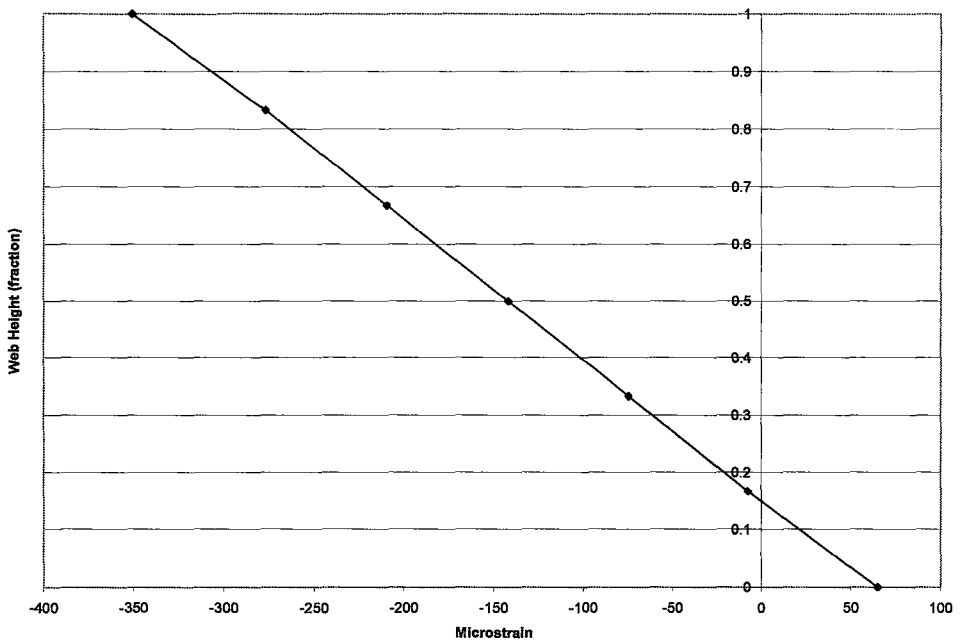

Figure 49: Longitudinal Strain – Location of Neutral Axis – W8x18

CHAPTER 4 PARAMETRIC STUDY

The finite element model developed in the previous chapter was shown to reasonably reflect the response of the beams tested in the experimental program. However, only two beam sections were tested. This chapter studies several other sections and their ability to reach certain design limits. The design limits generally considered by duct designers are first yield and overall section buckling. The post-buckled capacities, as well as the capacity beyond the elastic limit are not considered in this chapter.

The beams examined in this chapter are analyzed with the duct plate attached as before, and without the plate attached to determine the difference in capacity. The results of the analysis that includes the duct plate attached are then used to locate the neutral axis of each section. The neutral axis information is then used to acquire new geometrical parameters that may be used in an analytical analysis. Further analytical analysis is carried out to accommodate the load height factor and the effect of torsional bracing on the tension flange. The results from these calculations are then compared to the finite element results.

4.1 Finite Element Analysis of Stiffener Including Plate

Various beam sections with varying classes and heights were analyzed using the finite element model. The sections were selected by their b/2t ratio, where 'b' is the flange width, and 't' is the flange thickness. This ratio defines the class of the section. Section classes assist in determining the capacity of the compression flange to resist local buckling before overall buckling of the section. According to CISC Handbook of Steel Construction[9], a Class 1 section is controlled by yield and able to undergo large deformations without local flange buckling. A Class 2 section will reach yield but may experience local flange buckling in the plastic state. A Class 3 section has flanges that are long and thin that will buckle before the section is able to yield. A Class 4 section has flanges that are excessively thin and require special consideration in design. The limits for class designations were developed based on plate buckling theory. The American Institute of Steel Construction uses a similar approach to flange classification, but only uses three categories; compact, non-compact, and slender sections. The limits for the CISC classes and the AISC Compactness criteria are noted in Table 16.

For each range of section sizes between W6 and W12 listed in the AISC steel tables, a section from each class was found, with the exception of the W12's where only class 1 and 2 were available. Also, only one class 4 section was found within this range of beam sizes. The selection of beams chosen is listed in Table 17.

Table 17 lists the b/2t ratio, the class and compactness criteria, as well as the finite element results for the eigenvalues and stresses at buckling. The mode shape corresponding to the buckling load is also listed. For the buckling mode,

'Double' refers to a double curvature as illustrated in Figure 50, 'Flange buckling' refers to local flange buckling as illustrated in Figure 51, 'Single' refers to a single curvature as illustrated in Figure 52, and 'Half' refers to a half curvature as illustrated in Figure 53. Sections that have an elastic stress at buckling less than the nominal limit (345 MPa) are shown in bold.

Table 16: CISC and AISC flange buckling limits

Class Limits (CISC)			
1	2	3	4
$b/2t \leq 7.81$	≤ 9.15	≤ 10.77	> 10.77

AISC Compactness Limits		
Compact	Noncompact	Slender
$b/2t \leq 9.19$	≤ 13.43	> 13.43

Table 17: Yield and Buckling failure points for selection of beam sizes

Section	b/2t	CISC Class Criteria	AISC Compact section criteria	Buckling Eigenvalue	Elastic strain for unit load (μm/m)	Elastic Strain at buckling (μm/m)	Elastic Stress at buckling (MPa)	Mode of Buckling	Mode of Failure*
W6x16	4.98	1	Compact	13.307	-486	-6462	-1292.15	Double	Yield
W6x15	11.5	4	Noncompact	9.082	-544	-4937	-987.07	Flange buckling	Yield
W6x20	8.25	2	Compact	19.722	-398	-7850	-1569.62	Single	Yield
W8x10	9.61	3	Noncompact	4.598	-650	-2986	-597.14	Single	Yield
W8x18	7.95	2	Compact	11.339	-351	-3976	-795.05	Single	Yield
W8x21	6.59	1	Compact	14.418	-294	-4234	-846.62	Single	Yield
W10x12	9.43	3	Noncompact	4.598	-456	-2097	-419.29	Single	Yield
W10x19	5.09	1	Compact	9.472	-271	-2569	-513.77	Single	Yield
W10x33	9.15	2	Compact	22.974	-165	-3791	-757.97	Half	Yield
W12x14	8.82	2	Compact	4.55	-331	-1508	**-301.52**	Single	Buckle
W12x22	4.74	1	Compact	9.363	-201	-1878	-375.51	Single	Yield
W12x26	8.54	2	Compact	9.481	-167	-1584	**-316.75**	Half	Buckle

* Nominal yield stress = 345 MPa

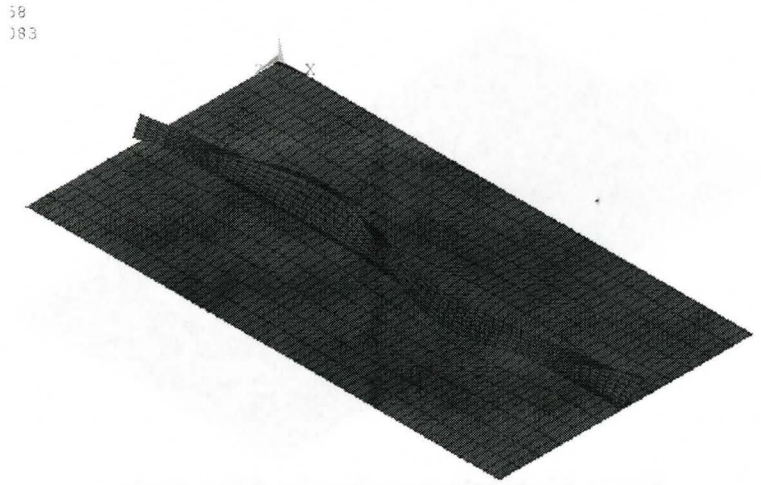

Figure 50: Double curvature buckling mode

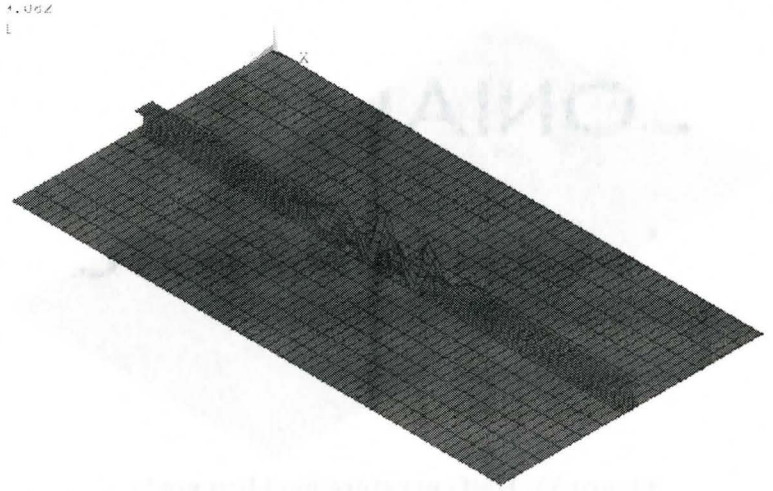

Figure 51: Local flange buckling mode

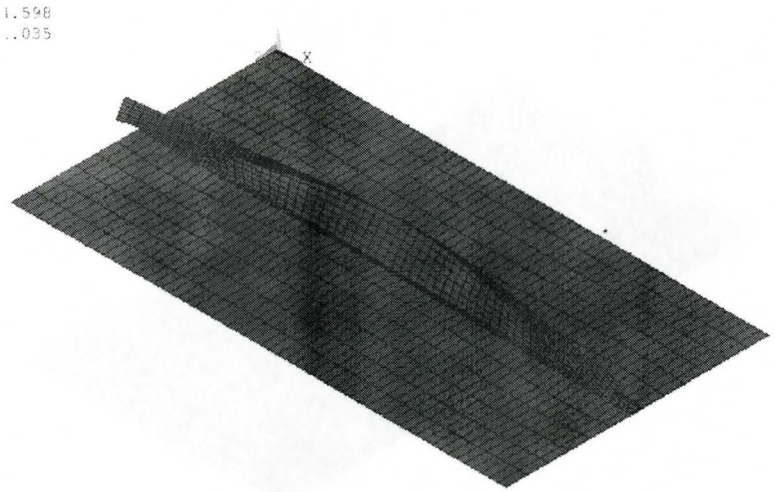

Figure 52: Single curvature buckling mode

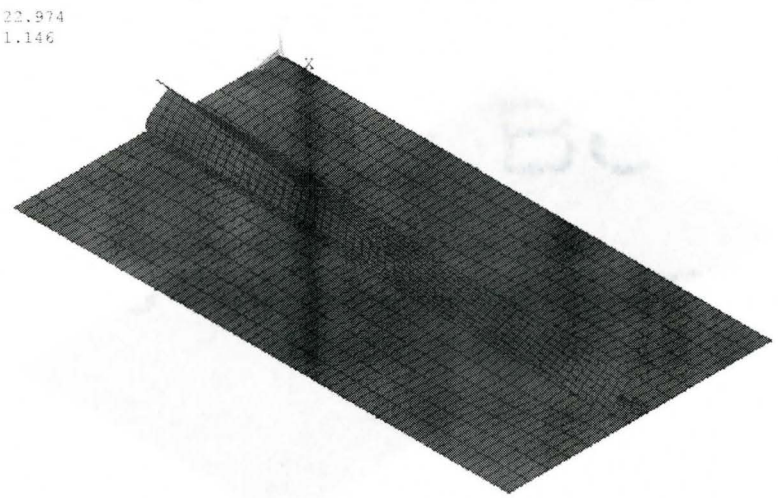

Figure 53: Half curvature buckling mode

The results show that only two sections reach the buckling limit at a load smaller than the yield limit. These are the W12x14 and W12x26. All other sections reach the yield limit first. For several sections, the buckling limit was high enough to predict linear elastic stresses three times the nominal yield value of the steel.

If the elastic strain at buckling was above the nominal yielding point of the steel, then the failure of the beam is deemed to be by yielding rather than by buckling. In some cases, buckling of the section may occur after the onset of first yield when portions of the beam are plastic, but practical design of stiffeners generally does not consider plastic analysis and is beyond the scope of this

analysis. The section is considered to have failed at either the point of first yield (extreme fibre yield) or by the onset of buckling.

Experimental results show that the post buckling capacity of the beam can be significant. Results of the experimental program showed that the W12x14 beam reached the point of buckling long before its final collapse. The rate of lateral deflection of the beam increased after the vacuum pressure reached approximately 33 kPa, indicating the buckling point had been reached. However, the beam did not collapse until approximately 45 kPa, a 40% greater capacity. The ultimate collapse was a result of local flange buckling despite being a class 2 section. As Table 17 illustrates, the point of overall buckling is achieved before the first yield (nominal yield at 345 MPa). At a point 40% higher than this, the beam has reached both plastic and post buckling behaviour before the ultimate collapse. In this regard, by using only first yield or onset of buckling leaves considerable room for maintaining a conservative design.

4.2 Finite Element Analysis of Sections Without Plate

The finite element analysis shown previously was repeated for the same selection of beams, but with the plate removed from the model. The imposed load was a uniform load along the length of the beam. The beams were simply supported, with one end fixed against displacement in all three axes, and the other end fixed against only vertical and lateral displacement. The boundary restraints were only applied to the bottom flange. The top flange and web were free to move in all directions. This analysis was performed to directly compare the effect of the plate on the capacity of the beams. Table 18 summarizes the data from this analysis.

Table 18: Yield and Buckling failure points for selection of beam sizes

Section	b/2t	CISC Class Criteria	AISC Compact section criteria	Buckling Eigenvalue from Ansys	Elastic strain for unit load ($x10^{-6}$)	Elastic Strain at buckling ($x10^{-6}$)	Elastic Stress at buckling (MPa)	Mode of Buckling	Mode of Failure*
W6x16	4.98	1	Compact	314.298	-4.11E-06	-1.29E-03	-258.19	Single	Buckling
W6x15	11.5	4	Noncompact	401.488	-4.41E-06	-1.77E-03	-354.22	Single	Yield
W6x20	8.25	2	Compact	658.541	-3.18E-06	-2.09E-03	-418.32	Single	Yield
W8x10	9.61	3	Noncompact	114.843	-5.63E-06	-6.46E-04	-129.25	Single	Buckling
W8x18	7.95	2	Compact	442.415	-2.83E-06	-1.25E-03	-249.96	Single	Buckling
W8x21	6.59	1	Compact	590.787	-2.35E-06	-1.39E-03	-277.43	Single	Buckling
W10x12	9.43	3	Noncompact	134.945	-4.02E-06	-5.43E-04	-108.59	Single	Buckling
W10x19	5.09	1	Compact	339.299	-2.29E-06	-7.76E-04	-155.17	Single	Buckling
W10x33	9.15	2	Compact	1618	-1.24E-06	-2.01E-03	-401.20	Single	Yield
W12x14	8.82	2	Compact	155.475	-2.95E-06	-4.59E-04	-91.71	Single	Buckling
W12x22	4.74	1	Compact	394.32	-1.69E-06	-6.66E-04	-133.14	Single	Buckling
W12x26	8.54	2	Compact	724.895	-1.29E-06	-9.38E-04	-187.50	Single	Buckling

* Nominal yield stress = 345 MPa

Table 18 illustrates that several sections (identified in bold) reached the buckling limit prior to reaching the nominal yield point. In the previous analysis in which the plate was part of the model, only two sections had reached the buckling limit first. Without the plate contribution however, the number of sections buckling before yielding increased to nine. Table 19 has reproduced the stress at buckling from both models for direct comparison.

Table 19 shows that the contribution of the plate has a substantial effect on the capacity of the beam. Aside from using a modified moment of inertia to limit deflection of the beam and thereby protect the local casing from buckling under positive pressure, a stiffener beam is currently sized without regard for the plate. From a practical viewpoint, it is recognized that the plate holds some restraining capacity. But this restraint is not applied directly to the compression flange and so gussets would be added to connect the compression flange to the plate. The items noted in bold will require gussets to reduce the unbraced length of the compression flange and allow the beam to be sized with a yielding limit state. By adding the plate to the analysis, the buckling load capacity is shown to increase on average by 327%.

Table 19: Stress at buckling limit - Stiffener with and without plate

Section	Elastic Stress at buckling Beam With Plate (MPa)	Elastic Stress at buckling Beam Without Plate (MPa)	% Difference
W6x16	-1292.15	**-258.19 (Y)***	501
W6x15	-987.07	-354.22	279
W6x20	-1569.62	-418.32	375
W8x10	-597.14	**-129.25 (Y)**	463
W8x18	-795.05	**-249.96 (Y)**	318
W8x21	-846.62	**-277.43 (Y)**	305
W10x12	-419.29	**-108.59 (Y)**	388
W10x19	-513.77	**-155.17 (Y)**	331
W10x33	-757.97	-401.20	189
W12x14	**-301.52 (Y)**	**-91.71 (Y)**	327
W12x22	-375.51	**-133.14 (Y)**	282
W12x26	**-316.75 (Y)**	**-187.50 (Y)**	168
			Mean = 327

* (Y) denotes section failed by yielding (345 MPa nominal yield stress)

4.3 Neutral Axis

When the location of the neutral axis is know, the factor F that determines the plate contribution can be derived as follows. The location of the neutral axis relative to the bottom of the plate is given by

$$NA = \frac{A_w\left(t + \frac{d}{2}\right) + A_p\left(\frac{t}{2}\right)}{A_w + A_p}, \tag{4-1}$$

where A_w is the beam area, t the plate thickness, d the beam height, and A_p the plate area. The plate area is a function of the factor, F and is given by

$$A_p = (Ft + b_f)t \tag{4-2}$$

The parameters for these equations are illustrated in Figure 54.

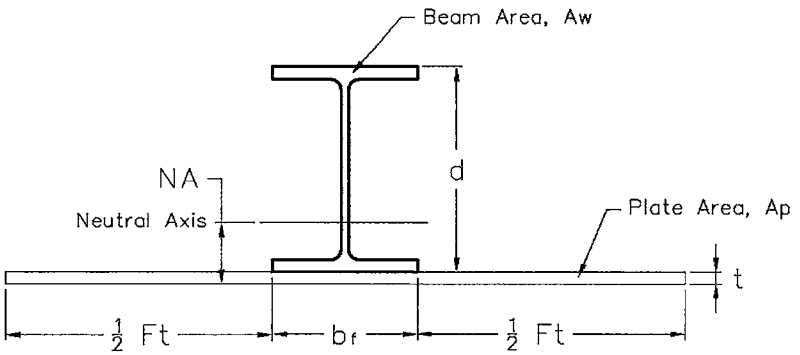

Figure 54: Parameters for Equation 4-1

Note that the flange width, 'b_f', is included in the plate area since the plate contribution factor is generally considered as the amount of plate beyond the flange toe. Here, F is a scalar value that is multiplied by the plate thickness resulting in a plate width.
Substituting A_p into Equation 4-1 yields

$$NA = \frac{A_w\left(t + \frac{d}{2}\right) + (Ft + b_f)t\left(\frac{t}{2}\right)}{A_w + (Ft + b_f)t} \tag{4-3}$$

Rearrange and solve for F:

$$F = \frac{A_w\left(t + \frac{d}{2}\right) + \frac{b_f t^2}{2} - \left(A_w + b_f t\right)NA}{t^2 NA - \frac{t^3}{2}} \tag{4-4}$$

As illustrated in Figure 54, Equation 4-4 was derived by locating the neutral axis with respect to the bottom of the plate. However, the finite element model was constructed using shell elements, and the bottom flange and the plate are actually coincident in space. The nodes of the plate and flange are separate except at the flange toe where the beam is 'welded' to the plate. This presents a slight discrepancy between the model and the actual structure. However, the plate and flange thicknesses are generally small relative to the overall height of the beam and the effect of the discrepancy can be considered negligible to the analysis.

The beam sections that were used in the previous section were analyzed to find the neutral axis of the composite beam/plate section. The axial strain of each node along the web height at the midspan of the beam was noted.

Table 20 lists the axial strain data along the webs of the various beams. The data has been normalized to show the strains as a fraction of the total beam height, and is plotted in Figure 55.

The neutral axis of the beam is located where the strain becomes zero. Table 21 summarizes the neutral axis heights for each beam and shows that the mean occurs at 14.8% of the beam height. Using Equation 4-4, the amount of plate that is needed to lower the neutral axis to that point is calculated. The column 'F' lists this scalar value for each beam. The mean value for 'F' is 414, meaning a plate width equivalent to 414 times the plate thickness, or '414t', contributes to the beam stiffness (varying between 361t to 485t). Figure 56 shows the distribution of the plate contribution factor.

The column representing 'Equivalent Plate Width' lists the actual width of plate considered to contribute to the beam, with a mean of 1890mm (74.4 in). This width does not include the width of plate under the beam flange. It should be noted that the actual width of plate used in the experimental test and in the finite element models was 2438mm (96 in) wide. Therefore it can be seen that the majority of the plate contributes to the stiffness of the beam. Referring to Figure 6 and Figure 7 of section 1.3.3, one did observe that the region of shear lag is significant. This shear lag area extends beyond the halfway point between the stiffener and the edge of the box which represents the location of the next stiffener. As such, the shear lag areas from each stiffener beam would have a significant overlap. The shear overlap would be additive where the plate strains do not exceed the yield limit, and would not diminish the effect of either adjacent beam. Considering the low height of the neutral axis on the beam/plate assembly, the top flange will reach the yield limit before the plate. Therefore by design, the plate will not reach yield limit and the overlapping shear lag will not affect the results shown here.

Table 20: Data from Neutral Axis Study

W6x15

Ex	Y	% of height
6.59E-05	0	0
-2.2E-05	0.998	0.167
-0.00012	1.997	0.333
-0.00023	2.995	0.5
-0.00033	3.993	0.667
-0.00043	4.992	0.833
-0.00054	5.990	1
	0.748	0.125

W6x16

Ex	Y	% of height
6.55E-05	0	0
-1.6E-05	1.047	0.167
-0.00011	2.093	0.333
-0.0002	3.140	0.5
-0.00029	4.187	0.667
-0.00038	5.233	0.833
-0.00049	6.280	1
	0.846	0.135

W6x20

Ex	Y	% of height
6.32E-05	0	0
-3.4E-06	1.033	0.167
-8E-05	2.067	0.333
-0.00016	3.100	0.5
-0.00023	4.133	0.667
-0.00031	5.167	0.833
-0.0004	6.200	1
	0.980	0.158

W8x10

Ex	Y	% of height
5.57E-05	0	0
-5.1E-05	1.315	0.167
-0.00017	2.630	0.333
-0.00029	3.945	0.5
-0.00041	5.260	0.667
-0.00052	6.575	0.833
-0.00065	7.890	1
	0.688	0.087

W8x18

Ex	Y	% of height
5.22E-05	0	0
-7.8E-06	1.357	0.167
-7.5E-05	2.713	0.333
-0.00014	4.070	0.5
-0.00021	5.427	0.667
-0.00028	6.783	0.833
-0.00035	8.140	1
	1.181	0.145

W8x21

Ex	Y	% of height
5.05E-05	0	0
-7.7E-07	1.380	0.167
-5.8E-05	2.760	0.333
-0.00012	4.140	0.5
-0.00017	5.520	0.667
-0.00023	6.900	0.833
-0.00029	8.280	1
	1.359	0.164

W10x12

Ex	Y	% of height
4.8E-05	0	0
-2.9E-05	1.645	0.167
-0.00011	3.290	0.333
-0.0002	4.935	0.5
-0.00028	6.580	0.667
-0.00037	8.225	0.833
-0.00046	9.870	1
	1.030	0.104

W10x19

Ex	Y	% of height
4.44E-05	0	0
-3.6E-06	1.707	0.167
-5.6E-05	3.413	0.333
-0.00011	5.120	0.5
-0.00016	6.827	0.667
-0.00021	8.533	0.833
-0.00027	10.240	1
	1.578	0.154

W10x33

Ex	Y	% of height
3.97E-05	0	0
9.87E-06	1.622	0.167
-2.4E-05	3.243	0.333
-5.8E-05	4.865	0.5
-9.3E-05	6.487	0.667
-0.00013	8.108	0.833
-0.00017	9.730	1
	2.158	0.222

W12x14

Ex	Y	% of height
4.13E-05	0	0
-1.6E-05	1.985	0.167
-7.8E-05	3.970	0.333
-0.00014	5.955	0.5
-0.0002	7.940	0.667
-0.00027	9.925	0.833
-0.00033	11.910	1
	1.439	0.121

W12x22

Ex	Y	% of height
3.75E-05	0	0
1.04E-06	2.052	0.167
-3.8E-05	4.103	0.333
-7.8E-05	6.155	0.5
-0.00012	8.207	0.667
-0.00016	10.258	0.833
-0.0002	12.310	1
	2.110	0.171

W12x26

Ex	Y	% of height
3.46E-05	0	0
4.37E-06	2.037	0.167
-2.9E-05	4.073	0.333
-6.3E-05	6.110	0.5
-9.7E-05	8.147	0.667
-0.00013	10.183	0.833
-0.00017	12.220	1
	2.331	0.191

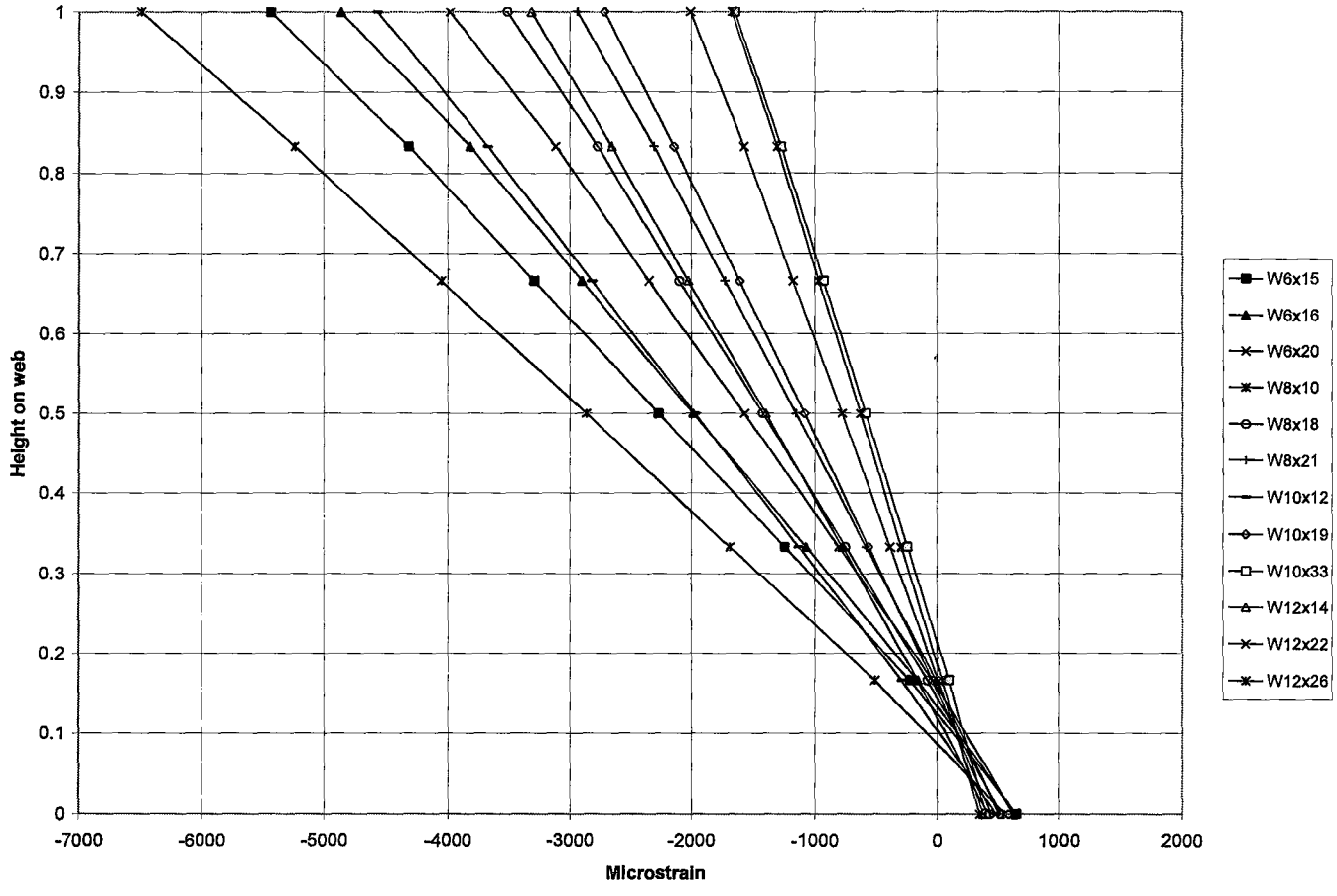

Figure 55: Location of Neutral Axis – Parametric Study

Table 21: Plate Contribution Factor, F

			Beam parameters				Equivalent plate width
	Neutral Axis	%	d	bf	A	F	F*t
W6x15	18.77	12.48	152.15	152.15	2871.0	457.4	2152.9
W6x16	21.23	13.47	159.51	102.36	3058.1	440.7	2074.2
W6x20	24.61	15.81	157.48	152.91	3800.0	421.1	1981.6
W8x10	17.28	8.73	200.41	100.08	1909.7	484.9	2281.8
W8x18	29.64	14.51	206.76	133.35	3393.5	412.1	1939.5
W8x21	34.12	16.42	210.31	133.86	3974.2	399.4	1879.7
W10x12	25.86	10.44	250.70	100.58	2283.9	435.7	2050.6
W10x19	39.60	15.41	259.08	102.11	3625.8	394.2	1855.2
W10x33	54.16	22.18	247.14	202.18	6264.5	361.7	1702.2
W12x14	36.13	12.09	302.26	100.84	2683.9	408.0	1920.2
W12x22	52.96	17.14	312.42	102.36	4180.6	380.9	1792.7
W12x26	58.52	19.08	309.88	164.85	4935.5	366.2	1723.4
	Mean (%)	14.8				414	
	SD (%)	3.7				35.2	
	COV (%)	25				8.5	

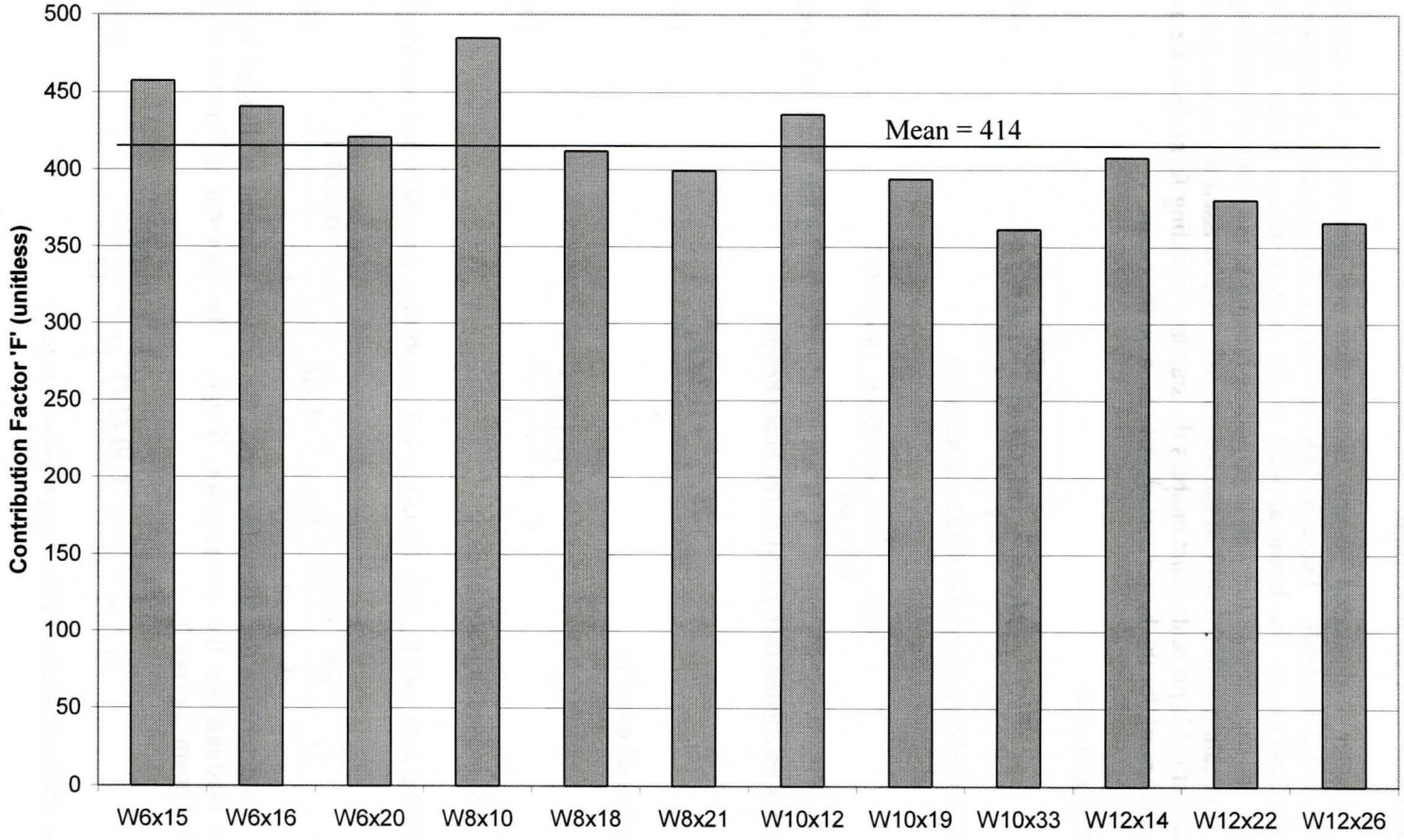

Figure 56: Plate Contribution Factor 'F'

4.4 Revised Analytical Method

Chapter 1 discussed several factors that are ignored in the standard stiffener design methods. These include accounting for the shift in the neutral axis, the loading on the beam applied to the bottom flange rather than the centroid, and the effect of the web in providing bracing to the compression flange.

In dealing with the shift of the neutral axis, as discussed in section 1.3.3, a general method is presented that enables the standard buckling formula to be used while accounting for the larger compressive area on the beam.

From Equation 1-1:

$$M_{cr} = \frac{\pi}{L}\sqrt{EI_y GJ + \left(\frac{\pi E}{L}\right)^2 I_y C_w} \tag{4-5}$$

The shear modulus, G, is calculated according to

$$G = \frac{E}{2(1+\mu)} = 0.385E \text{ , for } \mu=0.3 \tag{4-6}$$

where μ is the Poisson's ration. I_y is not greatly affected by the increase in beam height. J is calculated using 1.7d as the beam height;

$$J = \frac{2b_f t_f^{\,3} + (1.7d)t_w^{\,3}}{3} \tag{4-7}$$

C_w can be estimated by

$$C_w = \frac{(1.7d)^2 I_y}{4} \tag{4-8}$$

where 1.7d is used in place of d.

Substituting J, G, and C_w into Equation 4-5, combining constants and rearranging yields

$$M_{cr} = \frac{E\pi}{L}\sqrt{\frac{0.385}{3} I_y \left(2b_f t_f^{\,3} + 1.7dt_w^{\,3}\right) + \left(\frac{\pi}{L}\right)^2 \frac{(1.7d)^2 I_y}{4}} \tag{4-9}$$

To determine the allowable stress, the critical moment is divided by the section modulus for the compression flange. The moment of inertia of the modified beam is given by

$$I_x = 2\left(\frac{b_f t_f^{\,3}}{12} + A_f(0.85d)^2\right) + \frac{t_w(1.7d)^3}{12} \tag{4-10}$$

and the section modulus of the compression flange,

$$S_{xc} = \frac{I_x}{0.85d} \tag{4-12}$$

The allowable stress of the modified beam is then given by

$$F_b = \frac{0.85d\frac{E\pi}{L}\sqrt{\frac{0.385}{3}I_y\left(2b_f t_f^{\,3} + 1.7dt_w^{\,3}\right) + \left(\frac{\pi}{L}\right)^2 \frac{(1.7d)^2 I_y}{4}}}{I_x} \tag{4-13}$$

Equations 4-10 through 4-13 can be used to determine the critical moment of the beam section assuming a simply supported beam with no additional boundary conditions.

The bottom flange loading was discussed in section 1.3.2. A load applied to the bottom flange of a beam provides a restoring torque as the beam begins to twist under lateral torsional buckling. A revised moment modification factor, C_b, was used to account for this type of loading.

Tension flange bracing was described in section 1.3.1. The compression flange of a beam can be effectively braced if the tension flange is held to prevent rotation about the beam axis. By restraining the tension flange in this way, out of plane deflection, or buckling, must involve bending of the web. A sufficiently strong web will hold the compression flange in place without the use of additional gussets.

By applying in succession the critical moment equation for the beam with the shifted neutral axis, multiplying by a load height factor, and then adjusting the result to account for torsional bracing, a higher critical moment is then calculated. A less conservative stiffener capacity is thus obtained.

Table 22 lists the results of these successive calculations for the beam selection used previously. The formulae and input values used for the W12x14 section are shown in Appendix H.

Table 22: Revised analytical method results

	Variable	Unit	W12x14	W8x18	W6x20	W8x10	W8x21	W10x12	W10x19
Pressure at buckling	Papp	kPa (psi)	31.37 (4.55)	78.19 (11.34)	136.0 (19.72)	31.72 (4.60)	99.41 (14.42)	31.72 (4.60)	65.31 (9.472)
Equivalent moment from ANSYS	M_{ans}	kN*m (in*lb)	97.57 (863554)	243.15 (2152051)	422.91 (3743078)	98.60 (872664)	309.17 (2736421)	98.60 (872664)	203.11 (1797710)
Critical Moment	Mcr	kN*m (in*lb)	22.75 (201342)	59.14 (523446)	85.39 (755718)	15.13 (133942)	80.14 (709334)	18.40 (162808)	47.02 (416130)
% of Ansys			0.23	0.24	0.20	0.15	0.26	0.19	0.23
			Mean = 0.21 SD = 0.034 COV = 0.159						
Beam height	d_w	mm (in)	303 (11.91)	207 (8.14)	157 (6.2)	200 (7.89)	210 (8.28)	251 (9.87)	259 (10.2)
Flange thickness	t_f	mm (in)	5.7 (0.225)	8.4 (0.33)	9.3 (0.365)	5.2 (0.205)	10.2 (0.4)	5.3 (0.21)	10.0 (0.395)
Flange width	b_f	mm (in)	101 (3.97)	133 (5.25)	153 (6.02)	100 (3.94)	134 (5.27)	101 (3.96)	102 (4.02)
Flange area	A_f	mm^2 (in^2)	576 (0.893)	1118 (1.733)	1418 (2.197)	521 (0.808)	1360 (2.108)	537 (0.832)	1024 (1.588)
Web thickness	t_w	mm (in)	5.1 (0.2)	5.8 (0.23)	6.6 (0.26)	4.3 (0.17)	6.3 (0.25)	4.8 (0.19)	6.3 (0.25)
Torsional constant	J	mm^4 (in^4)	29303 (0.0704)	71592 (0.172)	102393 (0.246)	17731 (0.0426)	117377 (0.282)	22768 (0.0547)	96982 (0.233)
Warping constant	C_w	$10^9 mm^6$ (in^6)	21.64 (80.6)	32.76 (122)	30.34 (113)	8.3 (30.9)	40.82 (152)	13.67 (50.9)	27.93 (104)
Beam Y-Y moment of inertia	I_y	$10^3 mm^4$ (in^4)	982 (2.36)	3317 (7.97)	5536 (13.3)	870 (2.09)	4067 (9.77)	907 (2.18)	1786 (4.29)
Elastic modulus	E	GPa (ksi)	200 (29500)						
Shear modulus	G	GPa (ksi)	77 (11360)						
Nominal yield stress	F_y	MPa (ksi)	345 (50)						
Beam length	L	mm (in)	4572 (180)						
Stiffener spacing	b_s	mm (in)	1219 (48)						

Table 22 continued

Monosymmetric section									
Modified Beam height	d_m	mm (in)	514.3 (20.25)	351.5 (13.84)	267.7 (10.54)	340.61 (13.413)	357.6 (14.076)	426.2 (16.78)	440.4 (17.34)
Modified warping constant	C_{wm}	10^9 mm^6 (in^6)	64.96 (241.9)	102.45 (381.5)	99.2 (369.4)	25.24 (94.0)	129.94 (483.9)	41.19 (153.4)	86.6 (322.5)
Modified torsional constant	J_m	10^3mm^4 (in^4)	35.0 (0.0841)	75.7 (0.1819)	106.96 (0.2569)	18.6 (0.0446)	124.1 (0.2982)	26.1 (0.0628)	106.3 (0.2555)
Critical moment	M_{cr-m}	kN*m (in*lb)	32.60 (288516)	79.37 (702592)	109.26 (966997)	20.16 (178419)	104.28 (922975)	25.62 (226744)	59.83 (529576)
% of ANSYS (for comparison)			0.33	0.33	0.26	0.20	0.34	0.26	0.29
			Mean = 0.29 SD = 0.05 COV = 0.164)						
Load Height									
Beam constant	W_c		1.5081	1.2882	1.0666	1.2914	1.1332	1.3902	0.9993
Loading constant	A		1.12	1.12	1.12	1.12	1.12	1.12	1.12
Loading constant	B		1.456	1.433	1.395	1.434	1.408	1.446	1.381
Load height	Y_l	mm (in)	257 (10.12)	176 (6.92)	134 (5.27)	170 (6.71)	179 (7.04)	213 (8.39)	220 (8.67)
Moment modification factor	C_b		1.63	1.61	1.56	1.61	1.58	1.62	1.55
Moment capacity for monosymmetric section with load height consideration	M_{mslh}	kN*m (in*lb)	47.48 (420247)	113.8 (1007262)	152.4 (1349379)	28.9 (255867)	146.9 (1300018)	37.0 (327902)	82.6 (731266)
% of ANSYS (for comparison)			0.49	0.47	0.36	0.29	0.47	0.38	0.41
			Mean = 0.41 SD = 0.07 COV = 0.162						
Torsional bracing									
Casing thickness	t_{pl}	mm (in)	4.72 (0.1875)						
Casing strip I_{xx}	I_c	mm^4 (in^4)	228 (0.000549)						
Casing rotational stiffness	$beta_c$	kN*mm/ rad*mm (in*lb /rad*in)	12.509 (2812.2)						

Table 22 continued

Web rotational stiffness	$beta_{web}$	kN*mm/ rad*mm (in*lb /rad*in)	24.24 (5449.2)	53.94 (12125.9)	102.30 (22997.6)	22.47 (5051.5)	68.10 (15308.9)	25.08 (5637.7)	55.28 (12427.2)
Total casing and web rotational stiffness	$beta_{tot}$	kN*mm/ rad*mm (in*lb /rad*in)	8.25 (1854.9)	10.15 (2282.8)	11.15 (2505.8)	8.04 (1806.5)	10.57 (2375.8)	8.35 (1876.3)	10.20 (2293.3)
Moment capacity considering monosymmetric section, load height and torsional bracing.	M_{mslhtb}	kN*m (in*lb)	62.47 (552944)	140.72 (1245510)	189.19 (1674507)	47.51 (420534)	174.11 (1541034)	53.97 (477685)	102.62 (908280)
ANSYS Moment	M_{ans}	kN*m (in*lb)	97.57 (863554)	243.15 (2152051)	422.91 (3743078)	98.60 (872664)	309.17 (2736421)	98.60 (872664)	203.11 (1797710)
% of ANSYS (for comparison)			0.64	0.58	0.45	0.48	0.56	0.55	0.51
			Mean = 0.54 SD = 0.06 COV = 0.11						
Moment considering rigid casing	M_{mslhtb}	kN*m (in*lb)	84.25 (745641)	222.14 (1966102)	372.06 (3293014)	69.366 (613939)	279.11 (2470285)	77.47 (685622)	164.02 (1451716)
% of ANSYS			0.86	0.91	0.88	0.70	0.90	0.79	0.81
			Mean = 0.84 SD = 0.07 COV = 0.083						

The critical moments for each beam after each calculation step (each boundary condition considered) are illustrated in Figure 57. The bars illustrate the fraction of the critical moment that was predicted through the finite element modeling shown in section 4.1. Thus a bar reaching to 0.9 represents a critical moment equivalent to 90% of the predicted value according to the finite element analysis.

The left most bar for each section shows the result of the critical moment equation without any adjustments for boundary conditions. This represents the critical moment of the stiffener under current design rules. The mean value for this result is 0.21. The critical buckling formula alone accounts for approximately $1/5^{th}$ of the capacity of the stiffener beam as predicted by the finite element analysis.

The second bar from the left for each section shows the result of the critical moment equation if modified values are used to account for the larger area of compression due to the shift of the neutral axis. The mean value for this result is 0.29. This is an 8% increase over the buckling formula without accommodations for the larger compression area of the beam. The third bar from the left for each section shows the result of the critical moment equation if it is multiplied by the load height factor. The mean value for this result is 0.41. The fourth and fifth bar for each section show the results when torsional bracing is considered. Two cases were evaluated: Flexible casing plate and rigid casing plate. The flexible casing case considers a unit strip of metal that spans between adjacent stiffeners. The twisting rotation of the stiffener is resisted through the bending action of the metal strip. The formula used to establish the rotational stiffness of this strip is derived in Appendix J. This formula was derived with the aid of finite element analysis and considers the in-plane restraint of the plate as the beam rotates. This extra restraint results in some membrane tension in the plate which in turn provides more rotational stiffness. The mean value for the flexible casing result is 0.54.

It is realized that this flexible casing plate case is somewhat conservative. Although the formula considers some membrane action in the casing strip due to fixed end restraint, it does not account for the extra membrane tension field that is applied while the plate undergoes large deflections in response to the vacuum pressure. The deflections are large and the associated membrane stresses were shown to be significant as well. These additional membrane stresses provide a significantly higher stiffness to the unit strip of casing.

The unit casing strip also does not have uniform restraint down the length of the beam stiffener. The area of plate closer to the ends of the beam is affected by the sides of the duct and is rotationally stiffer than the strips at the centre of the beam. Therefore, the second case considered for torsional bracing assumes the extreme limit of rigid casing. This assumption may be somewhat unconservative. But as can be seen, the overall result remains less than the predicted buckling limit. The mean value for this result is 0.84. Each of these results only considers the limit of buckling. The failure mode of reaching first yield was not considered.

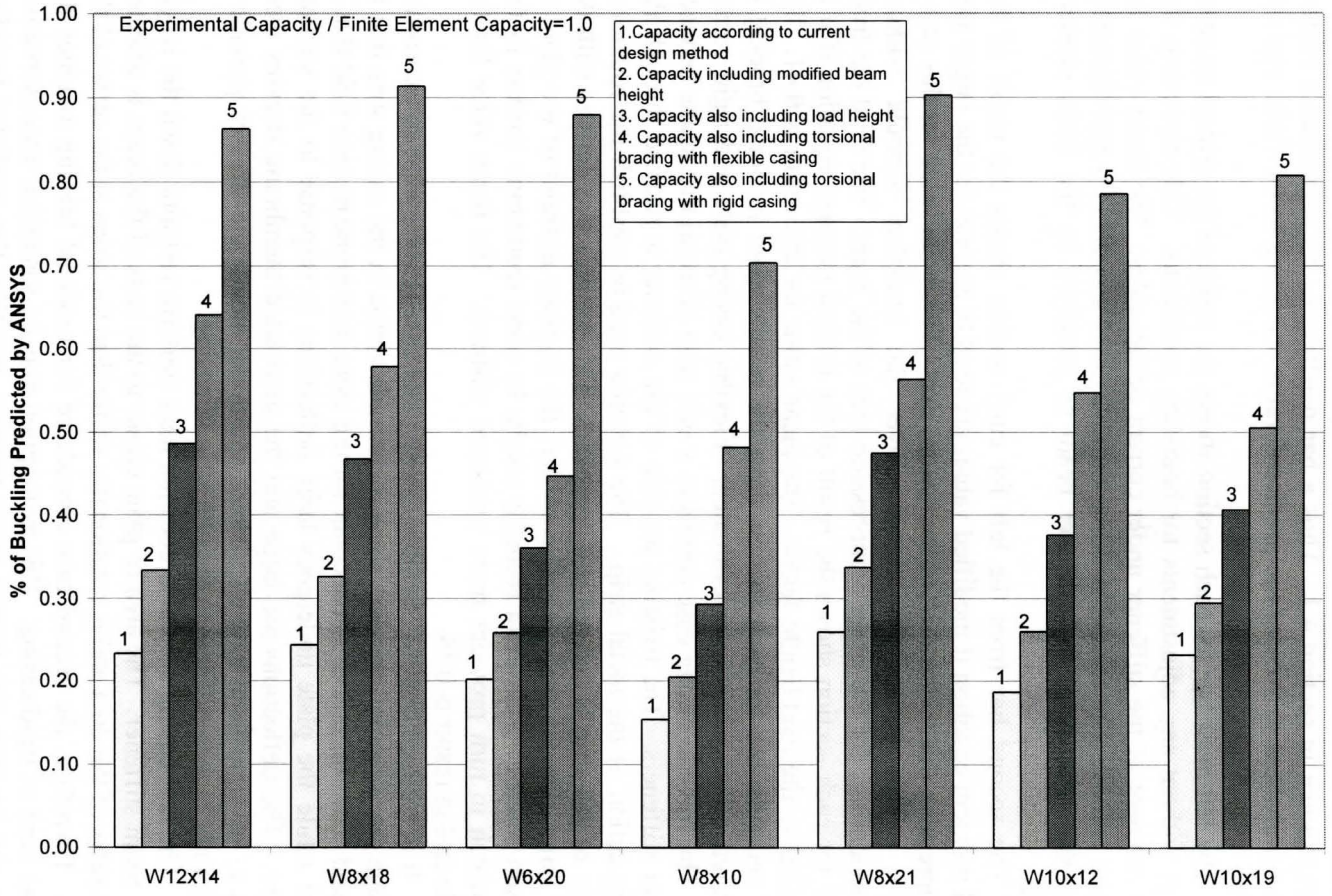

Figure 57: Beam Capacity with Various Load and Boundary Conditions

CHAPTER 5 SUMMARY, CONCLUSIONS, AND RECOMMENDATIONS

5.1 Summary

Industrial ducts are large structures that carry vast amounts of air or flue gas to and from industrial processes. The structural integrity of the ducts under load is maintained by ensuring the casing plate is sufficiently strong. As the width and depth of the ducts increases, the casing plate requires additional reinforcement and stiffening to withstand the applied loads. The stiffeners used for this purpose are commonly available steel shapes such as channels, angles and wide flange beams. The type and size of the stiffener depends on the length and the loads that must be resisted in order to maintain the integrity and shape of the duct.

This research has investigated the methods that are commonly used to analyze and design duct stiffeners. It was felt that these methods employ a large degree of conservatism and use assumptions that are normally applied to beams in buildings. Of particular interest was the practice of supplying gusset plates at the midspan of a stiffener if it is determined that the length of the compression flange is too long.

Also of interest was the amount of plate that is considered to contribute to the strength of a beam once they are welded together. A plate contribution factor is chosen based on assumptions and then used to establish a beam size that will be strong enough to resist the loads, and stiff enough to resist excessive deflections. The choice of a plate contribution factor value depends on the designer. This research identifies the amount of plate that contributes to the beam properties and relates it to commonly used values.

An experimental program was undertaken to investigate these concepts. Subsequently, a finite element model was developed to model the experimental program. Results from the finite element model were validated using the experimental data. A parametric study was carried out to determine the point of failure for each beam section, with failure being defined as either first yield or section buckling. An alternative analytical approach was proposed that includes the composite effect of the plate, the height of the load, and the ability of the casing and beam web to hold the compression flange and keep it from lateral buckling. The approach was shown to be still somewhat conservative.

5.2 Conclusions

This study has shown that the analytical design equations currently used to predict failure of stiffeners by buckling have a high degree of conservatism. Failure by yielding still needs to be checked independently. Excessive conservatism in design is uneconomical in that it adds substantial steel weight

resulting in higher capital cost, higher fabrication costs, and higher construction costs.

The results from this research program have led to the following conclusions:

1. The factor used to determine the plate contribution is grossly underestimated. The amount of plate that contributes to the composite section properties is found to be of the order of several hundred times the plate thickness.
2. The location of the neutral axis of the composite section is currently placed too high on the beam web. As a result, the capacity of the beam is underestimated.
3. The stiffness of the web to resist lateral buckling of the compression flange is overlooked. This research has shown that the web of a stiffener beam is an effective brace to prevent the lateral buckling of the compression flange.
4. Standard formulae used to calculate the capacity of a beam does not take into account the height of the applied load on the beam cross section. This research has shown that consideration of the load height provides a considerable increase in the calculated buckling capacity.

By incorporating the factors noted above, the size of a beam stiffener can be made smaller and more economical. This research has demonstrated that the consideration of these factors provides a solution that remains conservative and is below the point of failure by lateral buckling. The elastic response still needs to be checked as before, as is generally the governing mode of failure.

5.3 Recommendations for Future Research

The experimental program also revealed several items that need further investigation:

1. Stiffener beams on ducts are generally connected to each other at the corners to form a complete frame around the perimeter. The type of connection can vary. A common method is to use an 'L' shaped bracket that is welded to the webs of adjacent beams. The bracket provides additional boundary constraints on the ends of the beam that have not been considered here. The main purpose of the bracket (or any other attachment) is to provide a load path to accommodate the end reactions. The end reactions are taken into the adjacent beam in either the form of compression or tension loads depending on the pressure inside the duct. This forces each stiffener to act as a beam-column rather than as a simply supported beam. The extra compressive forces in the beam have not been considered and this presents a degree of unconservatism. However, this unconservative part of the design is overshadowed by the grossly conservative methods used otherwise. The brackets also provide a certain degree of lateral stiffness to the beam. This research did not consider any lateral support on the ends of the beam as a worst case check. The 'L'

brackets may provide relatively weak lateral support, but some support nonetheless. Further research should consider such support.

2. The experimental apparatus used in this research used a single stiffener on a large plate. The edges of plate parallel to the stiffener beam were supported by the box and intended to simulate the location of the next stiffener in a long line of stiffeners along a duct. The interaction between the plate and the stiffener was demonstrated and it was shown that the majority of the plate acted to influence the strength of the beam. Further research should include more than one stiffener section so that the plate contribution to each section can be determined.
3. The point of failure of the stiffener beam was taken as either first yield or the onset of buckling. It was found during the experimental program that the capacity of the beam beyond these points was substantial. The W12x14 beam exhibited post-buckling strength up to 45 kPa when the buckling limit was at 33 kPa. As it was, the beam ultimately failed by local flange buckling rather than overall section buckling. Likewise, the W8x18 beam passed the yield point and maintained its capacity well into the plastic region. The tests were only terminated after the beam bottomed out on the bottom of the box. Further study into the post yield and post buckling capacity should be conducted.
4. This research only examined wide flange shapes as stiffeners. It is recognized that many ducts are stiffened using other shapes such as channels and angles. These shapes are not symmetric about their strong axis and have a shear center offset from their centroid. This research has not addressed these other shapes and the effect of the unsymmetrical section.

REFERENCES

1. Air and Gas Duct Structural Design Committee of the Energy Division of the ASCE. The Structural Design of Air and Gas Ducts for Power Stations and Industrial Boiler Applications. Reston: American Society of Civil Engineers, 1995.
2. American Institute of Steel Construction. Manual of Steel Construction – Allowable Stress Design., 9th ed. Chicago: AISC, 1989.
3. American Institute of Steel Construction. Manual of Steel Construction – Load and Resistance Factor Design. 3rd ed. Chicago: AISC, 1999.
4. ANSYS Professional. Computer Software. ANSYS Incorporated, 2005.
5. Bleich, F. Buckling Strength of Metal Structures. New York: McGraw-Hill, 1952.
6. Blodgett, O. Design of Welded Structures. James F. Lincoln Arc Welding Foundation: Cleveland, 1966.
7. Brockenbrough, R.L., and B.G. Johnston. Steel Design Manual. Pittsburgh: United States Steel Corporation, 1968.
8. Canadian Standards Association. Limit States Design of Steel Structures. CAN/CSA-S16-01. Rexdale: CSA, 2003.
9. Canadian Institute of Steel Construction. Handbook of Steel Construction. 8th ed. 2nd Printing. Willowdale: CISC-IAAC, 2004.
10. Galambos, T.V. Guide to Stability Design Criteria for Metal Structures. 5th edition. Rolla: Structural Stability Research Council, 1998.
11. Gaylord, E.H., and C.N. Gaylord. Design of Steel Structures. 2nd edition. New York: McGraw Hill, 1972.

12. Heins, C.P., and R.A. Potochk. "Torsional Stiffening of I-Girder Webs." Journal of the Structural Division. American Society of Civil Engineers. Vol. 105. No. ST8. Proc. Paper 14788. August 1979: 1689-1698.

13. Humphreys, W. "Stress in Flat Rectangular Plates–With Deflection Exceeding One-Half Plate Thickness." Design News. May 26, 1965.

14. Milner, H.R. "The Buckling of Equal Flanged Beams under Uniform Moment Restrained Torsionally by Stiff Braces." Fifth Australian Conference on the Mechanics of Structures and Materials. Melbourne (1975): 405-420

15. Milner, H.R. "The Design of Simply Supported Beams Braced Against Twisting on the Tension Flange." Civil Engineering Transactions. Institute of Engineers. Australia. Vol. CE19. No. 1. (1977): 37-42

16. National Fire Protection Association. NFPA 85: Boiler and Combustion Systems Hazard Code. Quincy: NFPA, 2004.

17. Ojalvo, M., and R.S. Chambers. "Effect of Warping Restraints on I-Beam Buckling." Journal of the Structural Division. American Society of Civil Engineers. Vol. 103. ST12. December 1977: 2351-2360.

18. Szewczak, R.M., E.A. Smith, and J.T. Dewolf. "Beams with Torsional Stiffeners." Journal of Structural Engineering, American Society of Civil Engineers. Vol. 109. No. 7. July 1983: 1635-1647.

19. Taylor, A.C, and M. Ojalvo, "Torsional Restraint of Lateral Buckling", Journal of the Structural Division. American Society of Civil Engineers. ST2. April 1966: 115-129.

20. The Babcock & Wilcox Company. Steam/Its Generation and Use. 40th ed., Barberton: B&W, 1992.

21. Timoshenko, S.P., and J.M. Gere. Theory of Elastic Stability. 2nd ed. New York: McGraw Hill, 1961.

22. Valentino, J., and N.S. Trahair. "Torsional Restraint Against Elastic Lateral Buckling." Journal of Structural Engineering, American Society of Civil Engineers. Vol 124. No. 10. October 1998: 1217-1225.

23. Vacharajittiphan, P., and N.S. Trahair. "Warping and Distortion at I-Section Joints." Journal of the Structural Division, American Society of Civil Engineers. Vol. 101. No. ST8. August 1975: 1703-1705.

24. Winter, G. "Lateral Bracing of Columns and Beams." ASCE Transactions. American Society of Civil Engineers. Paper No. 3044. Vol. 125: 807-825.

25. Young, W.C. Roark's Formulas for Stress & Strain. 6th ed. New York: McGraw Hill, 1989.

26. Yura, J.A. "Fundamentals of Beam Bracing." Is Your Structure Suitably Braced? Milwaukee: Structural Stability Research Council, 1993.

27. Udall, J.D., S.E. Chidiac and B. Halabieh. "Effective Design of Stiffeners on Industrial Ducts." 1st Canadian Conference on Effective Design of Structures. McMaster University (2005): 237-246

APPENDIX A – DESIGN EXAMPLE

A design example is used to demonstrate the design processes. The example will only illustrate the design of a stiffener with a single pressure load. It is assumed that this pressure load is inclusive of other applied loads and represents the most critical combination of loads for this stiffener.

The parameters of the calculation are as follows:

- Stiffener – W12×14 (equivalent to W310×21)
- Stiffener span - 4570 mm (15')
- Stiffener spacing along duct- 1220 mm (4')
- Duct thickness – 4.7 mm (3/16")
- Temperature – ambient (70 deg F)
- Internal pressure – 8.717 kPa (35 in·H_2O)
- Stiffener material – 350 MPa (50 ksi)
- Elastic modulus – 200 GPa (29.5×10^6 psi)

A W12×14 section was chosen for its slenderness and poor ability to resist lateral buckling. The geometry of the duct is arbitrarily chosen to match the experimental arrangement described later.

Engineering firms have generally adopted the following method or conduct similar calculations with variations of this method. Currently there is no standard method presented in building structural or other codes.

The first step in the design process is to determine the spacing of the stiffeners. The ultimate goal of duct design is to create a structurally stable duct for the process it is used with. Therefore, stiffeners are added to reinforce the casing plate of the duct, thereby allowing larger ducts with larger air or gas capacity. The stiffeners are spaced to minimize the stress applied to the casing plate while maintaining an economical design. Should the width of the casing plate be sufficiently small no stiffeners are required. Casing stress can be calculated by assuming a unit width strip acting as a beam with uniform load, and limiting the bending stress. However, this provides a grossly conservative design since it does not consider the membrane tension capacity of the plate cross section. A more forgiving method is to use large deflection plate theory as described in Roark[25]. Roark's analysis uses tabulated values based on parameters including panel geometry, edge restraint conditions, etc. A formula has been developed that reasonably fits a curve connecting the values of Roark's table (Ref. 25, page 480).

After the spacing is defined, the load to the stiffener can be determined. The moment generated by negative pressure is calculated assuming a simply supported beam with uniform load. The applied bending stress on the stiffener resulting from this moment is affected by the composite action of the plate welded to the stiffener beam. The amount of plate that contributes to the bending properties of the beam is determined by the amount of plate that will

accommodate compression without buckling. Common values for this are between 20 times to 42 times the thickness of the plate, or 20t to 42t, depending on the design office.

The allowable bending stress for a W12x14 beam, considering the full span of beam as the length of the unbraced compression flange, is given by F_b. The equations for F_b determine the limit for failure by lateral torsional buckling. In the following example, the applied stress on the composite section is greater than the allowable stress. Therefore, the beam is not adequate for the loading under either the design limit or the actual buckling limit. The allowable bending stress can be increased by reducing the unbraced length of the compression flange. This is accomplished by providing a set of gusset plates between the flanges on both sides of the beam web. The gussets act to connect the outstanding compression flange to the tension flange that is presumed to be stabilized by the casing. Using half of the beam span for the unbraced length, the allowable stress increases and the section passes.

Design Example:

Conventional Stiffener Design Example:

Air duct
15 ft wide
35 inH2O internal negative design pressure
70 deg F
Grade 50 stiffener materials

Determine the size of the stiffener based on conventional methods.

Material Properties for nominal 50ksi steel:

$F_y := 50000\,psi$ Yield Stress

$E := 29500\,ksi$ Elastic Modulus

$G := 0.385E$

$F_t := \frac{2}{3}\cdot F_y$ $F_t = 33.333\ ksi$ Allowable tension design stress considering 33% safety factor

Duct Properties:

$t := \frac{3}{16}in$ duct casing thickness

$L := 15ft$ duct width (stiffener span)

$P := 1.264psi$ Internal pressure plus dead weight of casing and live load, equivalent to 35 inH2O

Determine the maximum stiffener spacing based on large deflection plate theory. For the purposes of this example, a pre-determined width of 48in is chosen.

$b := 48in$

Moment applied to stiffener beam from internal pressure and other loads

$M_{app} := \frac{P\cdot b\cdot L^2}{8}$ $M_{app} = 245.722\times 10^3\ lbf\cdot in$

$S_{req} := \frac{M_{app}}{0.66\cdot F_y}$ $S_{req} = 7.446\ in^3$ Minimum required section modulus
Note: The required section modulus may be decreased somewhat by the addition of a 'transient factor' applied to the allowable stress.

$I_{req} := \frac{5\cdot(240)\cdot P\cdot L^3\cdot b}{384\cdot E}$ Minimum required moment of inertia for deflection requirements. The factor '240' represents the deflection limit of L/240. This moment of inertia shall be for the composite beam and plate section.

$I_{req} = 37.483\ in^4$

Try W12x14 welded to 3/16" casing to get the required section modulus and moment of inertia

Determine moment of inertia of stiffener combined with attached casing:

$I_{stiff} := 88.6 \cdot in^4$

$d_{stiff} := 11.9in$ W12x14 section properties

$A_{stiff} := 4.16 \cdot in^2$

$t = 0.1875\ in$ Casing thickness

$w := 42 \cdot t$ effective width of plate to consider part of the composite beam

$I_{case} := \frac{w \cdot t^3}{12}$ $I_{case} = 4.326 \times 10^{-3}\ in^4$

$A_{case} := w \cdot t$ $A_{case} = 1.477\ in^2$ Casing properties

$d_{cg} := \frac{A_{case} \cdot \frac{t}{2} + A_{stiff} \left(t + \frac{d_{stiff}}{2} \right)}{A_{case} + A_{stiff}}$ $d_{cg} = 4.554\ in$ Location of center of gravity wrt bottom of casing

$I_{tot} := I_{case} + I_{stiff} + A_{case} \cdot \left(d_{cg} - \frac{t}{2} \right)^2 + A_{stiff} \left(\frac{d_{stiff}}{2} + t - d_{cg} \right)^2$ $I_{tot} = 128.41\ in^4 > I_{req} = 37.483\ in^4$

Composite section moment of inertia greater than minimum. Deflection will be less than L/240 at design pressures.

Elastic Section Modulus for compression flange:

$S_c := \frac{I_{tot}}{d_{stiff} + t - d_{cg}}$ $S_c = 17.046\ in^3 > S_{req} = 7.446\ in^3$ OK - Section will pass under elastic conditions. But first need to check for compression flange buckling to ensure section will pass.

Stress applied to compression flange

$f_b := \frac{M_{app}}{S_c}$ $f_b = 14.415\ ksi$

Determine allowable bending stress for stiffener based on using the full stiffener span for the unbraced length of the compression flange

Member dimensions: W12x14

$t_w := 0.2in$ $I_x := 88.6 \cdot in^4$ $J := 0.0704 in^4$

$d := 11.9in$ $I_y := 2.36 in^4$ $C_w := 80.6 in^6$

$b_f := 3.78in$

$A_f := 0.893 in^2$ $S_x := 14.9 in^3$

$r_t := 0.95in$ $Z_x := 17.4 in^3$

$L_b := 180in$ Stiffener unbraced length

Using the methods of AISC-ASD 9th ed:

Note: This is a conservative method that ignores either warping (non-uniform) or St. Venant (uniform) torsion. The factor L/rt is used to determine which torsional component is ignored.

$C_b := 1.12$ Moment modification factor for uniformly distributed load

$$L_c := \frac{20000 ksi}{\left(\frac{d}{A_f}\right) \cdot F_y} \qquad L_c = 30.017 in$$

Critical span for lateral overturning is controlled by d/Af

$$\frac{L_b}{r_t} = 189.474 > \sqrt{\frac{510 \times 10^3 ksi \cdot C_b}{F_y}} = 106.883$$

Therefore: $$F_{b1} := \frac{12 \cdot 10^3 ksi \cdot C_b}{\left(L_b \cdot \frac{d}{A_f}\right)} \qquad F_{b1} = 5.603 ksi < f_b = 14.415 ksi$$

Allowable bending stress — Applied bending stress

Removing a built in safety factor: $\frac{F_{b1}}{0.6} = 9.339 ksi$ **Section fails**

Using standard beam buckling formula for transverse loading:

$$M_{cr} := \frac{C_b \cdot \pi}{L_b} \cdot \sqrt{E \cdot I_y \cdot G \cdot J + \left(\frac{\pi \cdot E}{L}\right)^2 \cdot I_y \cdot C_w} \qquad M_{cr} = 201.342 \times 10^3 lbf \cdot in < M_{app} = 245.722 \times 10^3 lbf \cdot in$$

Section fails

This section is not acceptable. Even though the section was proved to pass elastically, and satisfied deflection criteria, the beam fails under buckling. To improve buckling capacity, a stiffener gusset can be added to reduce unbraced length. A gusset does not improve the elastic strength of the beam.

Decrease unbraced length by half with the addition of a gusset at midspan.

$L_b := \frac{L}{2}$ Stiffener span $L_b = 90\,in$

Using AISC-ASD 9th ed.:

$$\sqrt{\frac{102\cdot10^3\cdot ksi\cdot C_b}{F_y}} = 47.8 \quad > \quad \frac{L_b}{r_t} = 94.737 \quad > \quad \sqrt{\frac{510\cdot10^3 ksi\cdot C_b}{F_y}} = 106.883$$

$$F_{b2} := \left[\frac{2}{3} - \frac{\left(\frac{L_b}{r_t}\right)^2\cdot F_y}{1530\cdot10^3\cdot ksi\cdot C_b}\right]\cdot F_y \qquad F_{b2} = 20.239\,ksi \qquad \frac{F_{b2}}{0.6} = 33.732\,ksi \quad > \quad f_b = 14.415\,ksi$$

removing safety factor

Section passes

Using standard beam buckling formula

$$M_{cr} := \frac{C_b\cdot\pi}{L_b}\cdot\sqrt{E\cdot I_y\cdot G\cdot J + \left(\frac{\pi\cdot E}{L}\right)^2\cdot I_y\cdot C_w} \qquad M_{cr} = 402.685\times10^3\,lbf\cdot in \quad < \quad M_{app} = 245.722\times10^3\,lbf\cdot in$$

Section passes

Should this section still failed after the addition of a set of gussets, a second set would be added, with each placed at the 1/3 points on the beam span.

The addition of a gusset stiffener involves attaching two small plates to the web of the beam in order to provide a load path from the outstanding compression flange into the laterally braced tension flange. These sections of plate add cost to the structure primarily in terms of labour and time.

The philosophy of adding gussets to provide a load path to the braced flange does not take into account the stiffness of the web that already provides a load path.

APPENDIX B - STRAIN GAUGE LAYOUT

The following figures show the test apparatus from a plan view. The strain gauges in the figures are located in the precise location where they were placed on the test box. The '900' number beside each reflects the channel identification as output by the data logger. The letters in brackets beside the channel number represent the spreadsheet column letters for each channel once the data was imported into Excel. The spreadsheet columns are noted for reference only.

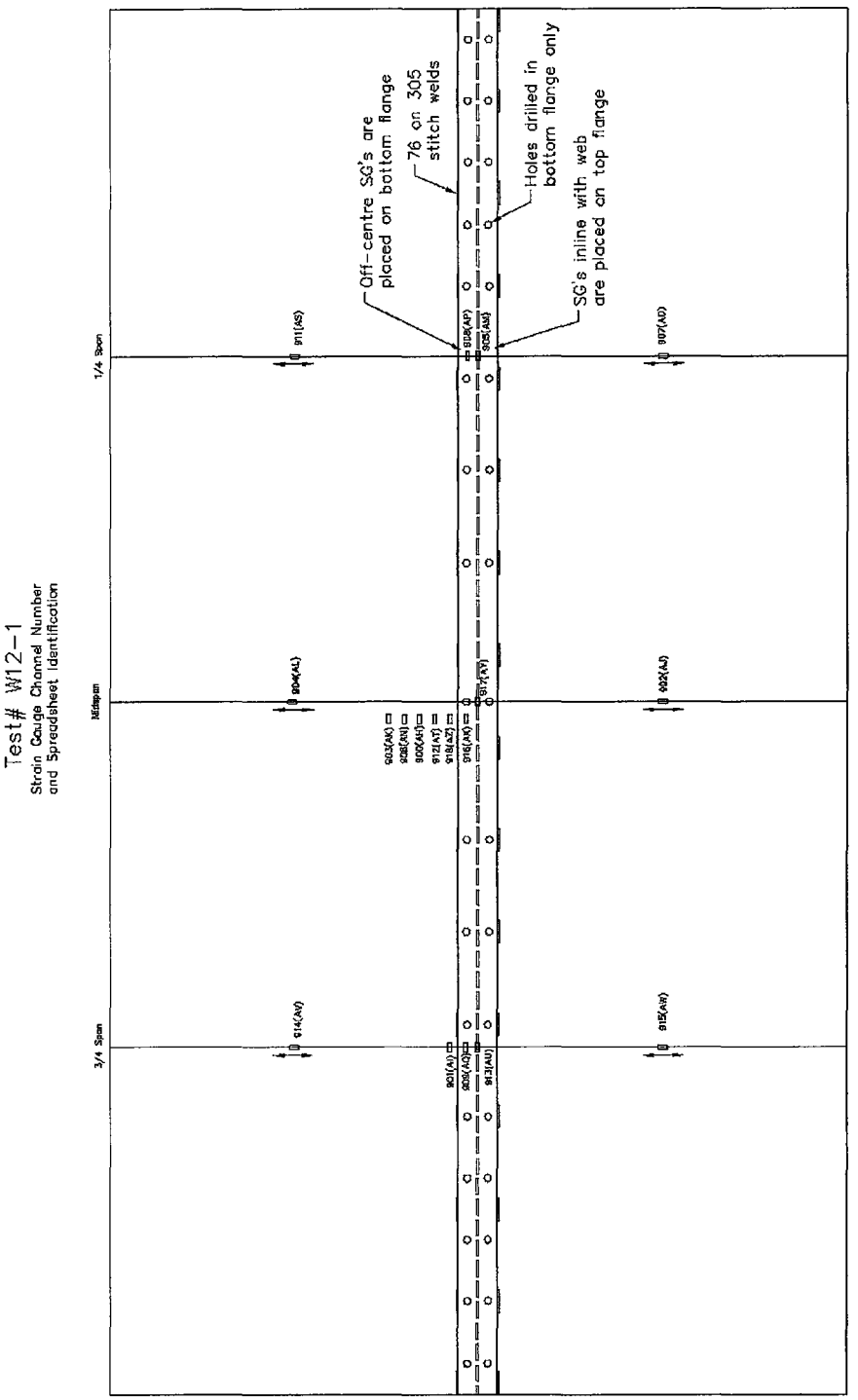

Figure 58: Strain Guage Layout W12-1

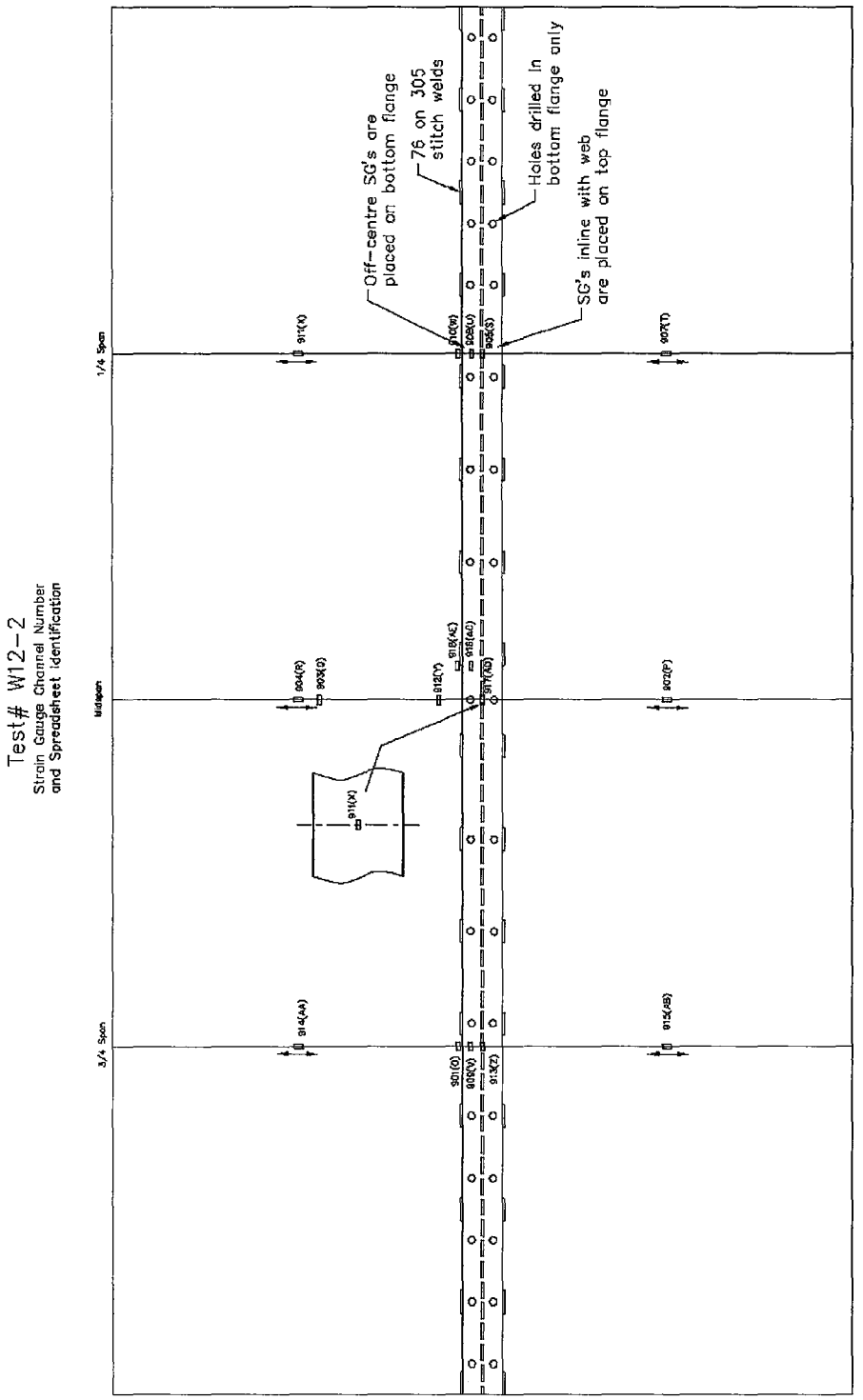

Figure 59: Strain Guage Layout W12-2

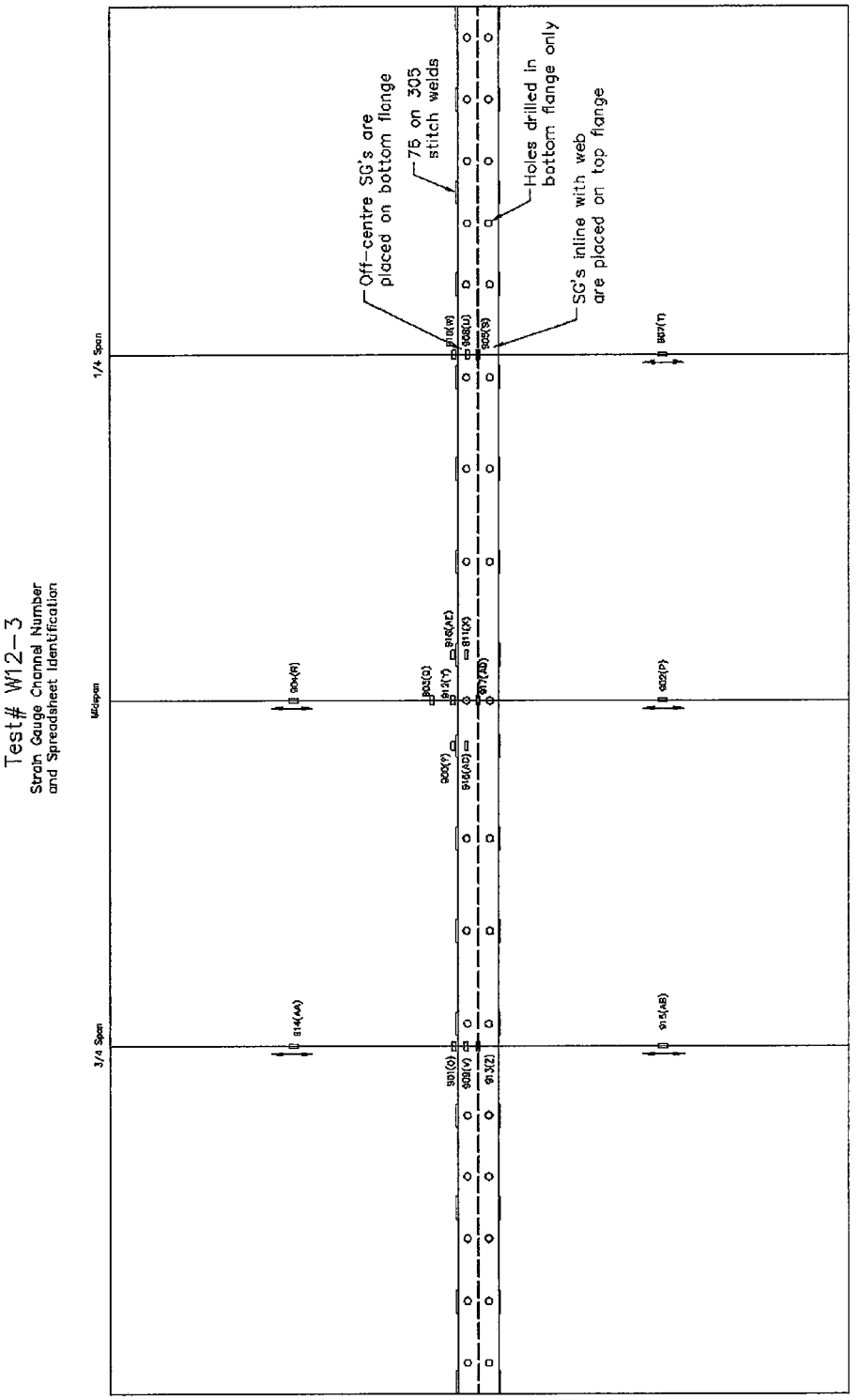

Figure 60: Strain Guage Layout W12-3

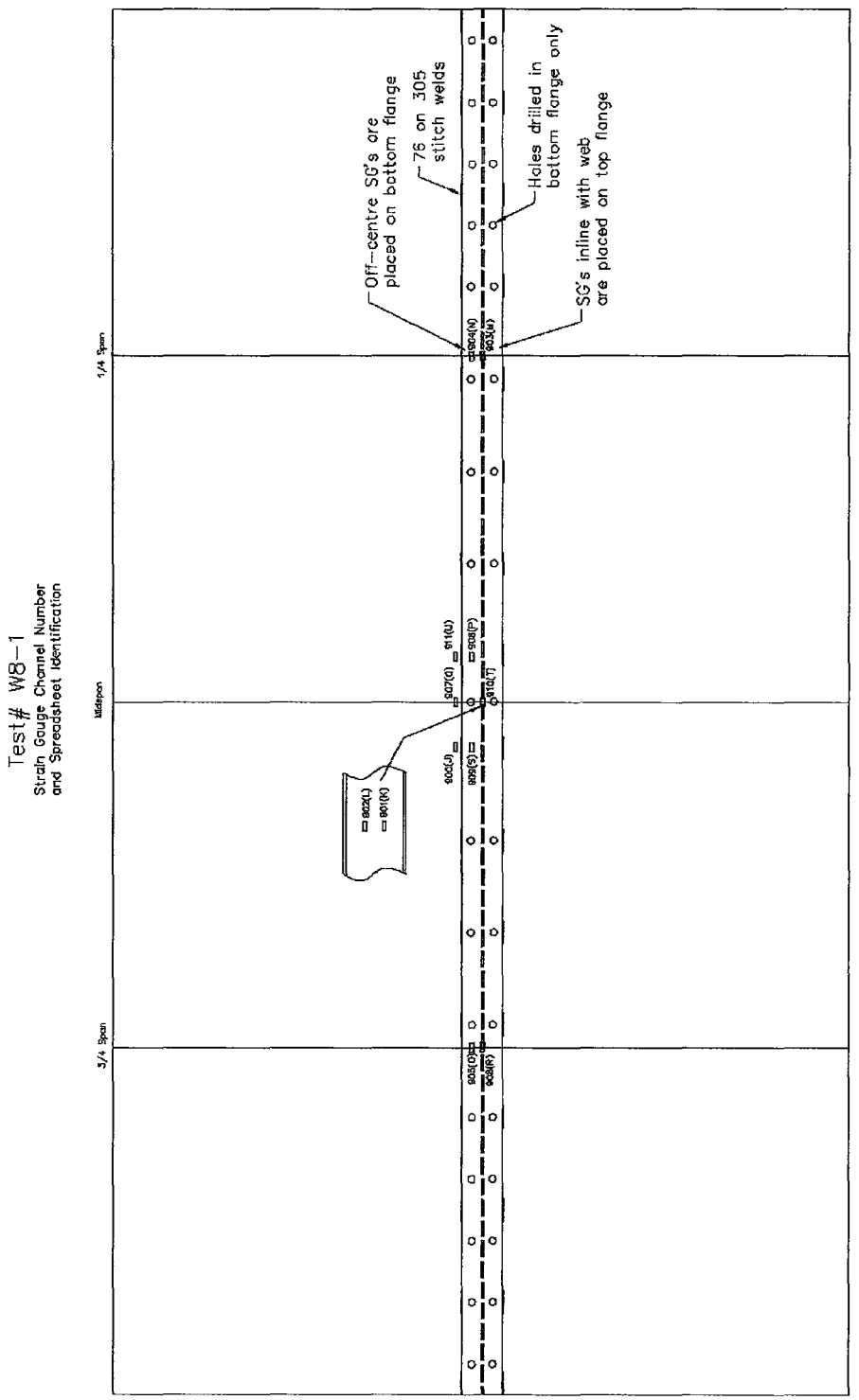

Figure 61: Strain Guage Layout W8-1

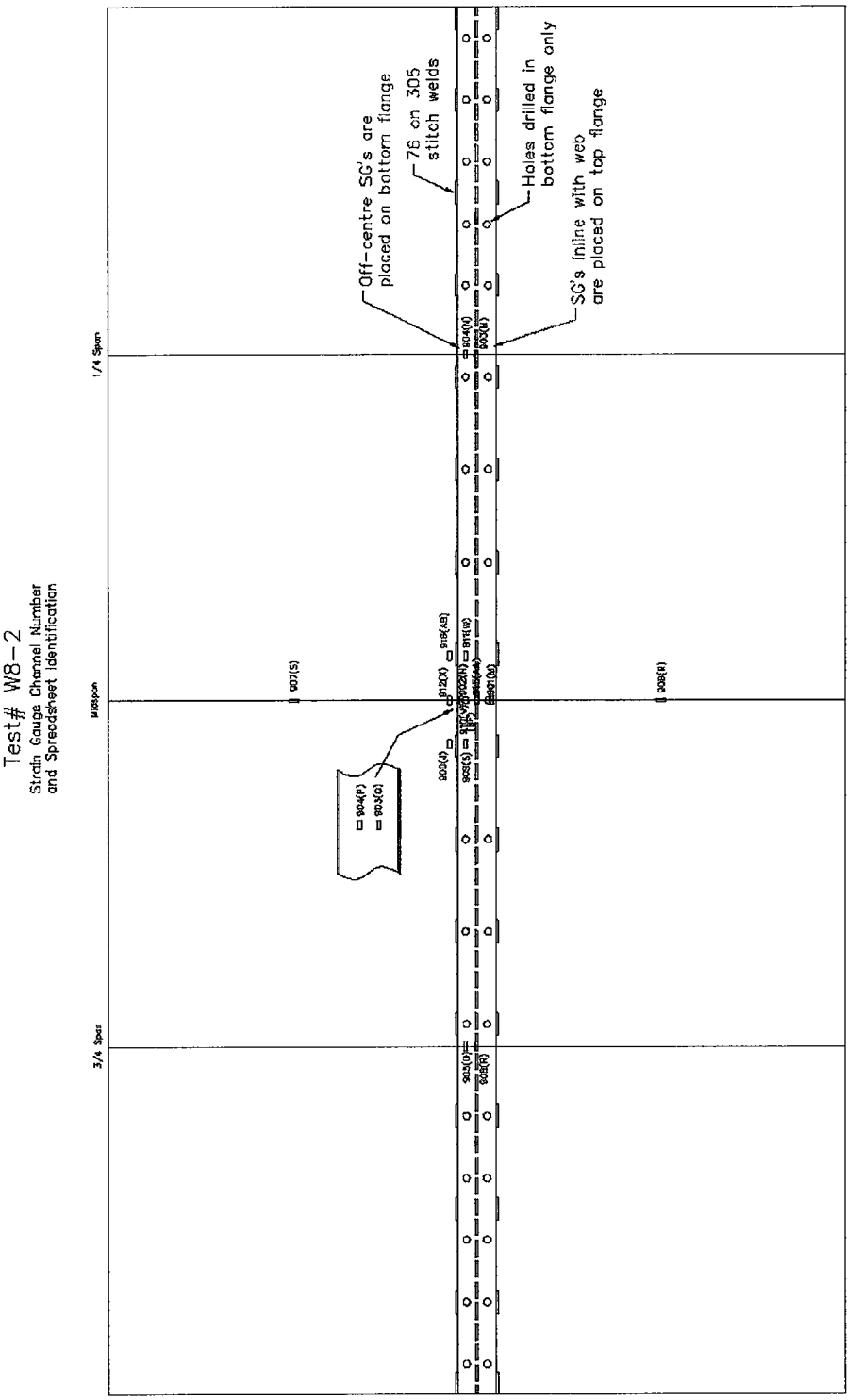

Figure 62: Strain Guage Layout W8-2

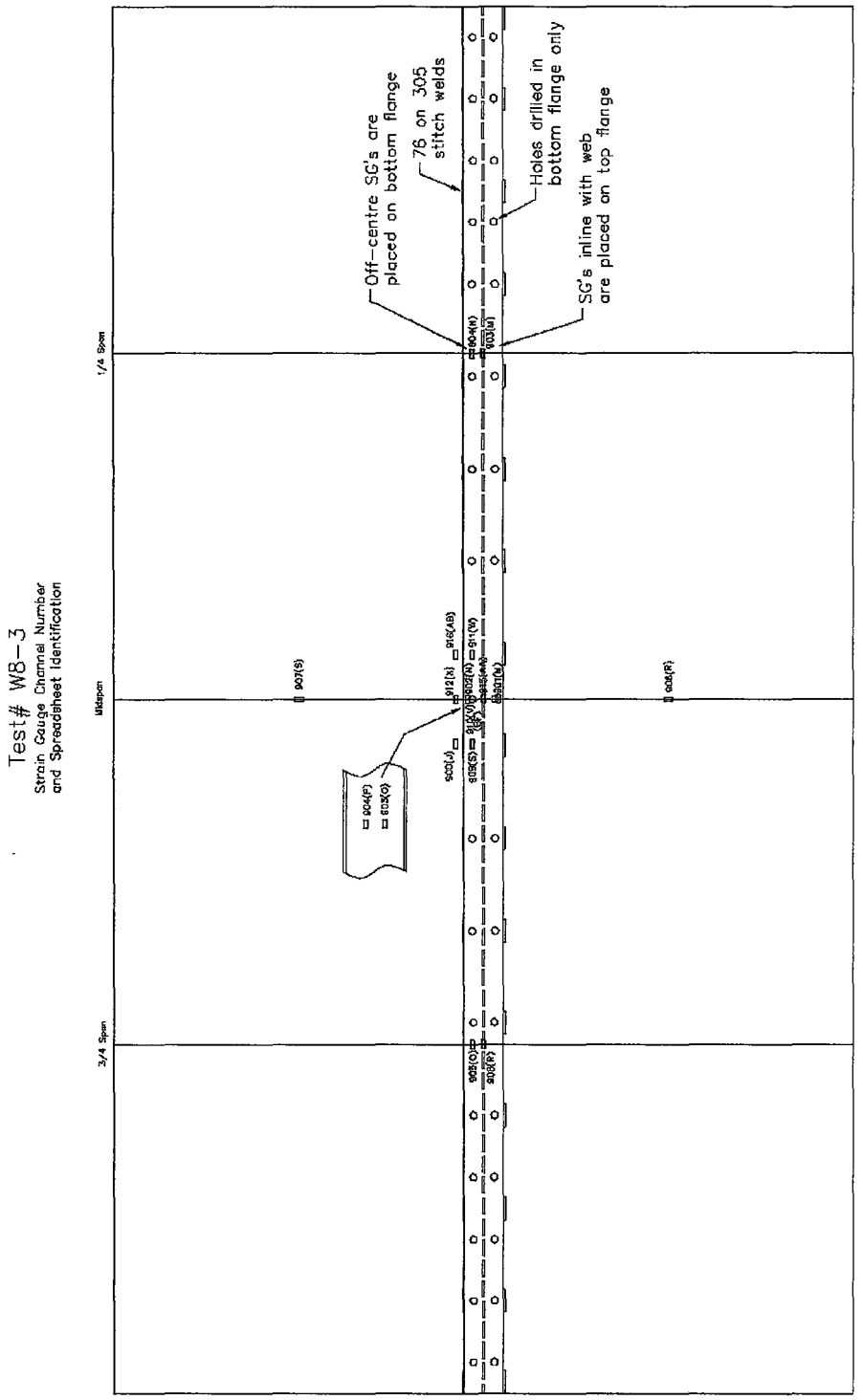

Figure 63: Strain Guage Layout W8-3

APPENDIX C – LVDT LOCATION AND CALIBRATION

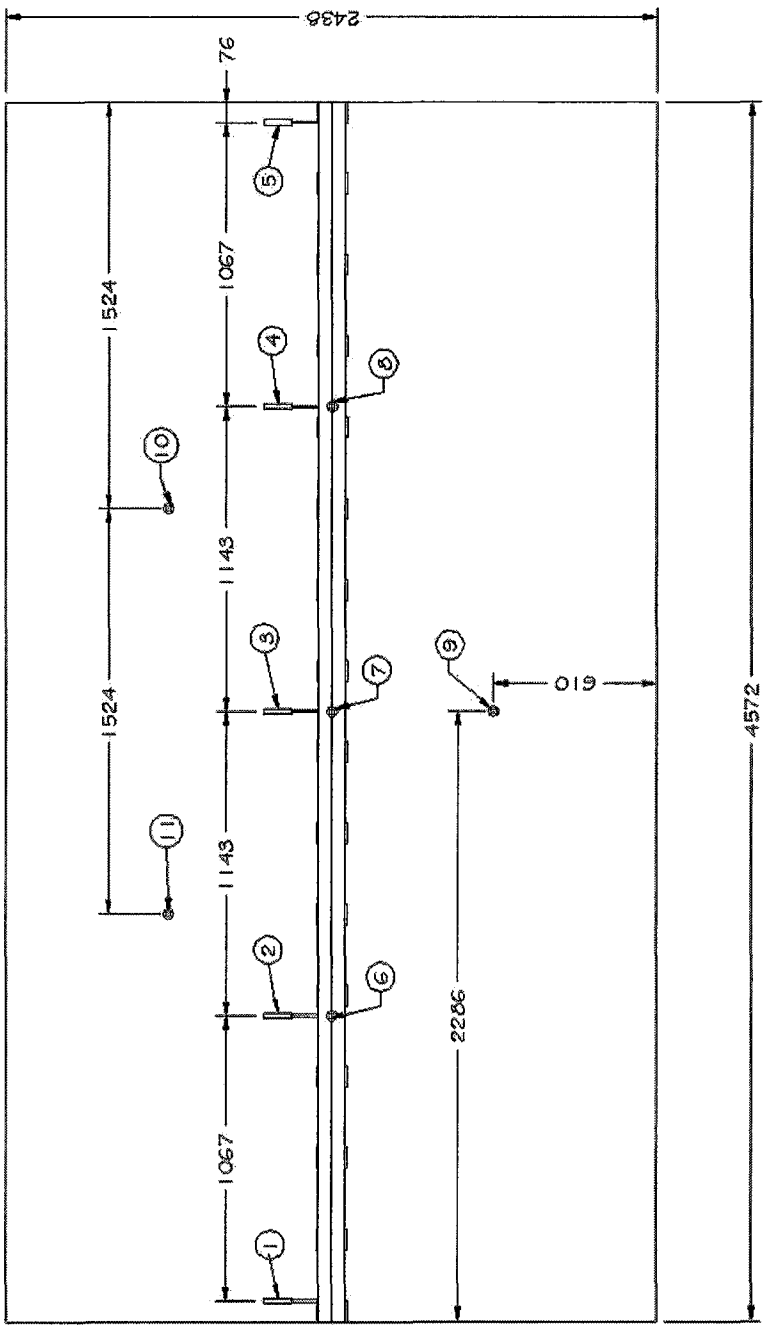

Figure 64: LVDT Layout

Table 23: LVDT Calibration Table

	2" LVDTs							4" LVDTs			
Displacement	LVDT#1	LVDT#2	LVDT#3	LVDT#4	LVDT#5	LVDT#6	LVDT#7	LVDT#8	LVDT#9	LVDT#10	LVDT#11
0	5.094	5.097	5.126	5.129	5.148	5.146	5.146	5.013	3.9891	4.9311	4.3725
0.05	4.973	4.974	5.002	5.004	5.042	5.026	5.054	4.948	3.9258	4.8662	4.3113
0.1	4.847	4.853	4.879	4.885	4.914	4.896	4.923	4.884	3.8608	4.8023	4.251
0.15	4.714	4.735	4.748	4.763	4.785	4.77	4.792	4.82	3.7963	4.738	4.1854
0.2	4.579	4.612	4.617	4.644	4.652	4.644	4.663	4.757	3.7314	4.6726	4.1234
0.25	4.4558	4.487	4.4909	4.525	4.525	4.519	4.54	4.693	3.667	4.6084	4.0597
0.3	4.327	4.3616	4.3602	4.4009	4.3979	4.3956	4.4121	4.628	3.6023	4.5438	3.9936
0.35	4.1919	4.2342	4.2268	4.2741	4.262	4.2738	4.2829	4.563	3.5396	4.4788	3.9311
0.4	4.0556	4.1002	4.0893	4.1435	4.1296	4.1519	4.1524	4.5	3.4738	4.4157	3.8633
0.45	3.9212	3.961	3.9532	4.01	3.9846	4.0239	4.0234	4.4351	3.4095	4.3507	3.7976
0.5	3.7843	3.8181	3.8176	3.8737	3.849	3.8934	3.8947	4.3705	3.345	4.2857	3.7324
0.55	3.6514	3.6853	3.6857	3.7417	3.7139	3.7669	3.7654	4.3074	3.2795	4.2219	3.665
0.6	3.5221	3.5473	3.5567	3.6096	3.5806	3.6402	3.637	4.2448	3.2153	4.1575	3.5996
0.65	3.3925	3.4168	3.4253	3.4779	3.4528	3.5102	3.5064	4.18	3.1516	4.0932	3.5344
0.7	3.2647	3.2884	3.2896	3.3528	3.3208	3.3818	3.3772	4.1165	3.0867	4.0279	3.4678
0.75	3.142	3.1667	3.1638	3.2301	3.1919	3.251	3.2482	4.0522	3.023	3.9636	3.4029
0.8	3.0158	3.0415	3.0366	3.1065	3.0695	3.1253	3.1208	3.9881	2.9594	3.9001	3.3375
0.85	2.8911	2.9144	2.911	2.9881	2.9463	2.9991	2.9916	3.9244	2.8938	3.8356	3.2729
0.9	2.7702	2.7924	2.7845	2.8657	2.8222	2.8748	2.8635	3.8596	2.829	3.7712	3.2093
0.95	2.6469	2.6707	2.6589	2.7436	2.7004	2.7472	2.7347	3.7948	2.7652	3.706	3.1462
1	2.524	2.5564	2.5312	2.6212	2.5776	2.6224	2.6057	3.7306	2.7015	3.6427	3.0821
1.05	2.3988	2.4428	2.4061	2.4973	2.4596	2.4966	2.4783	3.6662	2.6366	3.5776	3.0188
1.1	2.2624	2.3152	2.2692	2.3717	2.3327	2.3588	2.3511	3.6023	2.573	3.5134	2.9555
1.15	2.1164	2.1822	2.1287	2.2359	2.1975	2.2119	2.2216	3.538	2.5076	3.449	2.8919
1.2		2.0452	1.9892		2.0631	2.067	2.0939	3.4731	2.4432	3.3844	2.828
1.25		1.905	1.8542		1.9306	1.9282	1.9654	3.4095	2.3786	3.3203	2.7637
1.3			1.7209		1.7955	1.7852	1.8369	3.3445	2.3153	3.2555	2.6993
1.35						1.6435	1.7065	3.2807	2.2505	3.1919	
1.4								3.2158			

Slope	-0.387	-0.390	-0.382	-0.396	-0.386	-0.388	-0.389	-0.780	-0.776	-0.776	-0.772
Correlation	-0.999	-0.999	-0.999	-0.999	-0.999	-0.999	-0.999	-1	-1	-1	-0.9999

	Slope Mean		Slope Standard Deviation
2" LVDT	-0.3884	+/-	0.0042
4" LVDT	-0.7761	+/-	0.0030

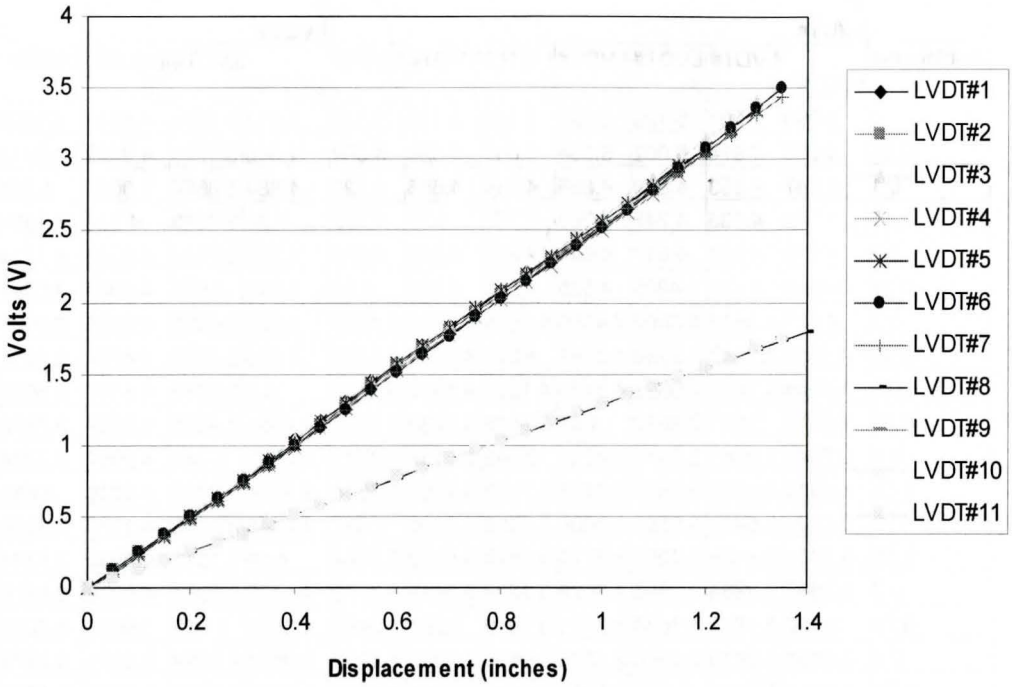

Figure 65: LVDT Calibration

Table 24: Pressure Transducer Calibration

mmHg	kPa	mV
0	0.0	0.2
5	0.66475	0.2
10	1.3295	0.4
15	1.99425	0.5
20	2.659	0.6
25	3.32375	0.8
30	3.9885	0.9
35	4.65325	1.1
40	5.318	1.2
45	5.98275	1.3
50	6.6475	1.5
55	7.31225	1.6
60	7.977	1.7
65	8.64175	1.9
70	9.3065	2.0
75	9.97125	2.2
80	10.636	2.2
85	11.30075	2.4
90	11.9655	2.5
95	12.63025	2.7
100	13.295	2.9
105	13.95975	3.0
110	14.6245	3.1
115	15.28925	3.2
120	15.954	3.3

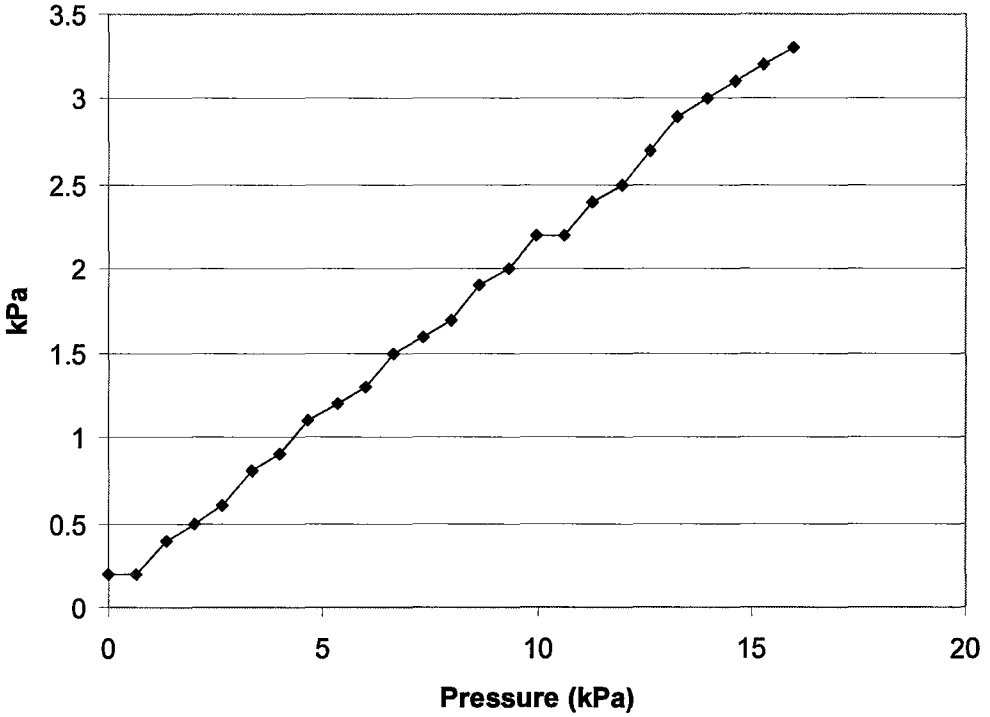

Figure 66: Pressure Transducer Calibration

APPENDIX D - ANSYS FINITE ELEMENT INPUT STRINGS

```
/PREP7

! Duct parameters
t=0.1875
L=15*12
B=8*12

! Beam Properties W12x14
BF=3.97
D=11.91
tw=0.2
tf=0.225

! Beam Properties W8x18
!BF=5.25
!D=8.14
!tw=0.23
!tf=0.33

! Define elements
ET,1,shell63
R,1,t
R,2,tf
R,3,tw

Load=1

! Define material
cs=1
mp,ex,cs,29.5e+6
mp,nuxy,cs,0.3
!mp,dens,cs,(0)
mat,cs

!  Plate
K,1,0,0,0,
K,2,0,0,(b/2-bf/2)
K,3,0,0,B/2
K,4,0,0,(B/2+bf/2)
K,5,0,0,B
K,11,L,0,0,
K,12,L,0,(b/2-bf/2)
K,13,L,0,B/2
K,14,L,0,(B/2+bf/2)
K,15,L,0,B

! SHORT SIDE OF PLATE
lstr,1,2    !L1
lstr,2,3    !L2
lstr,3,4    !L3
lstr,4,5    !L4
```

```
lstr,11,12  !L5
lstr,12,13  !L6
lstr,13,14  !L7
lstr,14,15  !L8

!  LONG SIDE OF PLATE
lstr,1,11   !L9
lstr,2,12   !L10
lstr,3,13   !L11
lstr,4,14   !L12
lstr,5,15   !L13

!  PLATE AREAS
al,1,10,5,9 !A1
al,2,11,6,10      !A2
al,3,12,7,11      !A3
al,4,13,8,12      !A4

! Line meshing factor
fact=3

! MESH PLATE
lsel,s,,,1
lsel,a,,,4
lsel,a,,,5
lsel,a,,,8
lesize,all,,,6

lsel,s,,,2,3
lsel,A,,,6,7
lesize,all,,,1
lsel,s,,,9,13
lesize,all,,,L/fact

asel,s,,,all
real,1
amesh,all

!  Beam

k,16,0,0,(b/2)
k,17,0,d,(b/2-bf/2)
k,18,0,d,(b/2)
k,19,0,d,(b/2+bf/2)

k,116,L,0,(b/2)
k,117,L,d,(b/2-bf/2)
k,118,L,d,(b/2)
k,119,L,d,(b/2+bf/2)

!  close face
lstr,2,16   !L14
lstr,16,4   !L15
lstr,16,18  !L16
```

```
lstr,17,18  !L17
lstr,18,19  !L18

!  end face
lstr,12,116 !L19
lstr,116,14 !L20
lstr,116,118      !L21
lstr,117,118      !L22
lstr,118,119      !L23

!  body
lstr,16,116 !L24
lstr,17,117 !L25
lstr,18,118 !L26
lstr,19,119 !L27

al,10,14,24,19    !A5 bottom flange
al,24,15,12,20    !A6 bottom flange
al,17,26,22,25    !A7 top flange
al,18,27,23,26    !A8 top flange
al,24,21,26,16    !A9 web

lsel,s,,,14,15
lsel,a,,,17,18
lsel,a,,,19,20
lsel,a,,,22,23
lesize,all,,,3    !flanges

lsel,s,,,24
lsel,a,,,25,27
lesize,all,,,L/fact     !beam length

lsel,s,,,16
lsel,a,,,21
lesize,all,,,6          !web height

!  mesh flanges
real,2
asel,s,,,5,8
amesh,all

!  mesh web
eshape,2
real,3
asel,s,,,9
amesh,all


fini
save

resume
/solution
antype,static,new
```

```
pstress,on

nsel,s,loc,z,b/2
nsel,r,loc,x,0
nsel,r,loc,y,0
d,all,ux,0
d,all,uz,0

nsel,s,loc,z,b/2
nsel,r,loc,x,L
nsel,r,loc,y,0
d,all,uz,0

nsel,s,loc,z,0
d,all,uy,0  !restraint on plate long edges
!d,all,uz,0
d,all,rotx,0

nsel,s,loc,z,b
d,all,uy,0  !restraint on plate long edges
!d,all,uz,0
d,all,rotx,0

nsel,s,loc,x,0   !restraint on short ends
nsel,r,loc,y,0
d,all,uy,0
!d,all,rotz,0

nsel,s,loc,x,L
nsel,r,loc,y,0
d,all,uy,0
!d,all,rotz,0

allsel

! Load Definition

asel,s,,,1,4
sfa,all,,press,-1
allsel

solve

fini

/post1

! Get stress/strain profile along web
nsel,s,loc,z,b/2
nsel,r,loc,x,L/2

*get,ncntweb,node,0,count
nn=0
*dim,wbstrn,array,ncntweb
```

```
*dim,yloc,array,ncntweb

*do,i,1,ncntweb,1
 nn=ndnext(nn)
 *get,wbstrn(i),node,nn,epel,x
 yloc(i)=ny(nn)
*enddo

!Get stress/strain profile along plate
nsel,s,loc,x,L/2
nsel,r,loc,y,0

*get,ncntplt,node,0,count
nn=0
*dim,pltstrn,array,ncntplt
*dim,zloc,array,ncntplt

*do,i,1,ncntplt,1
 nn=ndnext(nn)
 *get,pltstrn(i),node,nn,epel,x
 zloc(i)=nz(nn)
*enddo

!Get stress/strain profile along top flange
nsel,s,loc,x,L/2
nsel,r,loc,y,d

*get,ncntflg,node,0,count
nn=0
*dim,flgstrn,array,ncntflg
*dim,zloc,array,ncntflg

*do,i,1,ncntflg,1
 nn=ndnext(nn)
 *get,flgstrn(i),node,nn,epel,x
 zloc(i)=nz(nn)
*enddo


allsel

! Buckling Analysis
/solu
antype,buckle

bucopt,lanb,2
!bucopt,subsp,2

outpr,nsol,all

save,file
solve
finish
```

```
/solu
expass,on
mxpand,2
outpr
solve
fini
```

APPENDIX E – EFFECT OF VARIOUS BOTTOM FLANGE BOUNDARY CONDITIONS

This appendix is included to incorporate additional analysis that was performed for support of the thesis. However, it was removed from the main body of the document and presented here for information only.

The ANSYS finite element program was used to identify the affects of separate restraint boundary conditions and loading arrangements on the buckling capacity of a W12x14 beam. The results of each arrangement are compared to the theoretical buckling capacity considering uniform moment and various end restraints.

Table 1 lists the results of this boundary condition study. M_{cr} is the theoretical buckling capacity of the beam as determined by

$$M_{cr} = \sqrt{\frac{\pi^2 EI_y}{L^2}\left(GJ + \frac{\pi^2 EC_w}{L^2}\right)}$$

where, E = 200,000 MPa
$I_y = 983.5 \times 10^3$ mm^4
L = 4572 mm
G = 0.385·E
$J = 29.303 \times 10^3$ mm^4
$C_w = 21.644 \times 10^9$ mm^6

For this beam, $M_{cr} = 19.979 \times 10^6$ N·mm

The restraint boundary conditions considered are as follows:

- Ends held laterally – The web at the ends of the beam are prevented from moving sideways or twisting. This is a common arrangement accomplished in practice through the use of back to back clip angles, or with L-shaped gusset plates on duct stiffeners.
- Ends laterally free – If the web is free to twist or displace sideways (as in the case of the experimental program of this paper), the only restraint at the ends is to the bottom flange where a vertical restraint is placed. In addition, without any torsional restraint elsewhere on the beam, the section would have a meaningless eigenvalue solution with the buckling analysis. A torsional restraint is therefore applied to the bottom flange only at the ends to prevent such unstable motion.
- Bottom flange held laterally (DZ) – The bottom flange of the beam is prevented from sideways movement along the full span. This is essentially continuous lateral bracing, but only applied to the bottom flange. This restraint condition was discussed in section 1.3.1 Bracing of the Tension Flange.

- Bottom flange held rotationally (RX) – Similarly discussed in section 1.3.1, with the bottom flange prevented from rotating about the longitudinal axis of the beam, any twisting due to buckling must result in deformation of the web. Again, derivation of the buckling formulae is based on the assumption of the cross section remaining plane. Deformation of the web adds additional energy factors that are not normally considered.
- Bottom flange held in warping (RY) – By restraining the rotation of the nodes about the Y axis and allowing vertical (or horizontal) displacement, the bottom flange is held from axial displacements different than the web. By keeping these nodes from rotating, the effect of warping restraint is achieved.

The loads considered are equal and opposite end moments, and a uniformly distributed load. The end moments are created by applying equal and opposite point loads to the top and bottom flange at each end to create a force couple. The forces applied were unit forces. The resulting applied moment is the unit force multiplied the height of the beam. The uniformly distributed load is created by applying a unit load to each node along the full length. In one case, the UDL loads are applied at the midheight of the beam, which acts as the beam centroid and shear centre. In another case, the UDL load is applied at the bottom flange. By placing loads at the shear centre, the affect of second order moments is eliminated. As the beam begins to twist, the location of the load on the cross section will create an additional overturning moment if the load does not coincide with the shear centre. If the load is above the shear centre, the moment will increase with higher twisting deflections. If the load is below the shear centre, it will act to correct the twisting by creating a higher correcting moment with higher twisting deflections. This is discussed in section 1.3.2 Load Height.

Table 25: FE results for various loads and boundary conditions

Arrg't	Restraint Boundary Conditions	Applied Load	Applied Moment (N·mm)	FE Eigenvalue	Buckling Moment, M_b (N·mm)	C_b factor (M_b/M_{cr})
1	- Ends held laterally (DZ)	End moments	1320.4	15490	20.45×10^6	1.024
2	- Ends held laterally (DZ)	UDL at midheight	152550	151	23.06×10^6	1.154
3	- Ends held laterally (DZ)	UDL at bottom flange	152550	208	31.72×10^6	1.588
4	- Ends held laterally (DZ) - Bottom flange held laterally (DZ)	End moments	1320.4	75274 *	99.39×10^6	4.975
5	- Ends held laterally (DZ) - Bottom flange held rotationally (RX)	End moments	1320.4	52683	69.56×10^6	3.481
6	- Ends held laterally (DZ) - Bottom flange held in warping (RY)	End moments	1320.4	18006	23.78×10^6	1.190
7	- Ends held laterally (DZ) - Bottom flange held in warping (RY) - Bottom flange held laterally (DZ) - Bottom flange held rotationally (RX)	End moments	1320.4	93060 *	122.9×10^6	6.150
8	- Ends held laterally (DZ) - Bottom flange held in warping (RY) - Bottom flange held laterally (DZ) - Bottom flange held rotationally (RX)	UDL at bottom flange	152550	1147 *	175.0×10^6	8.759
9	- Ends laterally FREE (DZ) - Bottom flange held in warping (RY) - Bottom flange held laterally (DZ) - Bottom flange held rotationally (RX)	UDL at bottom flange	152550	835	127.4×10^6	6.376

In all cases, the bottom node at the ends was supported vertically and laterally. The left end was also held axially, while the left end was axially free. Each arrangement and the buckled shape is shown below. Eigenvalues in the table that are marked with an asterix * are beams that were forced into a second mode shape with a double curvature.

Arrangement 1 closely estimates the loading and restraint conditions of the ideal beam represented by the theoretical buckling equation. The ends are restrained from both vertical motion and rotation about the X-axis. The uniform moment loading is applied through a force couple spaced between the flanges at each end. The moment is applied uniformly across the length of the beam.

The buckling capacity as determined by ANSYS is 20.45×10^6 N·mm. This is 102.4% of the theoretical value. The C_b value is the ratio of the ANSYS result to the theoretical value. In this case, $C_b = 1.024$. This C_b value is used by designers to accommodate the increased (or decreased) capacity of a beam when it is loaded with a moment profile different than the uniform moment assumed by the buckling equation.

Arrangement 2 is a standard arrangement where a uniformly distributed force is applied across the span of the beam. The resulting C_b for this arrangement is 1.154, meaning the beam has 15.4% greater capacity than what the theoretical equation has determined. This can be compared to the published value of 1.12 for this loading arrangement.[8]

Arrangement 3 is the same as arrangement 2, except the UDL loading is moved to the bottom flange rather than being placed at the midheight. The resulting C_b for this arrangement is 1.588. This is an increase of 43% over the midheight loading. This can be compared to the results of bottom flange loading as discussed in section 1.4.2. Using the methods of the SSRC Guide[10], the C_b value for bottom flange loading on this beam section was calculated as 1.523.

Arrangements 4 through 7 demonstrate the effects of various bottom flange restraints. In each case, the loading was applied through the end force couples. The bottom flange in Arrangement 4 is only restrained from lateral displacement (DZ). This arrangement provided a significant increase in capacity, increasing the C_b from 1.024 to 4.975, a 486% increase.

The rotational restraint (RX) of the bottom flange in arrangement 5 provided a substantial increase in capacity. The C_b value for this arrangement is 3.481, a 340% increase from arrangement 1.

The warping restraint to the bottom flange (RY) in arrangement 6 gave a significant but less dramatic increase in capacity. The moment modification factor C_b increased from 1.024 to 1.19, a 16% increase.

Arrangement 7 provides the bottom flange with all three restraints, RX, RY, and DZ. Again, the loading is a uniform moment applied at the ends. The C_b of this arrangement is further increased to 6.15, a 600% increase. The buckled shape of the beam with this combination of restraints is forced into the second mode shape indicating a higher amount of energy is required to buckle in this shape.

Arrangement 8 provides the same restraint to the bottom flange and beam ends as arrangement 7, but the loading is changed from the uniform moment to a UDL on the bottom flange. The increase in capacity is increased further yet resulting in a C_b of 8.759. This buckled shape is also forced into the second mode.

It is noted that arrangement 8 closely represents the restraints of a stiffener on a duct. This model, however, does not include the affects of the composite plate and beam section which will further increase the beam capacity. This arrangement, however, does not represent the apparatus of the experimental program. In the experiment, the top flange and web at the ends of the beam were not restrained from rotation or deflection.

Arrangement 9 is the same as arrangement 8 except the lateral restraints are removed from the ends of the web. The resulting C_b of this arrangement as determined by BASP is 6.376, a 623% increase. This arrangement closely represents the testing apparatus used for the experimental portion of this thesis, with the exception of the plate and beam composite affects.

By relating these applied loads to an internal duct pressure on a 4572mm wide duct with 1219mm stiffener spacing, the internal pressure required to generate the buckling moment of arrangement 9 is 64.2kPa. These calculations are shown in Appendix F. It is noted that these pressures are substantially greater than the pressures predicted by the ANSYS modeling discussed previously.

From this analysis it is shown that the modified pressure loading does not have a large affect on the capacity of the beam. In this arrangement, the stiffeners are placed relatively close together and the tributary area that is supported by the end plates is quite small. As a result, the loading distribution shown in Appendix F is not greatly different than the idealized UDL. The affect of the modified loading diagram is expected to become greater with increased stiffener spacing that provides a larger tributary area to the end plates rather than the stiffener.

APPENDIX F – STIFFENER PRESSURE LOADING

The standard design methods use an idealized pressure loading model that considers a uniformly distributed load (UDL) across the entire span of the stiffener beam. As discussed in Section 2.5, the actual distribution is tapered at the ends as illustrated in the following figure. The plate between each stiffener is divided into four areas. The pressure applied to the small areas on the ends is supported by the adjacent face of the duct. Half of the remaining area goes to each stiffener in the pattern shown.

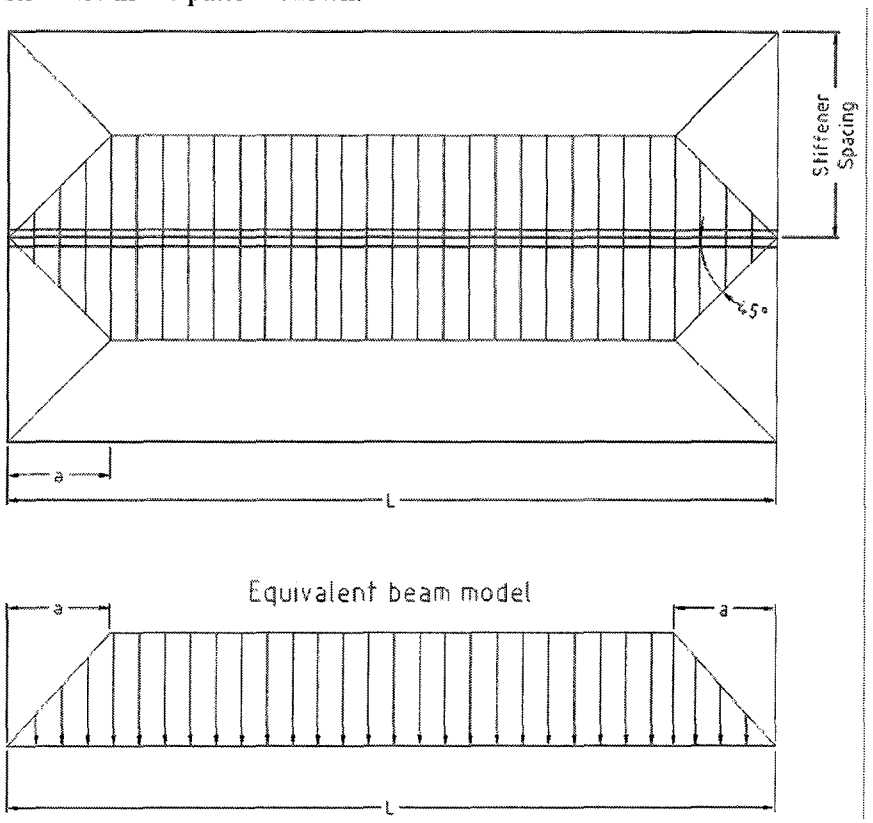

Figure 67: Pressure Distribution Model

$$M_{app} = \omega\left[\frac{L^2}{8} - \frac{a^2}{24}\right], \qquad \text{(F-1)}$$

where ω = P×b (internal pressure × stiffener spacing). For most stiffener arrangements, the $a^2/24$ is sufficiently small that it can be ignored. However, its effects may be useful if the stiffener size is optimized.

APPENDIX G – CASING STRESS CALCULATIONS

The following calculations determine the combined bending and membrane stresses on plate subjected to a uniform pressure load. The analysis carried out in this paper considered a stiffener spacing of 48in. This spacing was not justified. The following analysis, or something similar, is generally carried out first to establish the appropriate spacing of stiffeners in order to minimize the stresses on the casing plate.

The equation for 'b' below is an empirical derivation[13] of the tabular values in Roark[25].

Casing Stress Calculation:

Air duct
15 ft wide
35 inH2O internal negative design pressure
70 deg F
Grade 44 plate materials

Determine the maximum stiffener spacing using large deflection plate theory.

Material Properties:

$F_y := 44000\,psi$ 44W carbon steel plate

$E := 29.5 \times 10^6 psi$

$F_b := \left(\frac{2}{3}F_y\right) \cdot 1.5$ Bending stress using 1.5 shape factor for plate, and 2/3 design factor

$F_b = 44\,ksi$

Duct Properties:

$t := \frac{3}{16}in$ duct casing thickness

$L := 180\,in$ duct width (stiffener span)

$W := 35 inwg$ $W = 1.264\,psi$ Internal pressure plus dead weight of casing and live load

$W = 8.714\,kPa$

Determine the maximum stiffener spacing based on large deflection plate theory

$$b := \left[\frac{(0.6F_y)\cdot t^{1.08}}{0.81\cdot W^{0.77}\cdot E^{0.23}}\right]^{\frac{1}{1.08}}$$

$b = 61.448\,in$

$b = 1561\,mm$ Maximum spacing allowed (Ref. 17)

$b := 48in$ Actual spacing used in experimental program

APPENDIX H – DESIGN EXAMPLE FOR W12X14 FROM SECTION 4.4

Design Example

Determination of Moment Capacity Considering:
- Monosymmetric Sections
- Load Height Factor
- Torsional Bracing on Tension Flange

Beam section properties for W12x14:

$d_w := 11.91\,in$ beam height

$t_f := 0.225\,in$ flange thickness

$b_f := 3.97\,in$ flange width

$A_f := t_f \cdot b_f$ flange area

$t_w := 0.2\,in$ web thickness

$J := 0.0704\,in^4$

$C_w := 80.6 \cdot in^6$ torsional constants

$I_y := 2.36 \cdot in^4$ weak axis moment of inertia

Material properties:

$E := 29500\,ksi$ elastic modulus

$G := 0.385E$ shear modulus

$F_y := 50\,ksi$ yield strength

Stiffener and Duct Dimensions:

$L := 15\,ft$ beam span

$b_s := 48\,in$ stiffener spacing

Plate properties

$t_{pl} := 0.1875\,in$ plate thickness

Monosymmetric Section Properties

$d_m := 1.7 \cdot d_w$ $\quad d_m = 20.25\,in$ modified composite beam height

$C_{wm} := \frac{d_m^2 \cdot I_y}{4}$ $\quad C_{wm} = 241.87\,in^6$ modified beam warping constant

$J_m := \frac{\left(2 \cdot b_f \cdot t_f^3 + d_m \cdot t_w^3\right)}{3}$ $\quad J_m = 0.084\,in^4$ modified beam torsional constant

$M_{cr\_m} := 1.12 \cdot \pi \cdot \frac{E}{L} \cdot \sqrt{0.385 \cdot I_y \cdot J_m + \left(\frac{\pi}{L}\right)^2 \cdot I_y \cdot C_{wm}}$ $\quad M_{cr\_m} = 288.52\,in \cdot kip$ critical moment for modified beam section

Determine moment modification factor including load height

$$W_c := \frac{\pi}{L}\cdot\sqrt{\frac{E\cdot C_{wm}}{G\cdot J_m}} \qquad W_c = 1.51$$

$$A := 1.12$$

$$B := 1 - 0.154\cdot W_c^2 + 0.535 W_c \qquad B = 1.46$$

$$y := \frac{d_m}{2} \qquad y = 10.12\,in$$

$$C_b := A\cdot B^{\frac{2\cdot y}{d_m}} \qquad C_b = 1.63$$

$$M_{cmslh} := \frac{M_{cr\_m}}{1.12}\cdot C_b \qquad M_{cmslh} = 420.25\ in\cdot kip$$

Note: Mcr-v is divided by 1.12 since the term for Cb also contains the same factor

Determine additional strength from torsional bracing:

Determine the torsional stiffness of the casing in resisting twisting of the stiffener:

Consider 1" wide strip of plate with span equal to spacing between 2 stiffeners

$$I_c := \frac{(1\cdot in)\cdot t_{pl}^3}{12} \qquad I_c = 5.493\times 10^{-4}\,in^4$$

$$\beta_c := \frac{16.66\cdot E\cdot I_c}{2b_s\cdot(1in)} \qquad \beta_c = 2812.22\ \frac{in\cdot lbf}{rad\cdot in}$$

Determine the torsional stiffness of the beam web:

$$\beta_{web} := \frac{3.3\cdot E}{d_w}\cdot\left(\frac{t_w^3}{12}\right) \qquad \beta_{web} = 5.449\times 10^3\ \frac{in\cdot lbf}{rad\cdot in}$$

Total combined stiffness of casing and stiffener:

$$\beta_{tot} := \frac{1}{\frac{1}{\beta_c} + \frac{1}{\beta_{web}}} \qquad \beta_{tot} = 1854.93\ \frac{in\cdot lbf}{rad\cdot in}$$

Allowable moment for torsionally braced section:

$$M_{mslhtb} := \sqrt{M_{cmslh}^2 + \beta_{tot}\cdot E\cdot I_y} \qquad M_{mslhtb} = 553\ in\cdot kip$$

Buckling moment considering flexible casing

$$M_{mslhtb} := \sqrt{M_{cmslh}^2 + \beta_{web}\cdot E\cdot I_y} \qquad M_{mslhtb} = 746\ in\cdot kip$$

Buckling moment considering rigid casing

APPENDIX I – MATERIAL TEST RESULTS

Test specimens were cut from the webs of each beam to determine the yield strength and modulus of elasticity for each. The modulus of elasticity was noted at the point where the specimen was at the 2/3 yield stress level. The results are summarized in Table 10.

Table 26: Yield and Elastic Modulus Measurements

Speciman	Yield Strength (MPa)	Modulus of Elasticity (GPa)
W12x14 #1	402	201
W12x14 #2	399	193
W8x18 #1	373	245
W8x18 #2	384	205
W8x18 #3	380	307*
Average/SD/COV	388 / 11.1 / 2.9	211 / 20.1 / 9.5

* This value is ignored

The nominal minimum yield stress for all beams is 345 MPa (50 ksi). Each tensile test achieved a higher yield stress by an average of 12%.

The accepted modulus of elasticity for steel is 200 GPa. The average value obtained was 211 GPa. This value is within one standard deviation of the accepted value.

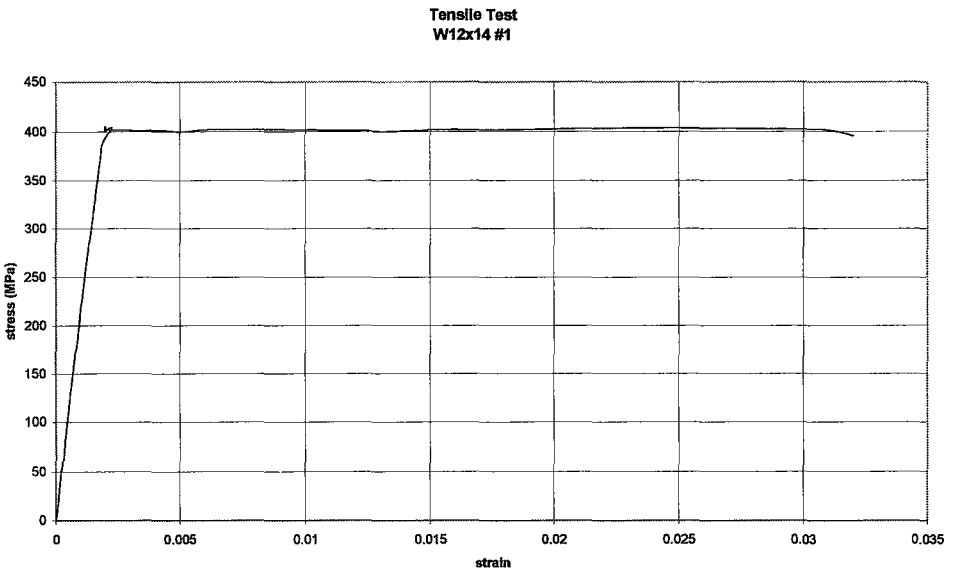
Tensile Test
W12x14 #1
stress (MPa)
strain
0
50
100
150
200
250
300
350
400
450
0
0.005
0.01
0.015
0.02
0.025
0.03
0.035

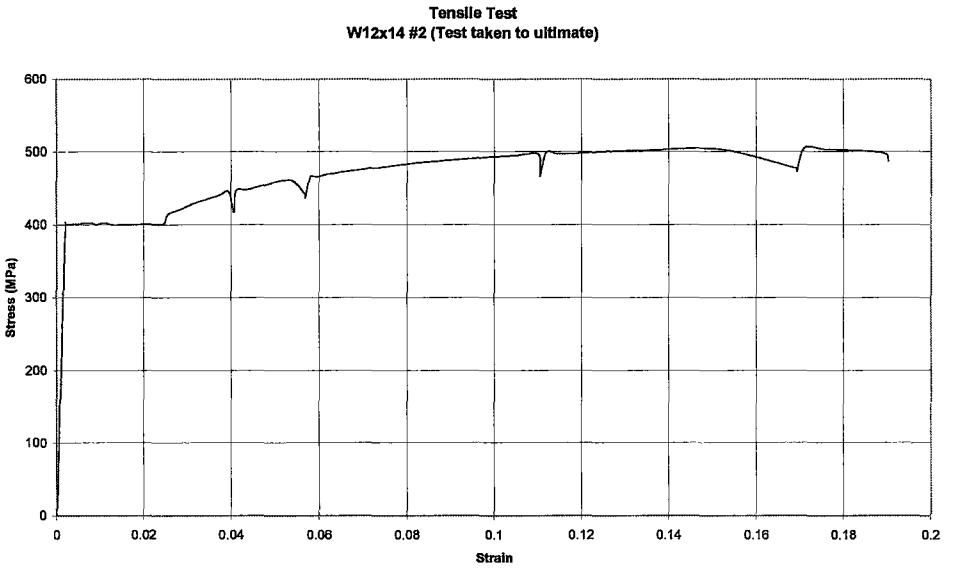
Tensile Test
W12x14 #2 (Test taken to ultimate)
Stress (MPa)
Strain
0
100
200
300
400
500
600
0
0.02
0.04
0.06
0.08
0.1
0.12
0.14
0.16
0.18
0.2

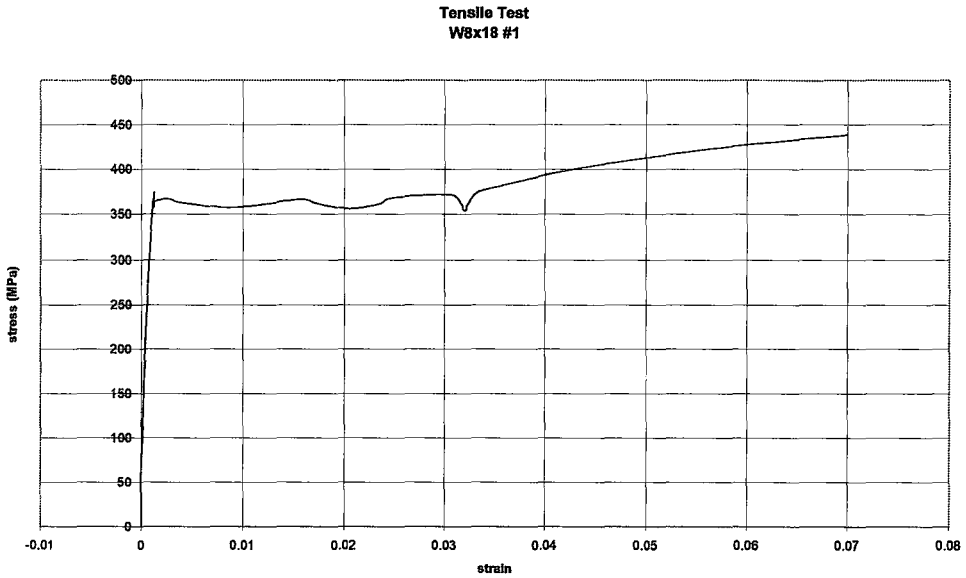
Tensile Test
W8x18 #1
stress (MPa)
strain
500
450
400
350
300
250
200
150
100
50
0
-0.01
0
0.01
0.02
0.03
0.04
0.05
0.06
0.07
0.08

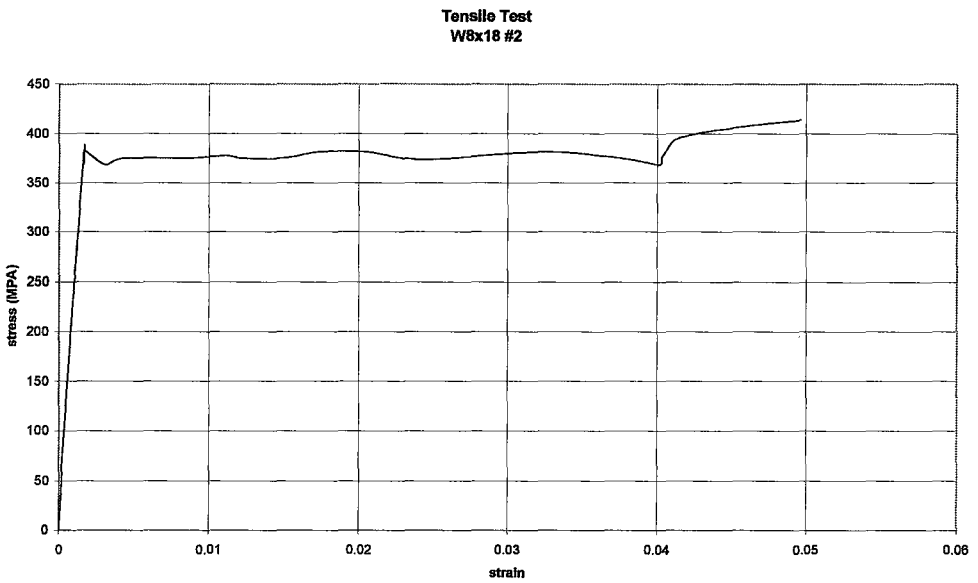
Tensile Test
W8x18 #2
stress (MPA)
strain
450
400
350
300
250
200
150
100
50
0
0
0.01
0.02
0.03
0.04
0.05
0.06

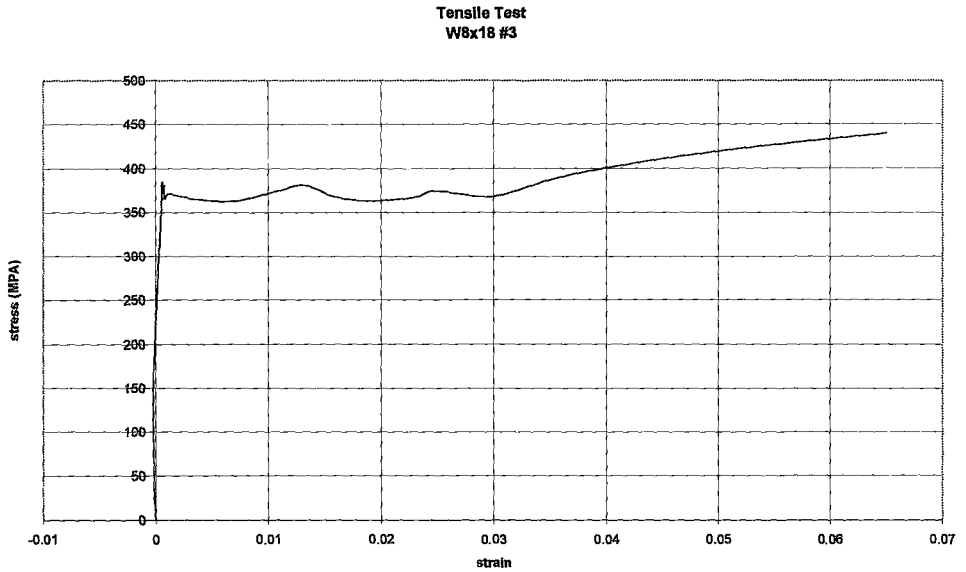
Tensile Test
W8x18 #3
stress (MPA)
500
450
400
350
300
250
200
150
100
50
0
-0.01
0
0.01
0.02
0.03
0.04
0.05
0.06
0.07
strain

APPENDIX J – DERIVATION OF CASING STRIP FLEXIBILITY

In Section 4.4 and Appendix H the flexibility of the casing was used to establish the amount of bracing given to the compression flange through the plate and web. A simply supported beam with a centre moment is a reasonable model to establish the relative rotation for a given load. However, it is realized that a strip of casing on a duct has additional boundary restraints that the simply supported model does not.

Figure 68(a) illustrates a simple beam with a moment applied at the midspan. This is the simply supported beam model. The rotation at the center of the beam is given by

$$\theta_{cL} = \frac{M_0 L}{12EI} \tag{J-1}$$

The stiffness of the plate is given by the force/displacement. Rearranging Equation J-1

$$\beta = \frac{M_0}{\theta_{cL}} = \frac{12EI}{L} \tag{J-2}$$

Figure 68(b) shows the same beam with the additional end restraints, $\theta(x=0,L) = 0$, and $\Delta x\ (x=0,L) = 0$. The axial restraint at the ends of the beam act to create membrane tension strain as the plate begins to deflect under the applied moment. This increases the stiffness of the plate to some degree.

A revised equation was derived with the use of the Ansys finite element program. The revised equation was to take the same form as Equation J-2 above. A strip of shell elements at varying lengths and thicknesses was modeled, and then a moment applied to the midspan. The moment was applied to the two nodes at the centre of the strip, 0.5 units on each node. Figure 69 shows the strip in the deflected shape. The Ansys input strings are included at the end of this Appendix.

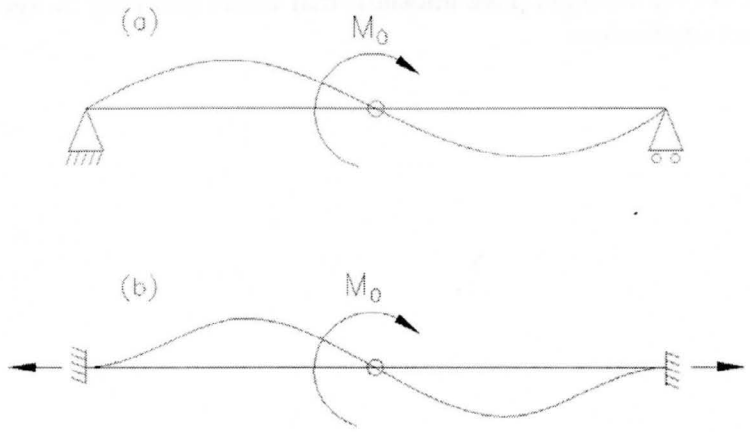

Figure 68: Casing Flexibility Model

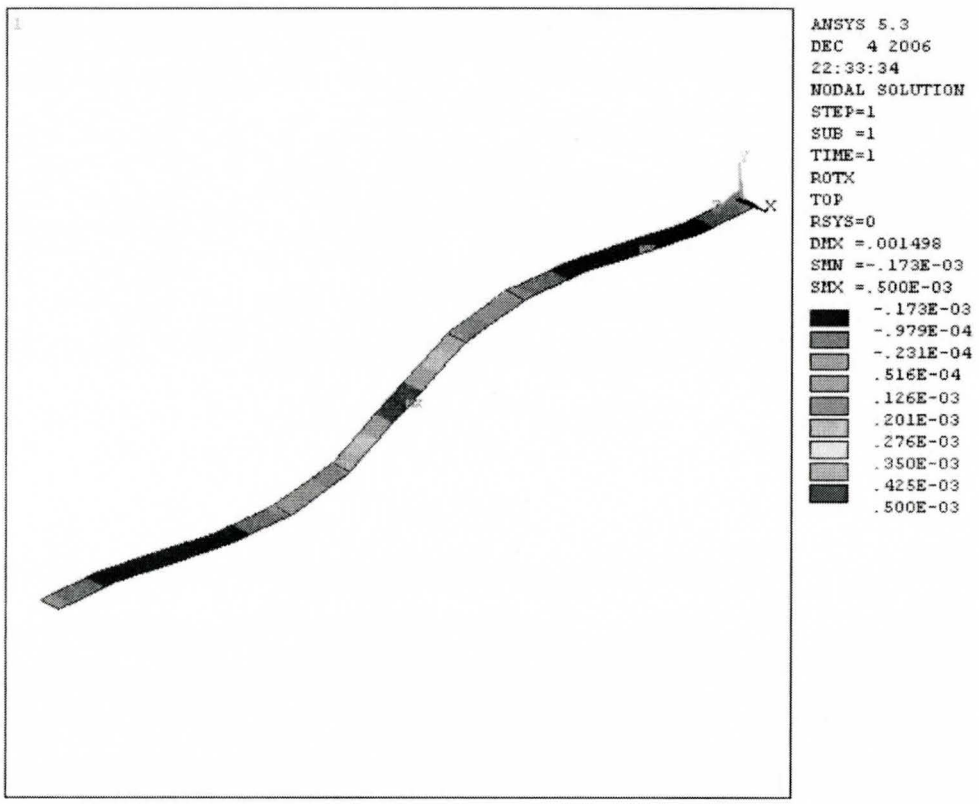

Figure 69: ANSYS Casing Strip Model

Table 27 lists the rotation of the strips as determined by the finite element output for various lengths from 40 inches to 80 inches, and thicknesses from 1/8"

to 3/8". These are the common plate thickness that would generally be specified in industrial duct applications.

Table 27: Plate stiffness data

Rotation at Center of Strip (rad)				
Length	Thickness			
	0.375	0.25	0.1875	0.125
80	3.70E-05	1.25E-04	2.96E-04	1.00E-03
70	3.24E-05	1.09E-04	2.59E-04	8.75E-04
60	2.78E-05	9.37E-05	2.22E-04	7.50E-04
50	2.31E-05	7.81E-05	1.85E-04	6.25E-04
40	1.85E-05	6.25E-05	1.48E-04	5.00E-04
Slope	4.6300E-07	1.5590E-06	3.7000E-06	1.2500E-05
Intercept	-2E-08	1.2E-07	0	0

Figure 70 illustrates the data from Table 27 graphically. The curves for each plate thickness are linear. Their slopes and zero-intercept are also given in Table 27. A cubic relationship between the various plate thicknesses for a given length can be seen. This is reflected in Equation J-2 in which the moment of inertia (which is proportional to t^3) is a factor in the stiffness, β.

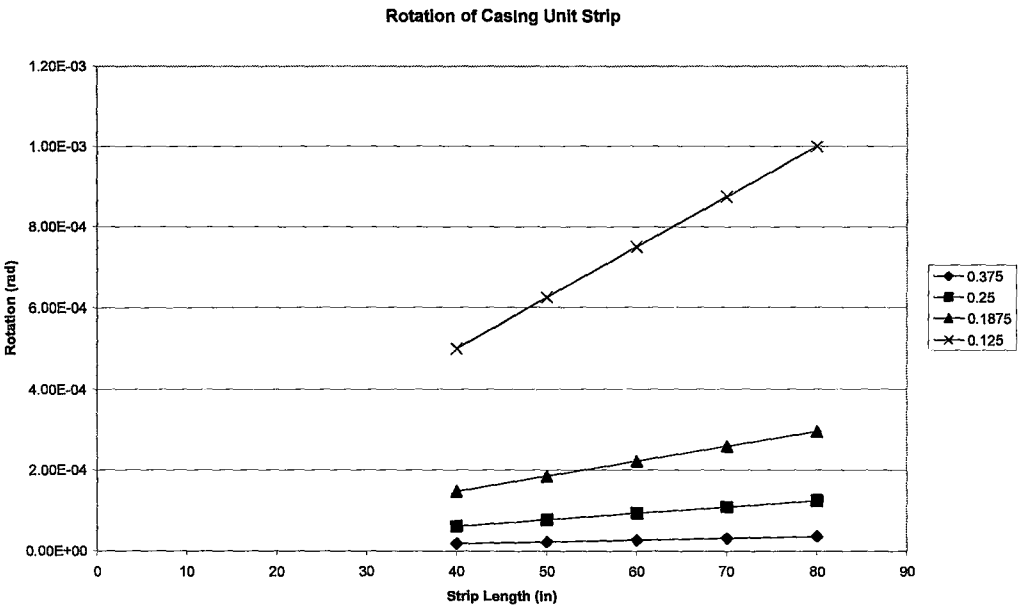

Figure 70: Casing Strip Flexibility Output

The slope of the above lines is given in *in·rad/in* units. Given that the equation for the stiffness, β, is the same form: $\beta = A \times \frac{EI}{L}$, then the slope of the above lines is given by

$$m = \frac{1}{AEI} \tag{J-3}$$

Substituting the slope values from Table 27 and solving for 'A':

$$A_1 = \frac{1}{m_1 EI_1} = \frac{1}{(4.63\times10^{-7})29{,}500{,}000\cdot\left(\frac{0.375^3}{12}\right)} = 16.66$$

$$A_2 = \frac{1}{m_2 EI_2} = \frac{1}{(1.559\times10^{-6})29{,}500{,}000\cdot\left(\frac{0.25^3}{12}\right)} = 16.699$$

$$A_3 = \frac{1}{m_3 EI_3} = \frac{1}{(3.70\times10^{-6})29{,}500{,}000\cdot\left(\frac{0.1875^3}{12}\right)} = 16.678$$

$$A_4 = \frac{1}{m_4 EI_4} = \frac{1}{(1.25\times10^{-5})29{,}500{,}000\cdot\left(\frac{0.125^3}{12}\right)} = 16.66$$

The stiffness of a strip of casing fixed from rotation and from axial displacement at the ends is given by

$$\beta_c = \frac{16.66\cdot E\cdot I}{L} \tag{J-4}$$

APPENDIX K - ANSYS INPUT STRING FOR CASING STRIP FLEXIBILITY

```
/PREP7
! Duct parameters
t=0.25
b=30*2
! Define elements
ET,1,shell63

R,1,t
! Define material
cs=1
mp,ex,cs,29.5e+6
mp,nuxy,cs,0.3
mp,dens,(0)
mat,cs

K,1,0,0,0
K,2,0,0,b/2
K,3,0,0,b
k,4,1,0,0
k,5,1,0,b/2
k,6,1,0,b

lstr,1,2
lstr,2,3
lstr,4,5
lstr,5,6
lstr,1,4
lstr,2,5
lstr,3,6

al,1,6,3,5
al,2,7,4,6

lsel,s,,,1
lsel,a,,,2
lsel,a,,,3
lsel,a,,,4
lesize,all,,,6

lsel,s,,,5
lsel,a,,,6
```

```
lsel,a,,,7
lesize,all,,,1

asel,s,,,all
real,1
amesh,all

nsel,s,loc,z,0
D,all,all,0

nsel,s,loc,z,b
D,all,all,0
allsel
fini

/solution

nsel,s,loc,z,b/2
f,all,mx,0.5
allsel
solve

fini

/POST1
PLNSOL,ROT,X,0
```